1990

Shift-invariant image reconstruction of speckle-degraded using bispectrum estimation

Steven M. Wear

Shift-Invariant Image Reconstruction Of Speckle-Degraded Images Using Bispectrum Estimation

by

Steven M. Wear, Capt, USAF

B.S.E.E. Oklahoma State University

(1985)

A thesis submitted in partial fulfillment of the requirements for the degree of Master of Science in the Center for Imaging Science in the College of Graphic Arts and Photography of the Rochester Institute of Technology.

May 1990

Steve M. Wear

Signature of the Author

Accepted by

Coordinator, M.S. Degree Program

COLLEGE OF GRAPHIC ARTS AND PHOTOGRAPHY
ROCHESTER INSTITUTE OF TECHNOLOGY
ROCHESTER, NEW YORK

CERTIFICATE OF APPROVAL

M.S. DEGREE THESIS

The M.S. Degree Thesis of Steven M. Wear
has been examined and approved
by the thesis committee as satisfactory
for the thesis requirement for the
Master of Science degree

Professor M. Raghuveer, Thesis Advisor

Professor N. Rao

Professor S. Dianat

14 May 90

Date

THESIS RELEASE PERMISSION FORM

Rochester Institute of Technology
College of Graphic Arts and Technology
Rochester, New York

Title of Thesis: **SHIFT-INVARIANT IMAGE RECONSTRUCTION OF SPECKLE-DEGRADED IMAGES USING BISPECTRUM ESTIMATION**

I, **Steven M.** Wear, hereby grant permission to the Wallace Memorial Library of R.I.T. to reproduce my thesis in whole or in part. Any reproduction will not be for commercial use or profit.

Steven M. Wear

Signature

5 JUL 90

Date

ABSTRACT

Coherent speckle noise is modeled as a multiplicative noise process that has a negative exponential probability density function. Using a homomorphic transformation, this speckle noise is converted to a signal-independent, additive process. The speckled images are randomly jittered from frame-to-frame against a uniform background to simulate image motion and/or platform jitter.

Multiple images are logarithmically transformed and ensemble averaged in the bispectral domain. The bispectrum ignores this image motion so no blurring results from the ensemble averaging. Object Fourier magnitude and phase information are also retained in the bispectrum so that the resultant image can be uniquely reconstructed. This value is then exponentiated to complete the image reconstruction process.

Since speckle masks the resolution of details in the noisy image and effectively destroys the object structure within the image, it is seen that image reconstruction using bispectrum estimation results in images that regain their object structure.

Both one-dimensional and two-dimensional images were tested using separate bispectral signal reconstruction algorithms for each.

ACKNOWLEDGMENTS

As with any work that so completely consumes an individual, one must rely on many people to fulfill that task that has been your life for so long. This is definitely the case for myself and the list of people who have helped me in some way would be endless. Thus, I must confine my thanks to a few people who have been instrumental in seeing this task completed. My thesis committee members have been extremely helpful in this work.

Professor Rao has given me excellent suggestions on improving the presentation of the material, expecially as regards the speckle modeling.

I would like to thank Professors Dianat and Raghuveer for allowing me to use their two-dimensional magnitude bispectrum reconstruction algorithm.

Professor Raghuveer has been particularly helpful in that he continually helped me search for ever-improving methods to overcome the problems I encountered when implementing the bispectral routines.

Similarly, early in this thesis work, Gopal Sundaramoorthy, a graduate student at R.I.T. working with the bispectrum, was very helpful in getting me started with the bispectrum and understanding its nuances.

Major Paul Idell, Capt Dave Voelz, and Capt John Gonglewski of the Air Force Weapons Laboratory were very helpful in helping me understand the parameters necessary to properly model coherent speckle.

Laura Abplanalp of Eastman Kodak played a pivotal role in helping me get the final product of this endeavor (the thesis itself) completed and published on a very short time schedule.

The ultimate thanks goes to my family who showed the patience and understanding necessary to allow me to complete this work.

DEDICATION

to

Judy, Marc, and Bethany

TABLE OF CONTENTS

TABLE OF CONTENTS (CONT'D)

LIST OF ILLUSTRATIONS

TABLE OF CONTENTS (CONT'D)

LIST OF ILLUSTRATIONS (CONT'D)

TABLE OF CONTENTS (CONT'D)

LIST OF ILLUSTRATIONS (CONT'D)

TABLE OF CONTENTS (CONT'D)

LIST OF ILLUSTRATIONS (CONT'D)

TABLE OF CONTENTS (CONT'D)

LIST OF ILLUSTRATIONS (CONT'D)

1.0 INTRODUCTION

When an object is illuminated by a coherent source of electromagnetic radiation, and this object has a surface structure that is rough on the order of a wavelength of the incident radiation. a speckle pattern results. A fully developed speckle pattern will appear chaotic and disorganized. Even when the speckled object is imaged, the presence of speckle noise is seen as a collection of spots superimposed on the actual image. Thus, speckle is considered as noise that degrades an image whereby information present in the image is masked. This noise can be present in either the pupil plane (farfield) or the image plane.

Studies related to the occurrence of speckle phenomenon are not new. Dainty (1984) relates a brief history of observations of speckle patterns, beginning with Newton s attempt to explain star twinkling. Exner, in the late 19th century. sketched a speckle pattern created by a candle seen through fogged glass. Dehaas. in the early 20th century. actually photographed such a pattern. In the early 1960's. with the advent of the laser, the investigation of this phenomenon accelerated. Coherent speckle phenomenon can occur is such diverse imagery as synthetic aperture radar (SAR). acoustic imagery. ultrasound. x-ray scattering. electron scattering. microwaves. and obviously laser illumination.

What really is important is how speckle degrades an image. Speckle increases the size of the minimum resolution patch obtained with a given aperture as compared to the same size aperture using incoherent illumination (Kozma and Christensen. 1976). The resolution of the image is reduced making certain feature identification difficult. The Maximum Likelihood Estimate (MLE) of a speckle image is obtained

from ensemble averaging. This technique is a highly effective way of removing speckle noise (Sadjadi, 1990; Jain and Christensen, 1980; Lim and Nawab, 1981). Multiple images are necessary to perform this procedure. Perfect registration of each image with the other is required so that the resultant, averaged image is not blurred. This concern often precludes using ensemble averaging due to the difficulty in registering images exactly. This is especially true when the image is changing its position from frame-to-frame.

A signal processing technique called bispectrum estimation can perform ensemble averaging on multiple, shifted, speckled images. The bispectrum is defined in this paper to be the Fourier transform of the triple correlation of an image. Image reconstruction with the bispectrum has the following beneficial properties:

1. The bispectrum is insensitive to linear phase shifts;

2. The bispectrum retains both Fourier magnitude and phase information;

3. The bispectrum is insensitive to certain additive noise processes.

This technique is a spectral domain technique as opposed to a spatial domain technique, where much of the current digital speckle reduction techniques operate. This thesis will review the statistics of speckle, speckle as noise, and how this noise affects the image. A thorough examination of speckle computer modeling will be conducted and several methods of generating speckled objects digitally will be reviewed in detail with examples of speckle imagery given. I will also review the bispectrum and how its use with homomorphic processing will aid in image recon-

struction of speckle-degraded images. Two separate bispectral reconstruction algorithms are used for one-dimensional and two-dimensional images.

2.0 BACKGROUND

The technique I will use to reconstruct the image of a speckled object will be a wholly digital technique. By this I mean that each speckled image will be in a digitized format and will be operated on totally using a computer on a pixel-by-pixel basis. I state this at the beginning so as to differentiate this technique from physical methods of reducing speckle. For example, McKechnie (1984) lists several methods one can do to reduce speckle before it is imaged, such as:

1. Illuminating the object with a temporally partially coherent source;

2. Illuminating the object with a spatially partially coherent source;

3. Observing the speckled object through a moving aperture that performs time-averaging as it moves across the pattern;

4. Observing the pattern through a finite aperture that acts as a low-pass filter.

Guenther, et al. (1978) has one of the earliest papers listing several different digital filters that could be applied to reduce speckle. They describe the basic ensemble averaging technique (where several images are averaged together to reconstruct the image) as well as the spatial processing technique using an averaging window (which moves across the image spatially). Two simple, digital, non-linear filters (square-root and squaring) are also described. Jain and Christensen (1980) review similar techniques as well as a homomorphic Wiener filter for digital speckle removal. Lim and Nawab (1981) compare other digital techniques for speckle reduction such as low-pass filtering in the frequency (Fourier) and density (logarithmic)

domains as well as a method they call the "short space spectral subtraction image restoration technique." They discuss briefly the homomorphic approach to image restoration using a filter built specifically for this method but do not describe this filter in any detail, though they do discuss the benefits of using the homomorphic approach. Sadjadi (1990) reviewed the before-mentioned averaging techniques, a median filter, local statistical filters, an adaptive filter, and a sigma filter and compared these with the homomorphic approach to speckle reduction. The homomorphic approach allows additive-noise reduction techniques to be applied to multiplicative noise conditions. A better description of a local statistics filter used in homomorphic processing is given by Arsenault and Levesque (1984). A general description of signal-dependent noise is presented in this article, also.

A comparison of phase-retrieval algorithms was performed by Fienup (1982) and some aspects of these algorithms are used to restore speckled images (Idell, et al. 1987). Cederquist, et al. (1988) used a phase retrieval algorithm for farfield, computer-generated speckle. These algorithms are useful because phase information is lost when spectral processing a recorded image using the power spectral density (PSD). Recovering the phase helps one reconstruct the image uniquely. Bispectral processing retains the phase of an object and it is this idea that makes it a possible technique to perform image reconstruction.

Kuan, et al. (1987), derived an adaptive restoration filter for speckled images. This article also brings up some important points. One key point is the difference between a noisy object and a noisy imaging system. A noisy object occurs when an incident coherent wavefront is scattered by the object such that random interfer-

ences occur among the dephased, but still coherent, reflected waves. This is the speckle case I am investigating. The noisy imaging system results from a randomly variable transmitting medium, such as the atmosphere, and this is the case for stellar speckle. Instead of being object-related, it is medium-related, i.e., a point is individually speckled throughout the image due to system effects. Crimmins (1985) used a geometric filter on speckled images and then compared his results with a 3X3 median filter used on the same images. Safa and Flouzat (1988) used morphological techniques on remotely-sensed speckled SAR images.

All of these previous noise-reduction methods operate on the speckled image in the spatial domain (except for the homomorphic Wiener filter). Recently, Marathay, et al. (1989) used computer-simulated speckle patterns and applied third and fourth order intensity correlations to restore the image. The speckle patterns generated were not imaged but rather found in the pupil plane. Newman and Van Vracken (1989) combine the bispectrum with photon-bias correction techniques (see Northcott, et al, 1988) to recover multiple, shifted objects in a uniform background of photon noise (e.g., Poisson). The signal-to-noise ratio (SNR) of these objects and background noise was less than one! Freeman, et al. (1988), used the bispectrum on one-dimensional (1-D), infrared, astronomical speckle data to recover the phase of a stellar object. Ayers, et al, (1988) compare the triple correlation with the Knox-Thompson phase retrieval technique for astronomical speckle and their results indicate that the triple correlation is more robust for recovering phase than the Knox-Thompson. Again, as a reminder, astronomical speckle is different than the speckle considered in this thesis. Astronomical speckle can also

be termed "incoherent speckle" while the speckle modeled in this thesis is coherent. Mavroidis, et al, (1990) found that the bispectrum could not be used for recovering coherently imaged objects through atmospheric turburlence. This was based on the theory of phase closure and its relation to the bispectrum. What they did not do was perform the homomorphic transformation before they attempted image recovery. As will be shown later, this is a key parameter to successfully reconstruct an image.

The goal of this thesis is to use recently developed algorithms for bispectrum estimation to reconstruct multiple, shifted images degraded by speckle noise. This is a conceptual study to determine if the bispectrum is robust enough to handle the image degradation resulting from speckle. The aim is to implement solutions from an engineer's viewpoint so that practical solutions can be obtained. Therefore, in some cases, a median filter may be applied, after bispectral averaging and the image reconstruction has been implemented, to further smooth the image.

3.0 SPECKLE

To properly model speckled images, I must attempt to review the underlying physics and mathematics behind speckle theory. Since speckle is random, it lends itself quite well to statistical analysis and the literature is very complete regarding this aspect of speckle. By using key concepts from this area, it will be shown that speckle obeys certain constraints that are conducive to computer modeling.

3.1 Electromagnetic Field

The general method I will use to describe the electric field vector of the propagating source is defined by several authors (Gaskill, Haus) and is reviewed here. Obviously any representation of the electric field vector must also obey Maxwell's equations, which in turn leads to the wave equation:

$$\nabla^2 E - \mu \epsilon \frac{\partial^2 E}{\partial t^2} = 0 \qquad (1)$$

where:

E is the electric field intensity vector E(x,y,z;t)

μ is the permeability

ϵ is the dielectric constant

∇^2 is the Laplacian operator: $\frac{\partial^2}{\partial x^2} + \frac{\partial^2}{\partial y^2} + \frac{\partial^2}{\partial z^2}$.

One solution to the wave equation is found by writing the vector E as (with r = (x,y,z) being a vector component):

$$E[\underline{r}; t] = A(\underline{r}) \exp[j2\pi\nu t] \qquad (2)$$

where:

$A(\underline{r})$ is the amplitude function

ν is the mean frequency.

In imaging I am concerned primarily with spatial quantities and not temporal ones. Thus, I can suppress the time dependence in the previous equation. Furthermore, since the electric field is, in general, a complex quantity, I can express it as:

$$A(\underline{r}) = \mathrm{Re}[A(\underline{r})] + j\,\mathrm{Im}[A(\underline{r})] = |A(\underline{r})| \exp[j\phi(\underline{r})] \tag{3}$$

where:

Re denotes the real part of the field

Im denotes the imaginary part of the field

$|A(\underline{r})|$ denotes the magnitude of the field

$\phi(\underline{r})$ denotes a phase function.

Therefore, this is the representation of the complex amplitude of the wave field. I will use this notation throughout the thesis. Another quantity of interest will be the intensity, defined as:

$$I(\underline{r}) = |A(\underline{r})|^2 \tag{4}$$

It is the squared modulus of the complex field. Implicit in the definition of the complex field that is a solution to the wave equation is that it is assumed to be perfectly monochromatic and linearly polarized. Linear polarization is required so that each component can be treated as a separate random walk (Goodman, 1986) and so that each component will be statistically independent. Monochromaticity is

required because if other wavelengths are present then each one can produce its own speckle pattern causing the overall statistics of the speckled image to be precluded by the effect of all the individual statistical distributions for each wavelength. The reflected field remains linearly polarized and monochromatic, though it does undergo a uniformly distributed phase change upon reflection.

3.2 Object Surface Statistics

Once this electromagnetic field strikes the object, it is reflected from this object. The surface is assumed to reflect all of the energy and any loss is due to the destructive interference of the reflected waves. It is at this point that the speckle phenomenon occurs. The derivation for the object field statistics that I will use is the classic random walk (Beckmann & Spizzichino, 1964; Goodman, 1976, 1984, 1985, 1986). This approach requires some assumptions as follows below.

A "rough surface" is a surface which scatters the energy of the incident plane wave into various and random directions upon reflection. The "smoothness" of this surface is dependent upon the relative wavelength-to-surface-roughness relationship. If this relationship is of the order of a wavelength (where a 2π phase excursion can occur that is uniformly distributed), speckle can occur. If the phase is not uniformly distributed then, even with the presence of a large number of scatterers (a central limit requirement [Stark & Woods,1986]), the speckle intensity will not have its required negative exponential distribution. Similarly, a large number of scatterers are required so that Gaussian random variables can be used as the field amplitude model. Shadowing effects (where a portion of the surface "shades" an adjacent scatterer) and multiple scattering from the surface are neglected: only one

reflection of the incident field occurs at the surface before it interferes with an adjacent coherent, reflected wave. The density of the scatterers (number/m^2) is not considered and there is always enough return signal to measure adequately, i.e, unconstrained intensity is assumed so as to preclude Poisson statistics (photocounts). I assume that this surface reflected field (or its analytic representation) can be modeled as a circular, complex, Gaussian random variable whose probability density function is given as:

$$p(A_r, A_i) = \frac{1}{2\pi\sigma^2} \exp\left[\frac{-((A_r)^2 + (A_i)^2)}{2\pi\sigma^2}\right] \tag{5}$$

where:

A_r is the real part of the field, $A(\underline{r})$

A_i is the imaginary part of the field, $A(\underline{r})$

σ is the standard deviation.

This is a complex Gaussian process where both components are independent, identically distributed with zero means and equal variances. By using a probability transformation one can show that (Goodman, 1984) the modulus of this Gaussian field is Rayleigh distributed:

$$p(|A(\underline{r})|) = \frac{|A(\underline{r})|}{\sigma^2} \exp\left[\frac{-|A(\underline{r})|^2}{2\sigma^2}\right] \tag{6}$$

where:

$$|A(\underline{r})| = \sqrt{(A_r)^2 + (A_i)^2}$$

It can be shown that the intensity $I = |A(\underline{r})|^2$ (Goodman, 1984) has a negative exponential probability density function given by:

$$p(I) = \frac{1}{2\sigma^2} \exp\left[\frac{-I}{2\sigma^2}\right] \tag{7}$$

From the previous development, $2\sigma^2 = <|a_k|^2>$, where $< >$ denotes the ensemble average. Notice that the value within the $< >$ is simply the individual phasor intensities. therefore I can rewrite Equation 7 in the more familiar form:

$$p(I) = \frac{1}{<I>} \exp\left[\frac{-I}{<I>}\right] \tag{8}$$

Another parameter is called the contrast of the speckle pattern and is defined as an inverse SNR. For fully-developed speckle. the contrast should equal one (Goodman, 1985: Cederquist. 1988). The contrast is given by:

$$C = \frac{\sigma}{<I>} \tag{9}$$

All of these first-order statistics will be important when I create computer-generated speckle because they will be used to verify that the speckle patterns are actually "speckled."

3.3 Propagation And Imaging Of The Speckle Field

Since I am dealing with images. their representation must of necessity be real and non-negative because image intensity (or its field modulus) can never be less than zero. Second-order statistics will help in describing the image formation process in

this case because these statistics define the spatial structure of the field (Dainty, 1976). I have reviewed several cases and will relate key results here. Goldfischer (1965) derived the autocorrelation (ATC) and the PSD for a uniform diffuse object viewed in the farfield at the pupil plane, thus not imaged. The farfield is that region a distance z from the object that satifisfies the constraints of $z >> \frac{\pi L^2}{\lambda}$ (Gaskill), where L is the size of the aperture and λ is the wavelength of the incident radiation.

The farfield, or Fraunhofer, diffraction pattern intensity is proportional to the complex ATC of the object and is thus a measure of the spatial frequency spectrum of the power. In other words, the ATC and the PSD are Fourier transform pairs (Yariv). Goldfischer's model used a uniform, and hence a statistically stationary object. Since images are, in general, non-stationary, it will be shown that his results are a special case of the more usual case of non-uniformity. Enloe (1967) later extended these results to an imaged, uniform object.

There exists a Fourier transform relationship between the speckle field and its farfield propagation, given by (Enloe):

$$A_1(\zeta,\eta) = \int_{-\infty}^{\infty}\int A_0(x,y)\exp\left[\frac{-j2\pi}{z\lambda}(x\zeta + y\eta)\right] dx\ dy \qquad (10)$$

where:

$A_0(x,y)$ is the object speckle field

$A_1(\zeta,\eta)$ is the farfield distribution.

At the farfield an aperture is located at the pupil plane. This aperture could be a pupil stop some distance from a lens or the lens itself. The lens then focuses this coherent radiation onto a detector located at the image plane. The resultant field at the image plane is given by:

$$A_2(\nu,\omega) = \int_{-\infty}^{\infty}\int H(\zeta,\eta)A_1(\xi,\eta)\exp\left[\frac{-j2\pi}{\lambda f}(\nu\zeta + \omega\eta)\right]d\zeta\ d\eta \qquad (11)$$

where:

$H(\zeta,\eta)$ is the System Transfer Function (Fourier transform of pupil function)

f is the focal length of the lens

ν,ω merely denote a different coordinate system from that of the object.

The lens acts as a Fourier transformer (Goodman, 1968). Thus the field at the image plane is the Fourier transform of the field in front of the lens, modified by the aperture. The intensity at the image plane is found from Equation 11 times its complex conjugate (denoted by *) by:

$$I(\nu,\omega) = A_2(\nu,\omega)(A_2(\nu,\omega))^* \qquad (12)$$

Notice that the intensity at the image plane is nothing more than the autocorrelation of the object convolved with the imaging system.

3.4 Nonstationary, Second-Order Image Statistics

The previous development was for stationary objects. Lowenthal and Arsenault (1970) studied the case of an imaged, nonstationary object being speckled. Their development is important because several important relationships regarding the

object structure and the second order statistics of the speckle field arise. To begin with, the object f(r) is composed of two components: t(r) is the actual object function that acts to modulate the rough surface, which is denoted by d(r). This non-uniform object is represented by (neglecting the vector representation for r for notational simplicity):

$$f(r) = t(r)d(r) \tag{13}$$

The image plane field, g(r), is related to the object field via the convolution operator (*) with the system impulse response, h(r):

$$g(r) = f(r)*h(r) \tag{14}$$

Relating d(r) to the statistics discussed previously, d(r) is stationary and a circular, complex Gaussian random variable with independent real and imaginary parts having zero means and equal variances. The function can also be thought of as wideband, random noise (Lim and Nawab, 1981). An important point here is that, even though the object is non-stationary, its noise function is stationary and thus for all cases of t(r), we can find the parameters of g(r). Referring to Equation14, I can express the mean of the image as (h(r) is the same function throughout the ensemble):

$$< g(r) > = < f(r) > * h(r) \tag{15}$$

Since $< d(r) > = 0$, then $< f(r) > = < t(r) > < d(r) > = 0$, and therefore $< g(r) > = 0$. The variance of the amplitude(or field) is given for real, non-negative images as (from the standard relationship $\sigma^2 = < x^2 > - < x >^2$ (Friedan):

$$(\sigma_g(r))^2 = < |g(r)|^2 > - |< g(r) >|^2 \tag{16}$$

Since the image mean is zero and the magnitude squared of the amplitude equals the intensity, I can rewrite the variance of the image amplitude as:

$$(\sigma_g(r))^2 = <I(r)> \tag{17}$$

This interesting result says that the variance of the image amplitude is equal to the mean of the image intensity. For the variance of the intensity I can write:

$$(\sigma_I(r))^2 = <I(r)^2> - <I(r)>^2 \tag{18}$$

The definition of a statistical ATC function is given by Goodman(1985) for the intensity (since intensity is real) as:

$$R_{II}(r_1, r_2) = <I(r_1)I(r_2)> \tag{19}$$

This function allows us to compare the intensities at r_1 and r_2 over the ensemble. By letting $r_1 = r_2 = r$, can rewrite Equation 18 as:

$$(\sigma_\Pi(r))^2 = R_\Pi(r,r) - <I(r)>^2 \tag{20}$$

It can be shown (Goodman, 1985) that another way to write Equation 19, with $r_1 = r_2 = r$, is given by:

$$R_\Pi(r,r) = <I(r)><I(r)> + |R_{gg}(r,r)|^2 \tag{21}$$

where $R_{gg}(r,r)$ is the ATC of the image amplitude and, from the relationship between Equation 12 and Equation 19, is equal to $<g(r)(g(r))^*>$ (since amplitude can be complex, in general). For t(r) and h(r), though, this will always be a real

function, so I can write $R_{gg}(r,r) = \langle |g(r)|^2 \rangle = \langle I(r) \rangle$. Equation 21 can be written as:

$$R_{\Pi}(r,r) = \langle I(r) \rangle^2 + \langle I(r) \rangle^2 = 2\langle I(r) \rangle^2 \qquad (22)$$

Using this result in Equation 20 gives $(\sigma_{\Pi}(r))^2 = \langle I(r) \rangle^2$, which, upon taking the square root of both sides and dividing by the ensemble averaged intensity, gives us the same result as Equation 9 for the contrast. So the rms of the intensity equals the mean intensity even for non-stationary objects. The difference here is that, in general, the variance is not a constant but is a result of the ensemble average and the image coordinates. Consider the mean intensity of the image given as, by definition, $\langle I(r) \rangle = \langle g(r)\, g(r)^* \rangle$. However, as shown above, this is nothing more than the ATC of g(r), given as $\langle I(r) \rangle = R_{gg}(r,r)$

Another important property is the ATC of the image. Returning to my original notation, where d(r) is assumed stationary, its ATC can be written as $R_{dd}(r_1, r_2) = R_{dd}(r_1 - r_2) = \delta(r_1 - r_2)$ since I assume the ATC peak to be very narrow for the wideband noise (δ represents the Dirac delta function). The ATC of the speckled object f(r) then becomes:

$$R_{ff}(r_1, r_2) = \langle t(r_1)\, d(r_1)\, t^*(r_2)\, d^*(r_2) \rangle$$

$$R_{ff}(r_1, r_2) = \langle t(r_1)\, t(r_2)^* \rangle R_{dd}(r_1, r_2) \qquad (23)$$

$$R_{ff}(r_1, r_2) = t(r_1)\, t(r_2)^*\, \delta(r_1 - r_2)$$

Note that $R_{ff}(r_1, r_2)$ is still a function of r_1 and r_2 and not just $r_1 - r_2$, even though d(r) is stationary, since I have retained the nonstationarity of t(r). So the image amplitude ATC can be expressed in integral form as:

$$R_{gg}(r_1, r_2) = \int_{\Pi_0} |t(r_0)|^2 h(r_1 - r_0) h(r_2 - r_0)^* dr_0 \tag{24}$$

where the integration is over the object plane Π_0 and a linear filter operation is assumed with the impulse response h(r). Again letting $r_1 = r_2 = r$, and using the relation from a previous paragraph of $< I(r) > = R_{gg}(r,r)$ in the expression above (Equation 24) I can write (* denotes convolution):

$$< I(r) > = |t(r)|^2 * |h(r)|^2 \tag{25}$$

From Goodman (1968) this equation is of the form of the transfer function for a system illuminated by incoherent light (where $|t(r)|^2$ is the source intensity and h(r) is the system impulse response).

Thus, the transfer function that determines the mean intensity in the image is the incoherent transfer function of the system, even for an optical system illuminated by a coherent diffuse object field! One can see from Equation 25 that the PSD of a speckle pattern has the shape of the ATC of the squared modulus of the pupil function (Goodman,1985).

Labeyrie and Dainty (1973) use the principle of Equation 25 to analyze atmospheric speckle. I mention this because it relates a practical application of this expression. By measuring the image intensities and summing their individual Fourier

transforms from each realization, and then dividing this result by the time-averaged modulus of each transfer function, the Fourier magnitude of the object's intensity can be reconstructed.

Miller, et al, (1975) use a more rigorous approach to come to the same conclusions as given above. They find that the intensity is, in general, a nonstationary random process so the ATC must be a function of two variables. They make the point that these second-order results are good for both Fresnel (so-called near field) and Fraunhofer diffraction but that the usual ATC/PSD Fourier relationship does not necessarily hold. For nonstationary images, the PSD of the intensity is given as:

$$S_I(\zeta) = < \left| \int_{-\infty}^{\infty} I(r) \exp\left[-j2\pi\zeta r\right] dr \right|^2 > \qquad (26)$$

where $S_I(\zeta)$, the PSD, is the average value of the modulus squared Fourier-transformed image intensity and ζ is a spatial frequency vector.

This relationship was extended by April and Lowenthal (1984). They showed that Equation 26 is really only one of two parts of the PSD of the image intensity. The complete PSD is given as $S_I(\zeta) = S_I(\zeta)_1 + S_I(\zeta)_2$ (eq. 26 is $S_I(\zeta)_1$). This is derived simply by taking the PSD of Equation 21. The first term is the object and the second term is the speckle noise. $S_I(\zeta)_2$ is written as:

$$S_I(\zeta)_2 = \int_{-\infty}^{\infty}\int \left| < g(r_1) g^*(r_2) > \right|^2 \exp\left[-j2\pi\zeta(r_1 - r_2)\right] dr_1 \, dr_2 \qquad (27)$$

The key point in all of this is that the noise spatial frequencies are across the same frequency region as the incoherent transfer function relationship given by Equation 26. This was proven by April and Lowenthal experimentally. Using the speckled image of a Ronchi ruling, they showed that it is the incoherent cutoff frequency (which is twice the coherent cutoff frequency (Goodman (1968) and Gaskill)) that determines the distribution of the spatial frequencies present in the diffuse coherent light. Note that all indication of the object's presence is still lost in a speckled image if the incoherent cutoff frequency is less than the fundamental frequency of the Ronchi ruling. Kozma and Christensen (1976) also experimentally verified that the aperture of a coherently illuminated system must be twice as large as an equivalent incoherently illuminated system to achieve the same resolution for each. They compared bar targets of varying spatial frequencies illuminated by both incoherent and coherent sources.

To summarize all of these points, it was shown that, even using nonstationary statistics, the rms intensity still equals the mean intensity and so, for fully developed speckle, the contrast is one. Also, nonstationary statistics do not change the fact that the rough surface is a complex Gaussian random variable leading to a negative exponential distribution in intensity. Finally, the signal was shown to be the object intensity attenuated by the incoherent transfer function of the system. Therefore, information transmission with coherent diffuse illumination is dependent on the incoherent bandwidth of the optical system.

3.5 Multiplicative Noise Model

These results are the basis for the noise model used by most researchers (Kuan, et al, 1987; April and Arsenault, 1976, 1984, 1986; Guenther, et al, 1978; Jain and Christensen, 1980). They describe speckle noise as multiplicative in the sense that the speckled object's intensity is a product of the incoherent signal and a noise function.

Therefore, the amount of speckle noise is proportional to the image. The signal-dependent nature of speckle is due to the fact that the rms amplitude of the speckle noise is proportional to the image. This model is described by (Tur. et al, 1982) as:

$$I_s(r) = \alpha I_o(r) I_N(r) \tag{28}$$

where:

$I_S(r)$ is the speckled intensity

$I_o(r)$ is the incoherent image intensity of $t(r)$

$I_N(r)$ is the speckle noise intensity of $d(r)$

α is a proportionality constant dependent upon the system parameters.

The above model breaks down if the object has details beyond the resolution capabilities of the coherent optical system used to image the object. In other words, if the bandwidth of the image is greater than the bandwidth of the optical system, the multiplicative model will not be applicable. Lim and Nawab (1981) ensure this condition will not occur by sampling the speckled image coarsely enough so that all points in the degraded image will be considered independent. The sampling distance must be larger than the correlation length of the speckles at neighboring pixels to ensure a spatially uncorrelated random field in the image (Sadjadi, 1990).

This is the case for most speckle computer models. In this thesis, I will assume that my coherent system can resolve all of the details of the object surface, t(r).

3.6 Speckle Computer Models

Having resolved that a speckled image is a signal-dependent, multiplicative noise process, I now turn to how I want to model this on the computer. There are several methods I can choose to do this. Before I describe them, I will review speckle.

A speckled object results when a coherent, electromagnetic wave reflects from a rough surface which contains a very large number of scatterers. This rough surface varies randomly and uniformly at depths on the order of a wavelength of the incident radiation. The reflected, dephased, yet still coherent wave interferes with itself and speckle is detected. The object structure modulates the speckle and surface roughness greater than one wavelength of the incident radiation produces no greater amount of speckle. Once the surface roughness exceeds the coherence length of the source, though, speckle will cease since it no longer has the modulo 2π (or integer multiples thereof) phase shift. The speckles "wash out" due to the loss of coherence of the source. This is the idea behind speckle reduction techniques that are performed physically.

The negative exponential probability distribution of speckle intensity has been experimentally verified (Dainty, 1976). This probability density function (pdf) can result from a circular, complex Gaussian random variable with the real and imaginary components having zero means and equal variances (Goodman, 1985). The

standard deviation and the mean of the intensity are equal for fully developed speckle, giving a contrast (C) ratio (an inverse SNR) of one.

The most direct way to model this is given by Guenther, et al, (1978). The speckle field can be described as (using m,n as pixel locations):

$$a(m,n) = a_R(m,n) + j\, a_I(m,n) \tag{29}$$

where $a_R(m.n)$ and $a_I(m.n)$ are zero mean. Gaussian random variables for the real and imaginary components, respectively, with variances of $\sigma_a^2 = E\{a_R^2(m.n)\} = E\{a_I^2(m.n)\}$. The speckle intensity becomes:

$$g(m.n) = a_R^2(m.n) + a_I^2(m,n) = |a(m.n)|^2 \tag{30}$$

To model digital speckle, I first generate, for each pixel, a pseudo-random pair of Gaussian random variables of zero mean and equal variances based on the field strength (square root of the intensity) of the object at each pixel. The Gaussian random variables of zero mean and unity variance are created by a routine from Forsythe. Figure 1 is a typical histogram of the Gaussian random variable I have created for a given seed (7654321). I then take the complex absolute value squared of this quantity to obtain the speckle intensity. Different realizations are provided by using different starting random seeds for each new image. The optical system is ignored in this approach and completely uncorrelated speckle is produced. I call this technique the Direct Digital Model (DDM). Its flowchart is shown in Figure 2.

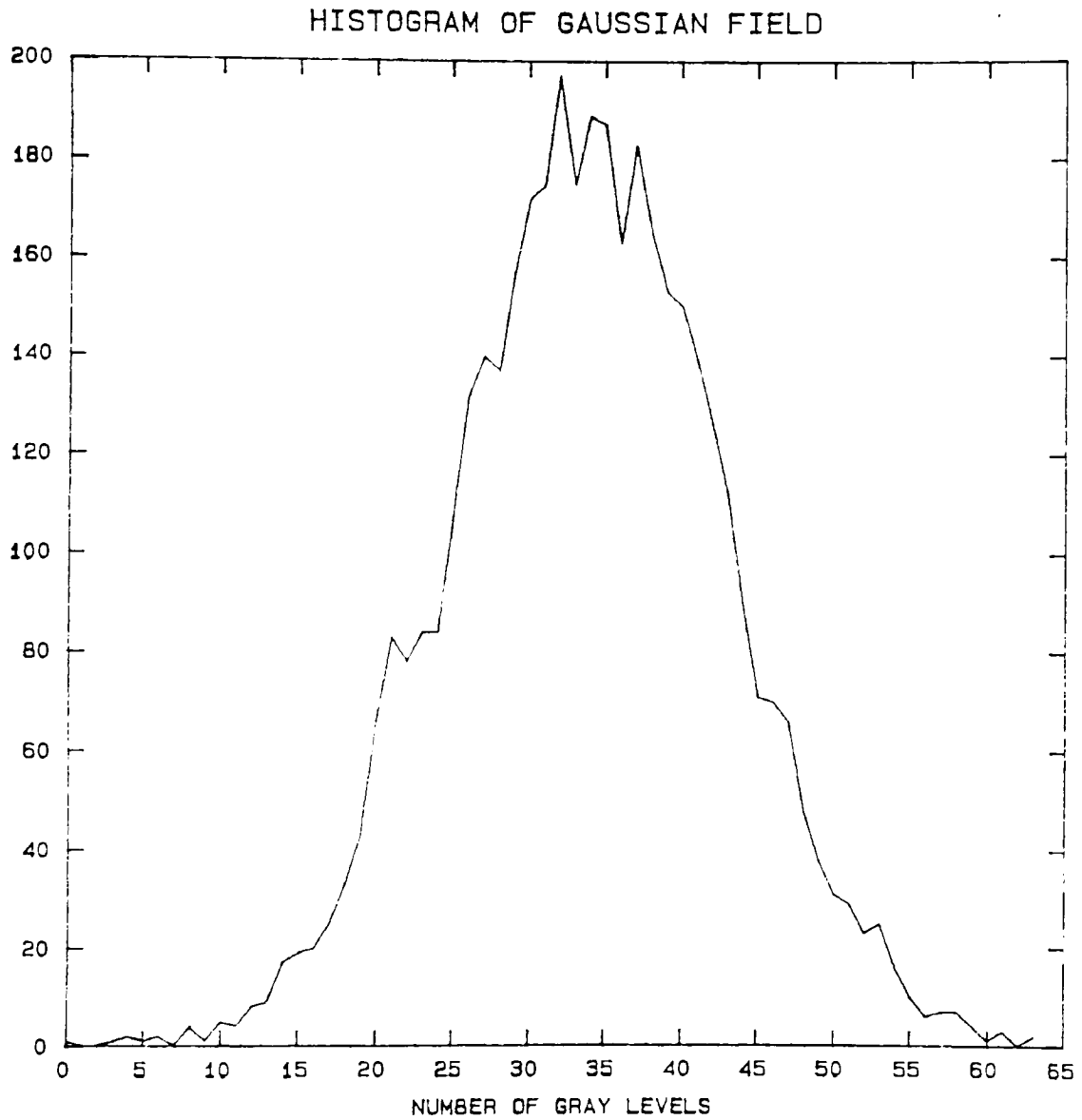

Figure 1. Typical Histogram of a Gaussian Random Number Function Generated by Forsythe Routine

DIRECT DIGITAL MODEL

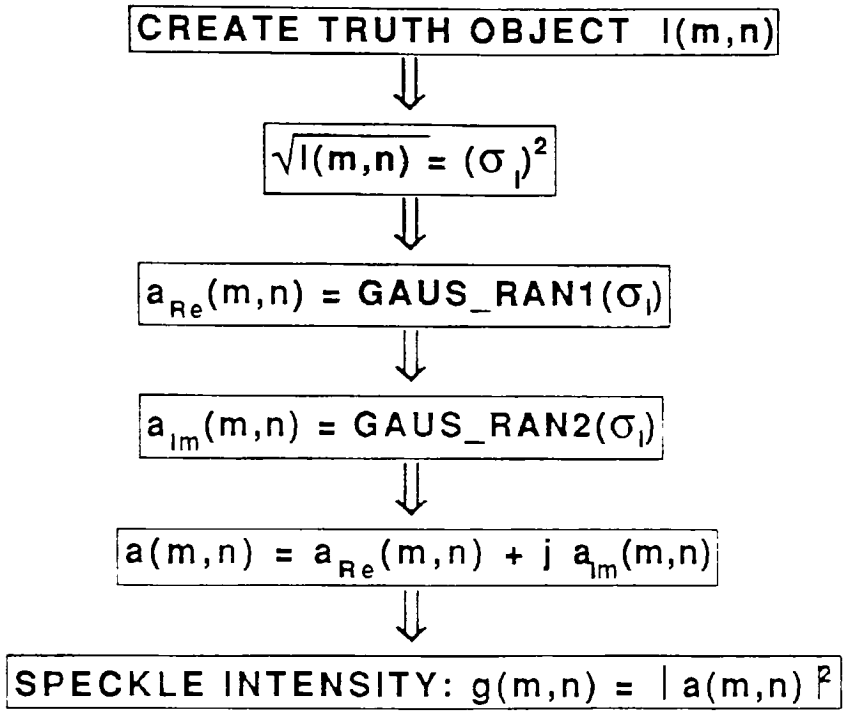

Signal dependency occurs because the rms of the field is proportional to the input signal.

The function, a(m,n), is a circular, complex, Gaussian random variable with zero mean real and imaginary components having independent, identically distributed variances.

Figure 2. Flow Diagram for Direct Digital Model

This result can be extended to include the optical system by propagating the speckle **field** to the farfield and multiplying this by the coherent transfer function of the aperture. Inverse Fourier transforming this function (focusing through a lens) and then taking the magnitude squared (square law detector) gives a speckled object that includes the coherent point spread function (psf) of the optical system (Enloe, 1967; Goodman, 1968). I call this technique the Transfer Function Model (TFM). Its flowchart is seen in Figure 3.

A technique used by Marathay, et al, (1989) and Voelz, et al, (1988) is to create a random, uniform phase of modulo 2π and then, using Euler's relationship $\exp[j\theta] = \cos\theta + j\sin\theta$, multiply the phase by the object field at each pixel location. From Friedan, this phase is given by:

$$f(m,n) = \pi\ (2R-1) \tag{31}$$

where $0 \leq R \leq 1$ is a uniformly distributed, pseudo-random number produced by a random number generator. The key here is that the phase is statistically independent of the original object. I call this technique the Random Phase Model (RPM). See Figure 4 for its flowchart.

TRANSFER FUNCTION MODEL

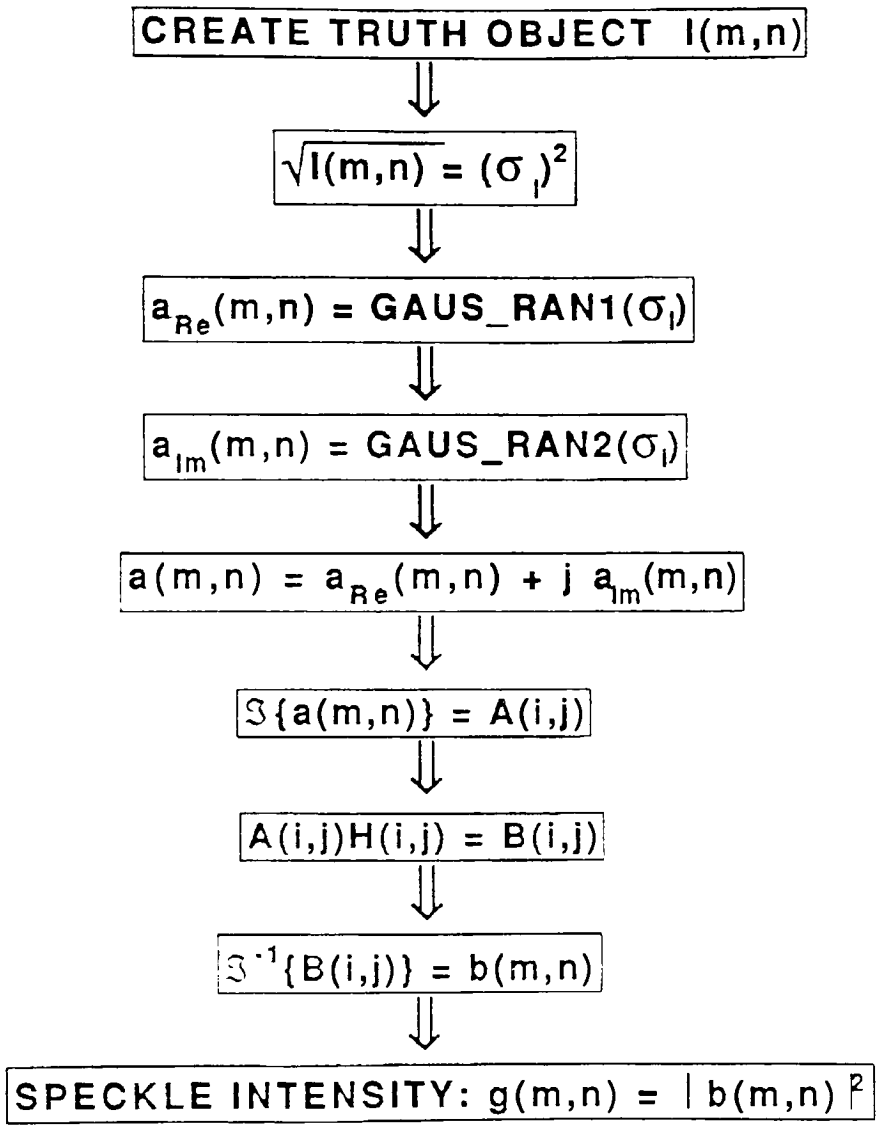

H(i,j) is the coherent transfer function of the optical system

Figure 3. Flow Diagram for Transfer Function Model

RANDOM PHASE MODEL

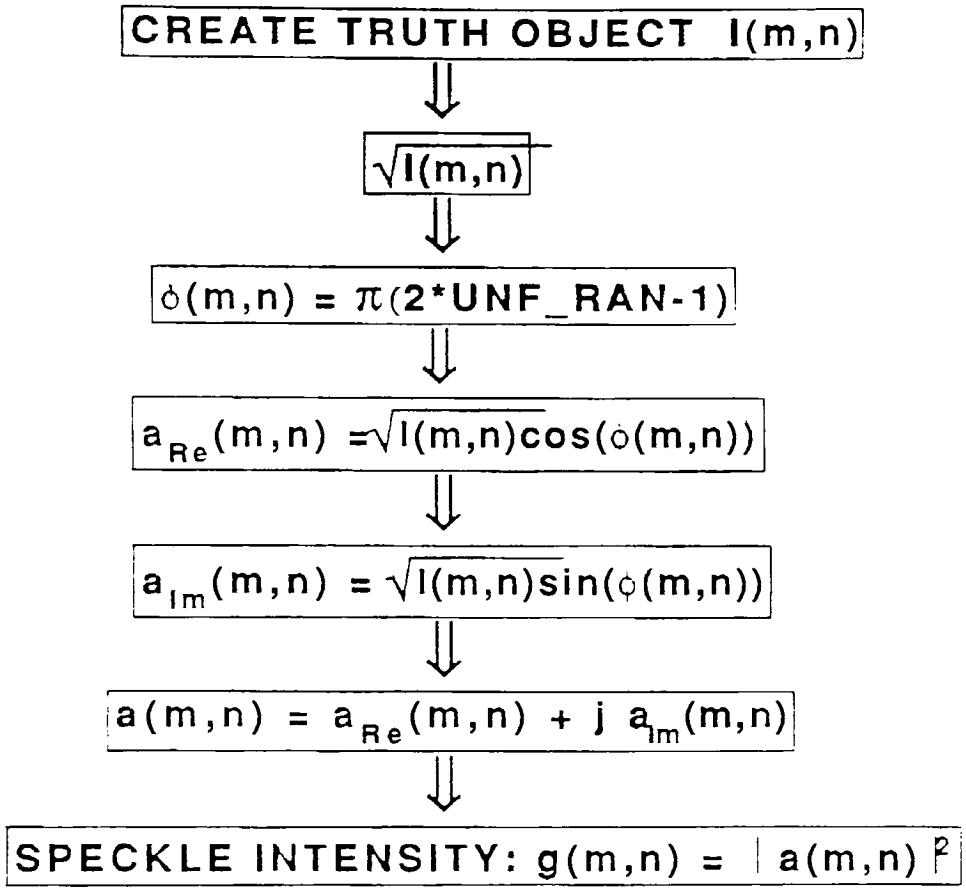

The phase is statistically independent of the original object and is modulo 2π ($-\pi \leq \phi \leq \pi$)

Figure 4. Flow Diagram for Random Phase Model

Another way to obtain g(m,n) above is given by Kuan, et al, (1987). They describe the complex quantity b(m,n) as:

$$b(m,n) = \sum_i \sum_k h(m-i, n-k)\sqrt{f(i,k)}\, \exp[j\theta(i,k)] \qquad (32)$$

where h(i.k) is the coherent psf of the system for pixels i,k. Kuan terms Equation 32 as the single phase speckle model. He extends this model to what he calls the multiple phase model by rewriting Equation 32 as:

$$b(m,n) = \sum_i \sum_k h(m-i, n-k)\sqrt{f(i,k)}\quad a(i,k) \qquad (33)$$

where a(i.k) is a circular, complex, Gaussian random variable. Kuan prefers this latter model because it reduces the sampling rate to that which accurately reflects the speckle statistics and "abstracts the dependence of the speckle model on the object surface." I have modeled this by creating a(i,k) as discussed for the DDM, multiplying this by the object field and then convolving this quantity with h(i.k) in the spatial domain. Thus, h(i.k) is a 3X3 spatial window of equal strengths (1'9) that moves across the image correlating the object from pixel-to-pixel (see Gonzalez and Wintz). Adjacent pixels are no longer uncorrelated. Notice that the TFM uses a coherent transfer function that operates in the frequency domain upon the **entire** image simultaneously. Its correlation is much weaker than this technique. The magnitude squared of this quantity gives the speckled object intensity. I call this model the Correlated Window Model (CWM). Figure 5 shows the CWM flowchart.

CORRELATED WINDOW MODEL

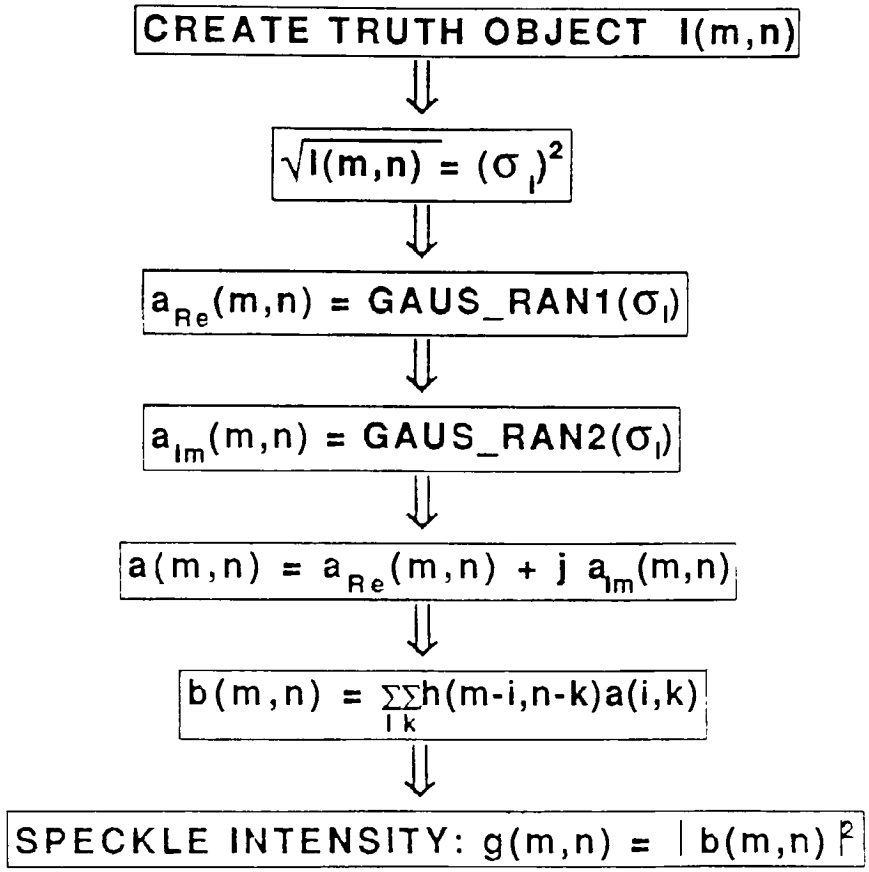

The function, h(i,k) is a 3X3 spatial window of equal strengths (1/9).

Figure 5. Flow Diagram for Correlated Window Model

The CWM is probably the most physically accurate of the speckle models since the assumption of the existence of totally independent scatterers on the diffuser, d(r), is not realistic for high quality optical systems (Fujii, et al, 1976). These systems tend to correlate the scattering spots because they are so smooth across the surface. Most researchers ignore this model because it severely complicates the statistical nature of the resultant image thus complicating any statistical filters used to reduce the speckle noise. As Kuan shows in his paper, the reconstructed image is more blurred than the original, and I found that to be the case in this paper, also.

As proven in earlier sections, a speckled object has the following relationship (in Kuan's notation):

$$g(m,n) = I(m,n)\,u(m,n) \tag{34}$$

where u(m,n) is a signal independent, white noise process with a negative exponential pdf and I(m,n) is the incoherent image of the original image. This leads to another method of generating speckle images that are "correct" statistically. First create u(m,n), a function that has an intensity that obeys a negative exponential pdf with unity mean and unity variance. Then multiply this by the original object thereby creating a signal-dependent, multiplicative noise process with the requisite negative exponential pdf. I call this model the Negative Exponential Model (NEM). The NEM flowchart is seen in Figure 6.

NEGATIVE EXPONENTIAL PDF MODEL

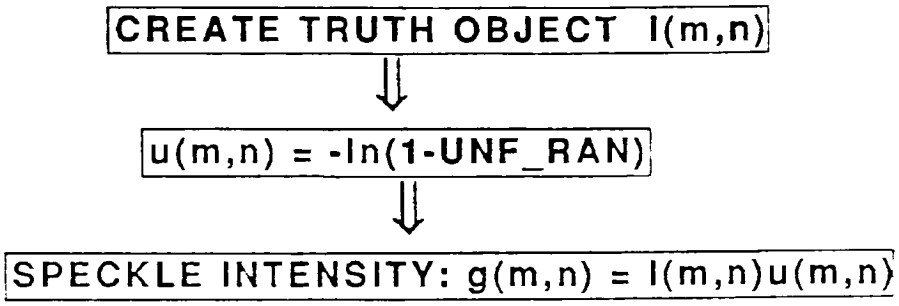

The function, u(m,n), is found from the probability transformation of a uniform pdf to a negative exponential pdf.

Figure 6. Flow Diagram for Negative Exponential pdf Model

The value of u(m,n) can be found from the following equation (see Friedan

$$u(m,n) = -\ln(1 - R) \qquad (35)$$

where R has the same meaning as in Equation 31 and ln is the natural logarithm.

Similar to the development of the NEM is the following technique. Arsenault and April (1976) showed that the natural logarithm of a speckled object has an approximately Gaussian pdf and is additive. To take advantage of this property, I create a Gaussian random variable, a(m,n), as above and add it to the natural logarithm of the original object, I(m,n). I then exponentiate this sum to obtain the speckle intensity. To see this:

$$p(m,n) = \ln(I(m,n)) + a(m,n) \tag{36}$$

by exponentiation:

$$g(m,n) = \exp\left[p(m,n)\right] \tag{37}$$

I call this model the Additive Gaussian Model(AGM) and its flowchart is seen in Figure 7a. Figure 7b is the histogram of the function, a(m,n), used to create this speckle. These last two methods are statistically correct but they may be difficult to model physically.

All six of these speckle models are imaged, i.e., the speckled object exists in the image plane and not the pupil, or Fourier plane. Several authors (Marathay, et al. 1989; Voelz, et al. 1988; Idell, et al, 1987) model this latter speckle condition but it is not considered in this thesis. Welford (1976) reviews the difference between imaged and non-imaged speckle statistics and states that similar statistics will result as long as the phase excursion is large, the number of effective scatterers is large, and the imaging system is not telecentric (i.e., the optical path length from object plane to image plane is the same along all principal rays). All optical systems considered in this thesis are aberration-free.

ADDITIVE GAUSSIAN MODEL

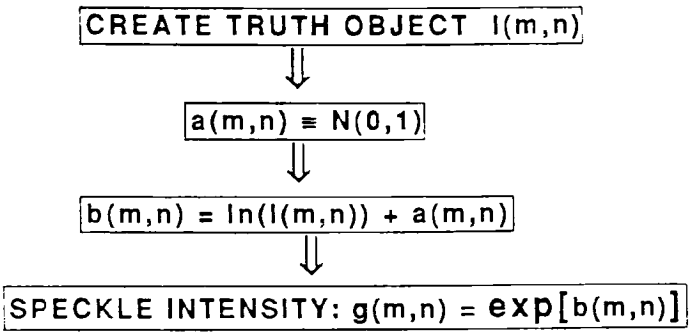

Forces the logarithm of the speckle intensity to have a Gaussian noise pdf.

Figure 7a. Flow Diagram of Additive Gaussian Model

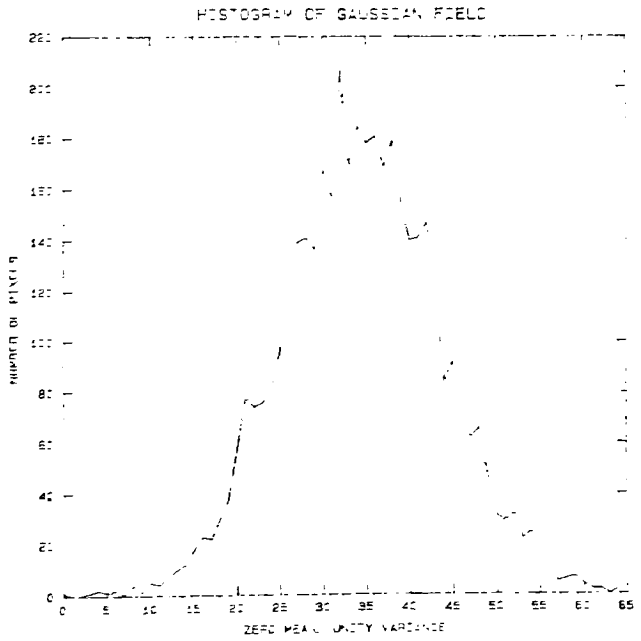

Figure 7b. Histogram of Zero Mean, Unitary Variance Gaussian Function

Dainty (1980) lists several other types of speckle that are seen but these cases have different statistics than the modeled versions in this thesis and are merely listed here:

1. *Non-circular Gaussian speckle* - the phase is not uniformly distributed from $-\pi$ to π but the number of scatterers (N) is still large.

2. *Small -N speckle* - the number of scatterers are small and thus non-Gaussian statistics result.

3. *White light speckle* - spatially coherent yet partially temporally coherent radiation is used for illumination.

4. *Spatially partially coherent speckle* - similar to stellar speckle where atmospheric turbulence provides the "speckled" appearance.

5. *Depolarized speckle* - the object depolarizes the incident radiation upon reflection.

The next section will review the checks necessary to verify the speckle models and give examples of each.

3.7 Speckle Verification

There are four key ways to ensure an image is "correctly" speckled, i.e., it meets the proper first order statistics that define speckle noise. These four checks for fully developed speckled objects are that its:

1. Field modulus histogram has a Rayleigh pdf.
2. Intensity histogram has a negative exponential pdf.
3. Natural logarithm of the speckle intensity has an approximately Gaussian pdf. i.e., exp[-g-exp(-g)] pdf seen in Figure 8.
4. Contrast ratio is approximately one.

Checks one through three are shown in the following figures. Check four can be found one of two ways. If my image fills the entire array I can compute the global mean and global variance to obtain the global contrast. If not, I have to obtain these values locally by, for the mean:

$$\mu(m,n) = \frac{1}{9} \sum_{i=-1}^{1} \sum_{j=-1}^{1} g(m+i, n+j) \tag{38}$$

for the standard deviation:

$$\sigma(m,n) = \sqrt{\frac{1}{9}\left[\sum_{i=-1}^{1} \sum_{j=-1}^{1} (g(m+i, n+j))^2 - \frac{1}{9}\mu(m,n)^2\right]} \tag{39}$$

for the speckle contrast (Crimmins, 1985):

$$C = \frac{1}{(N-2)^2} \sum_{m=2}^{N-1} \sum_{n=2}^{N-1} \frac{\sigma(m,n)}{\mu(m,n)} \tag{40}$$

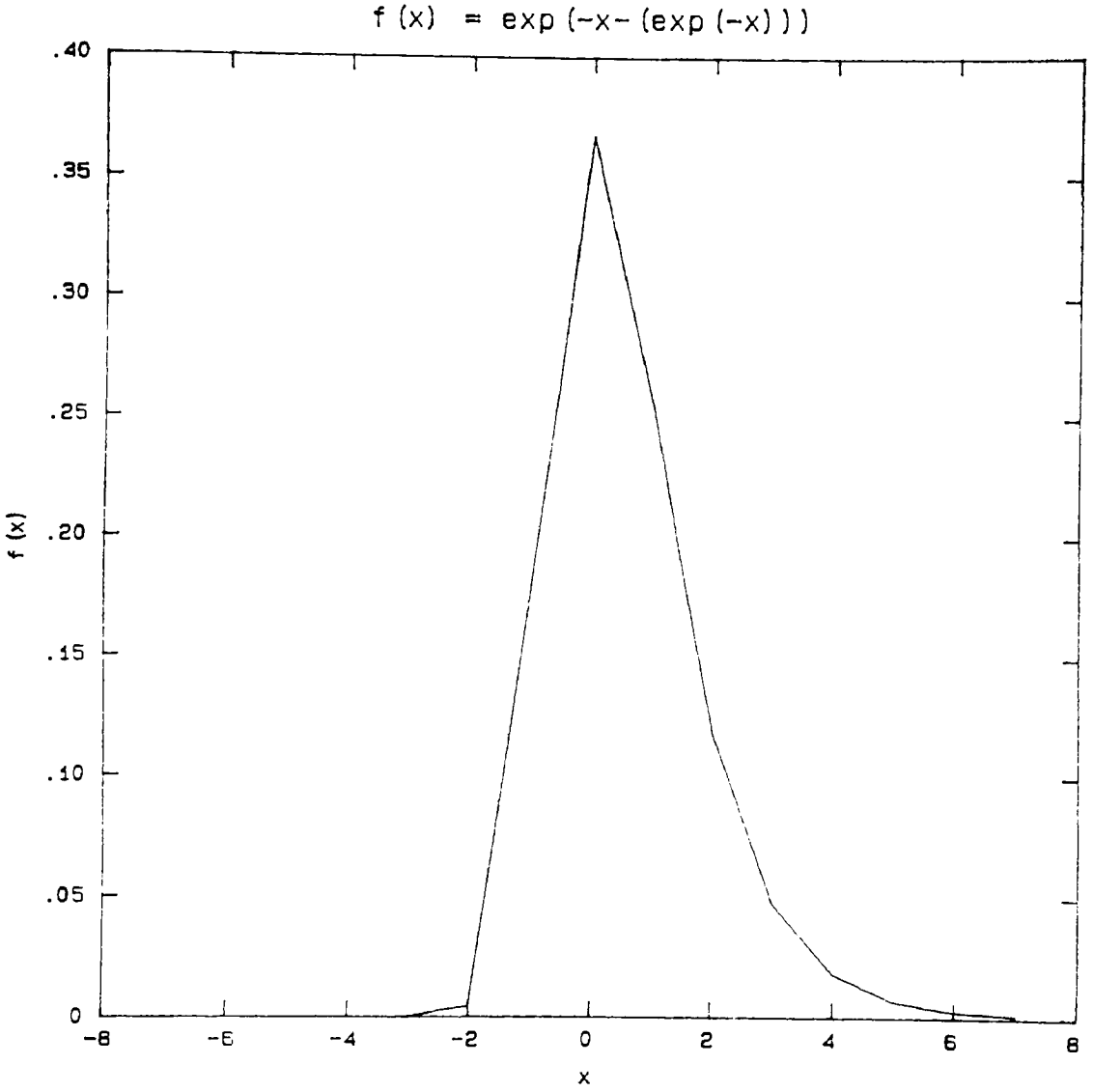

Figure 8. Plot of exp(-x-(exp(-x))) Function

I compute these values for each speckled image. To compare each of these modeling techniques I use the same truth object. For pure speckle statistics, I use a uniform "wall" as an object that is the same size as the array (64X64) and has an uniform pixel intensity value of one. For a constrained object I use a $sinc^2$ (x/16,y/16) in a 64X64 array (see Figures 9a and 9b). Several different plots will be shown for each method, depending on the parameters I want to use to describe the statistics of that particular method. An explanation will accompany each plot. The same starting random number seed was given for all models (seed=7654321).

Figures 10a through 10e demonstrate the DDM. Figures 10a–d show the speckle statistics for a uniform "wall." The contrast is 0.9942375 and the skewness of the logarithm of the intensity is 1.2944. Notice that the histograms match the exact statistical criteria that represent their given phenomenon (intensity, field, log(intensity)). The speckle phase is a white noise process. Figure 10e is an example of a $sinc^2$(r/16) speckled via the DDM. Its imaged contrast is 0.9873512.

Figures 11a through 11f demonstrate the CWM. Figure 11a is a depiction of a speckle pattern seen due to a uniform "wall." Its contrast is 1.0278078. Notice that there is no difference between the statistical histograms or the phase of this method and that of the DDM. That is because this technique is similar to the DDM except for the 3X3 spatial correlating window. The correlating makes the logarithm of the speckle intensity slightly more symmetrical than the DDM (skewness=1.2122, so closer to zero than the DDM for the same implementation) indicating the localized Gaussian psf's are playing a small role.

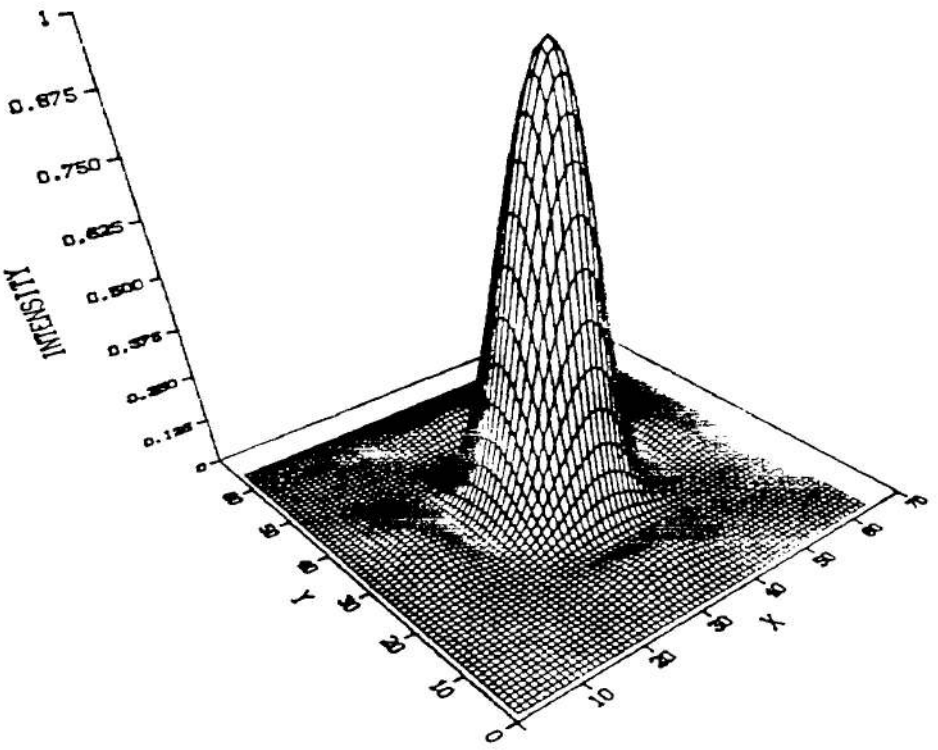

Figure 9a. Three-dimensional Plot of $Sinc^2(X/16,Y/16)$Truth Object

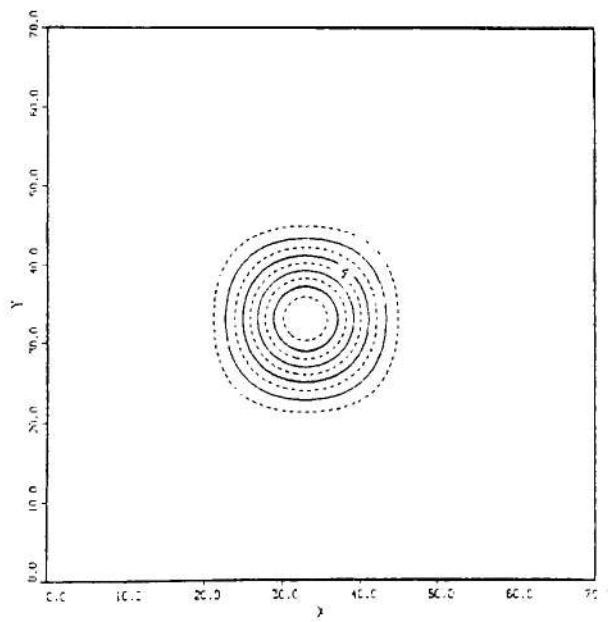

Figure 9b. Two-dimensional Contour Plot of Truth Object

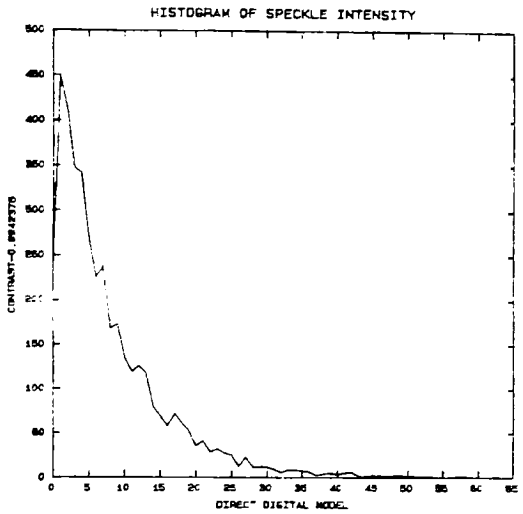

(a)

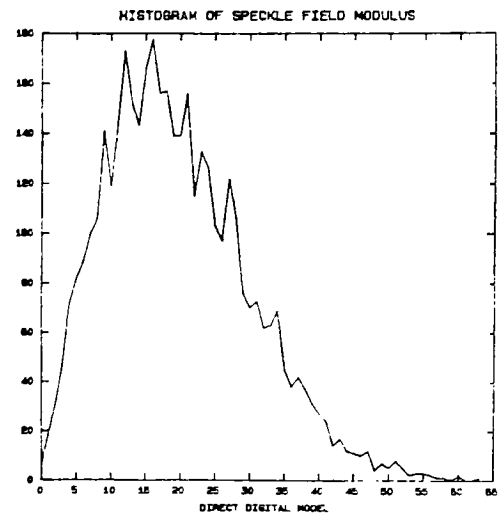

(b)

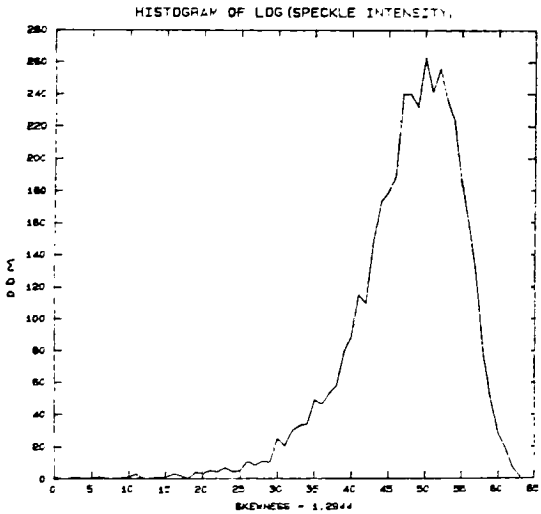

(c)

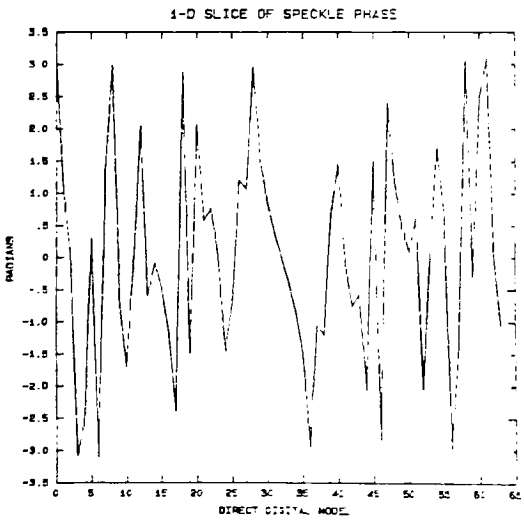

(d)

Figure 10a-d. Statistical Histograms and Phase for Direct Digital Model

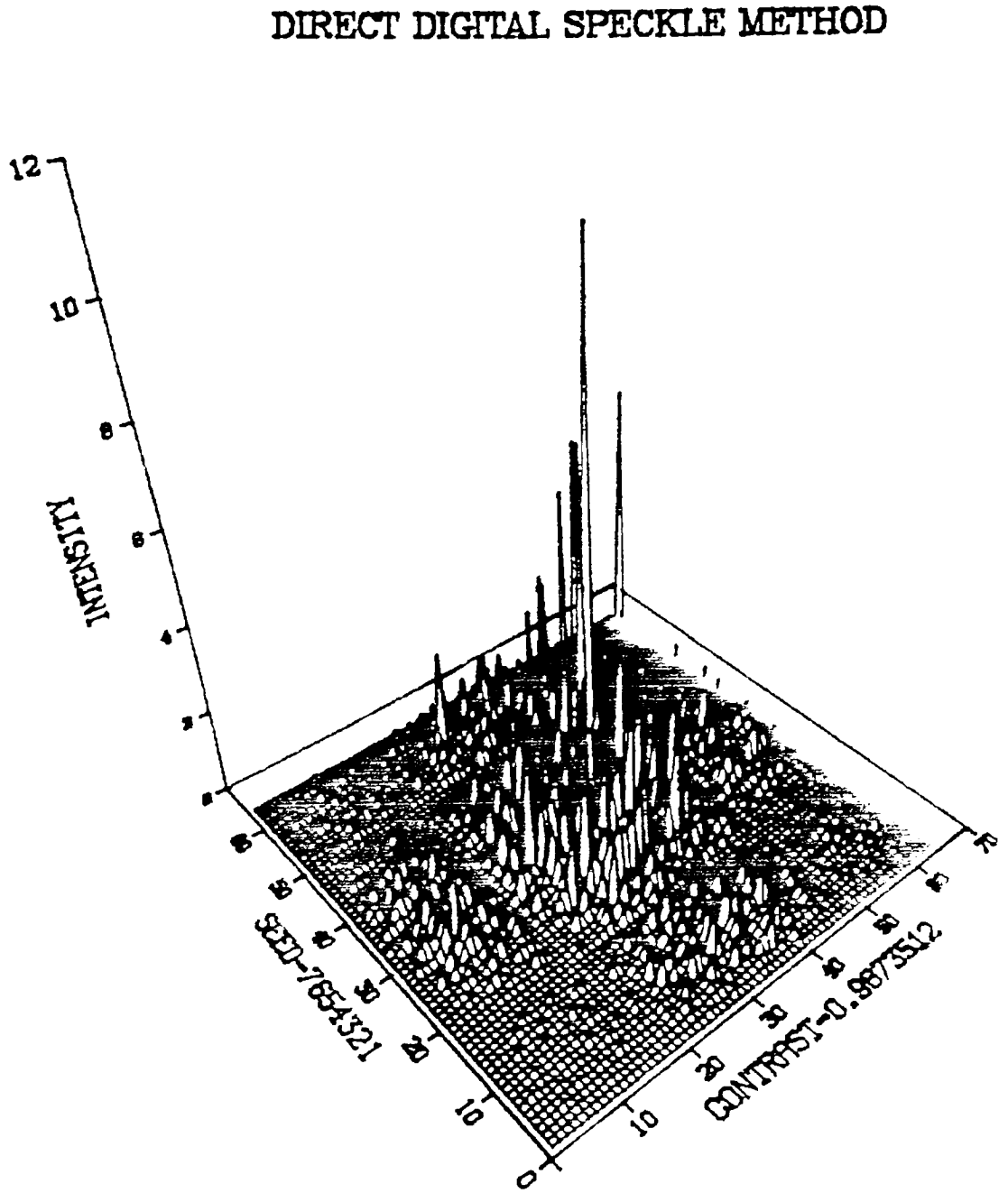

Figure 10e. Truth Object Speckled Using the DDM

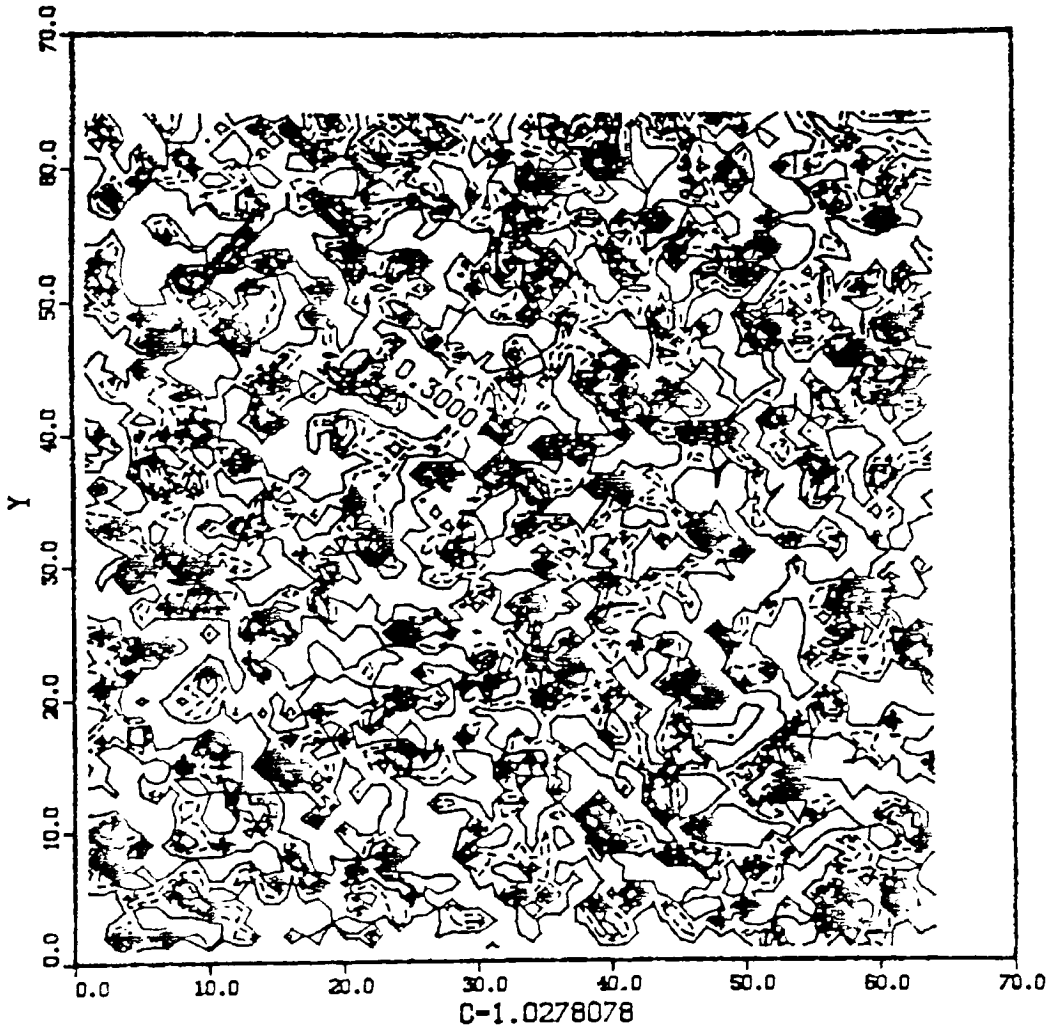

Figure 11a. A Uniform "Wall" Speckled Via the CWM

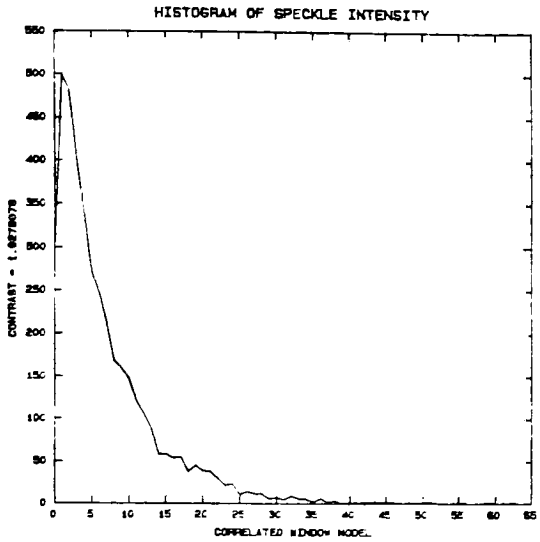

(b)

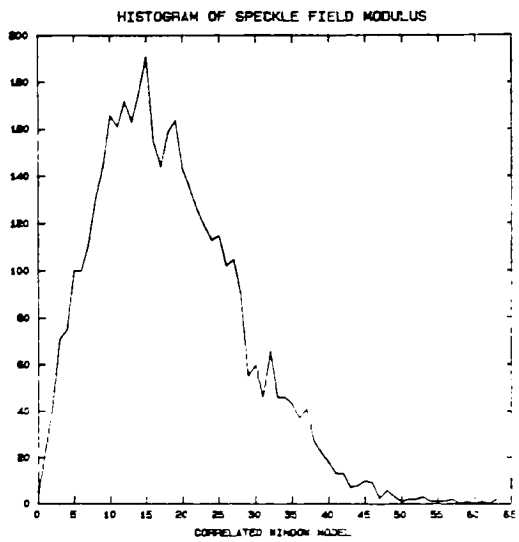

(c)

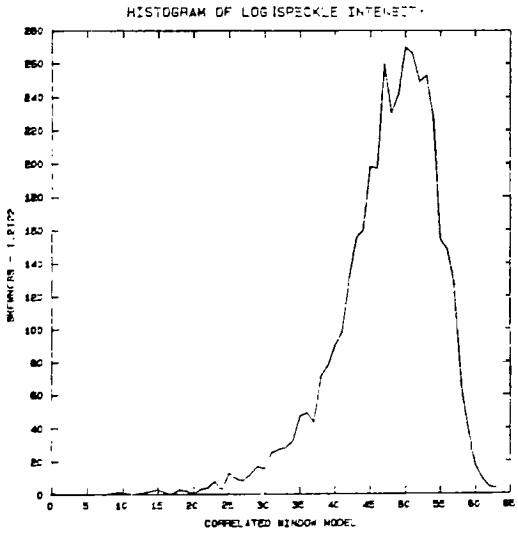

(d)

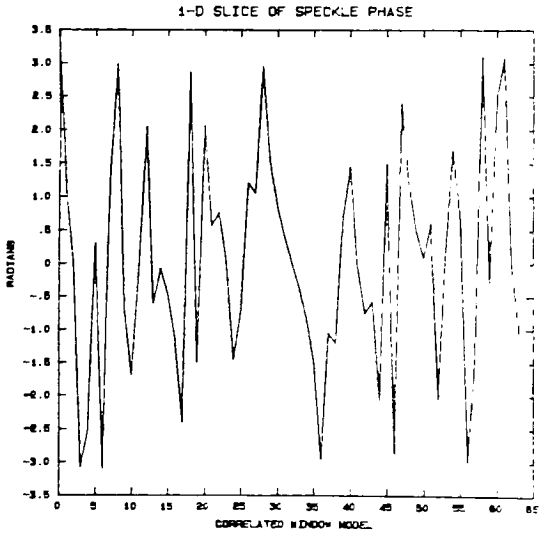

(e)

Figure 11b–e. Statistical Histograms and Phase for the CWM

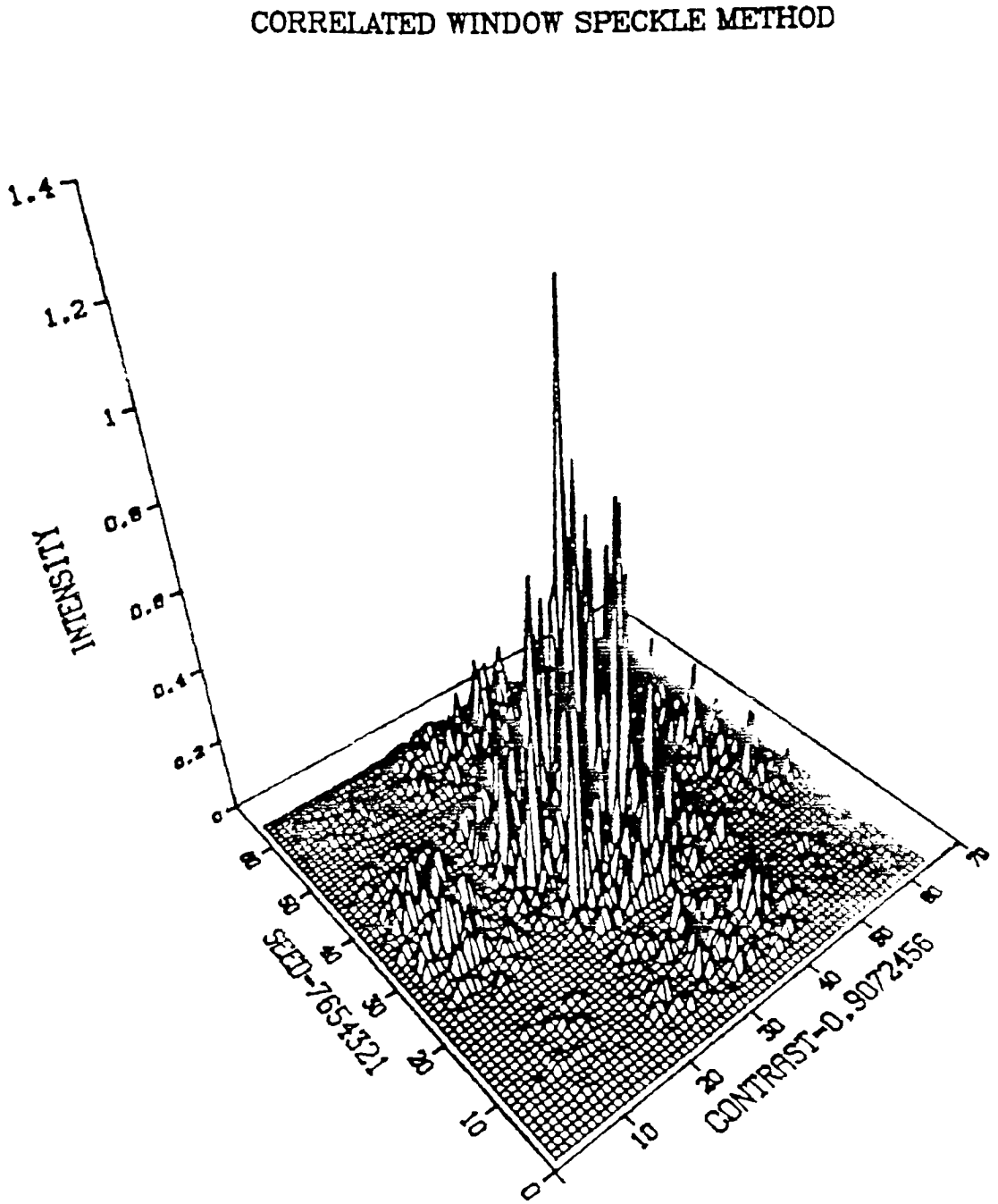

Figure 11f. Truth Object Speckled Via the CWM

Figures 12a through 12c demonstrate the TFM. The TFM is another modification to the DDM using a coherent transfer function. The statistics of this technique are too dependent on the choice of the transfer function to be universally applicable. For example, Figure 12a is the speckled $sinc^2$ (C=0.9634319) using a rectangular aperture of width N=64 pixels. Figure 12b is the same object but with a circular aperture of diameter N=64 pixels. Notice how the speckle is much smoother. Figure 12c is the image if I used an incoherent transfer function and the circular aperture with the TFM.

Figures 13a through 13g demonstrate the RPM. Figure 13a shows the imaged, speckled $sinc^2$ (C=0.7850590). Using the modification in Figure 13b, where I propagate the speckle field to the farfield (via Fourier transformation (Goodman, 1968)), I obtain the speckle pattern shown in Figure 13c (C=1.001926). Comparing these figures with their contrast ratios, it is obvious that the best way to use this technique is for pupil-plane speckle and **not** for image-plane speckle (see Voelz, et al, 1988 and Marathay, et al, 1989). The skewness for the farfield case was 1.20904. This technique could also be used to create the speckle field and then be imaged via a coherent transfer function similar to the TFM.

Figures 14a through 14e demonstrate the NEM. The imaged speckle contrast for this model is 1.071339. By forcing the object to have a negative exponential pdf with unit mean and variance, it is not surprising that the histograms fulfill the statistical criteria so well. Figure 14c is the histogram of the speckle intensity for the "wall" object (C=.9949181). The skewness is 1.3722.

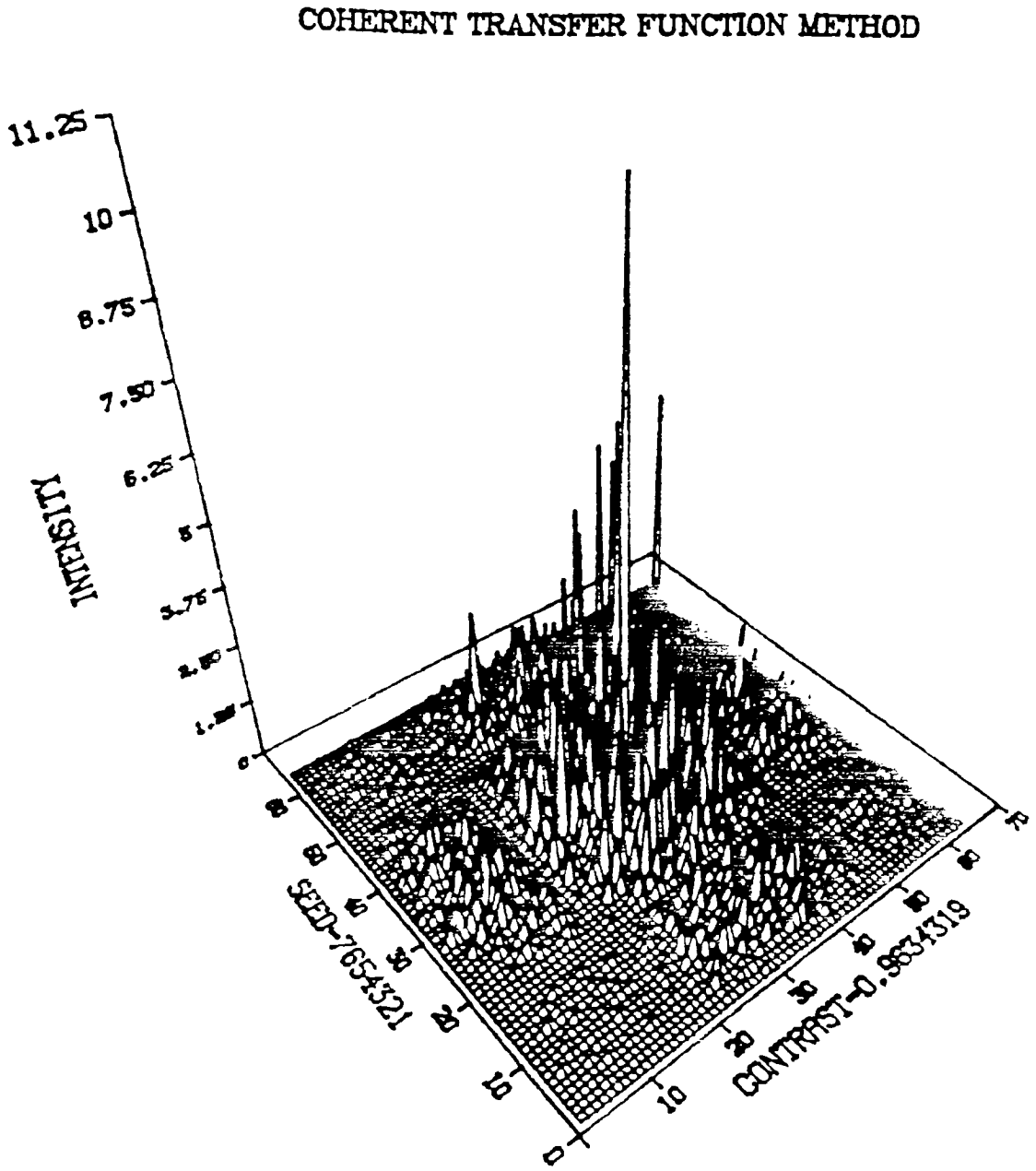

Figure 12a. Truth Object Speckled Via the TFM. Coherent Transfer Function Was a 64 x 64 Rectangular Aperture

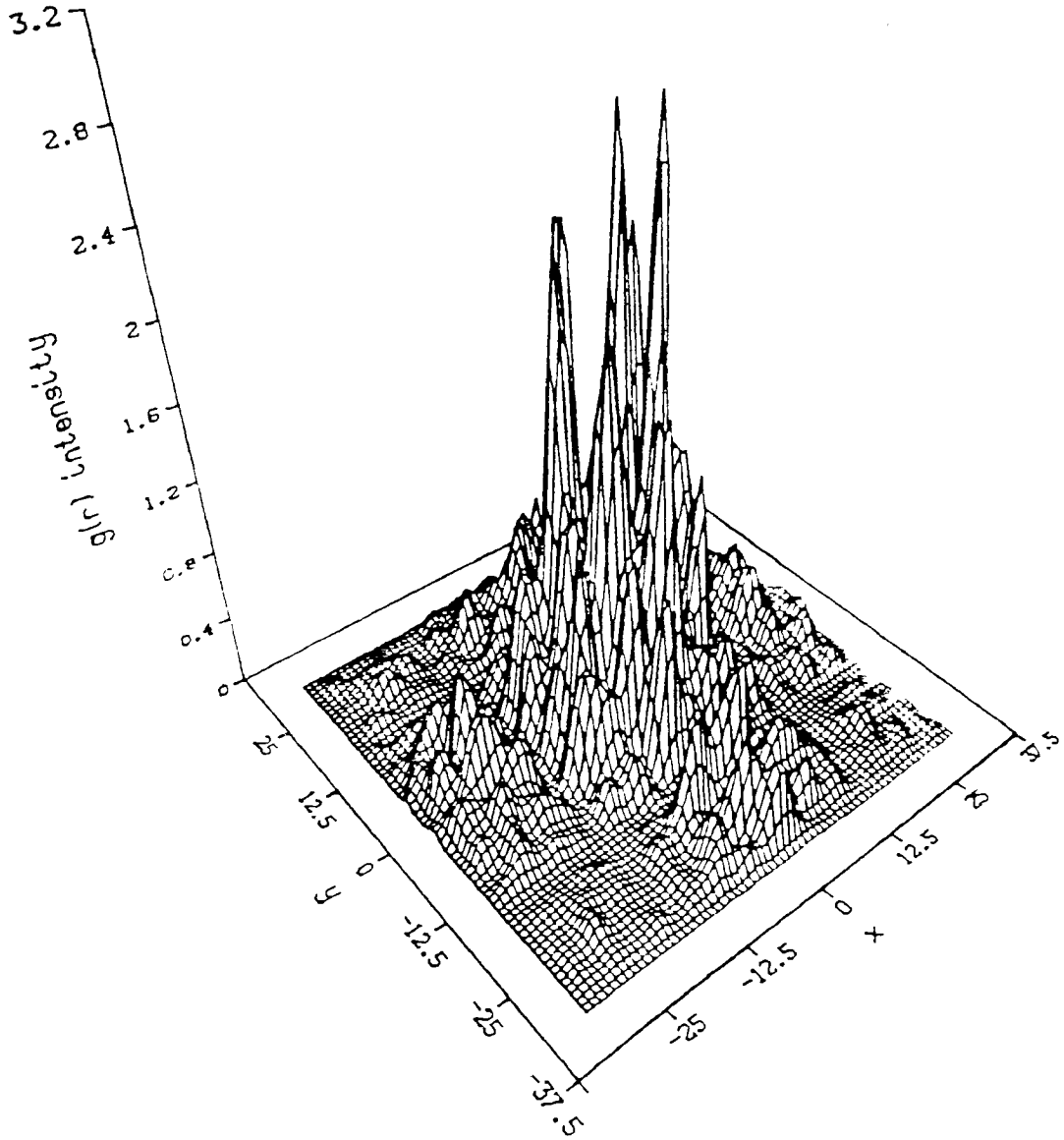

Figure 12b. Truth Object Speckled Via the TFM. Coherent Transfer Function Was a Cylindrical Aperture (Diameter = 64 pixels)

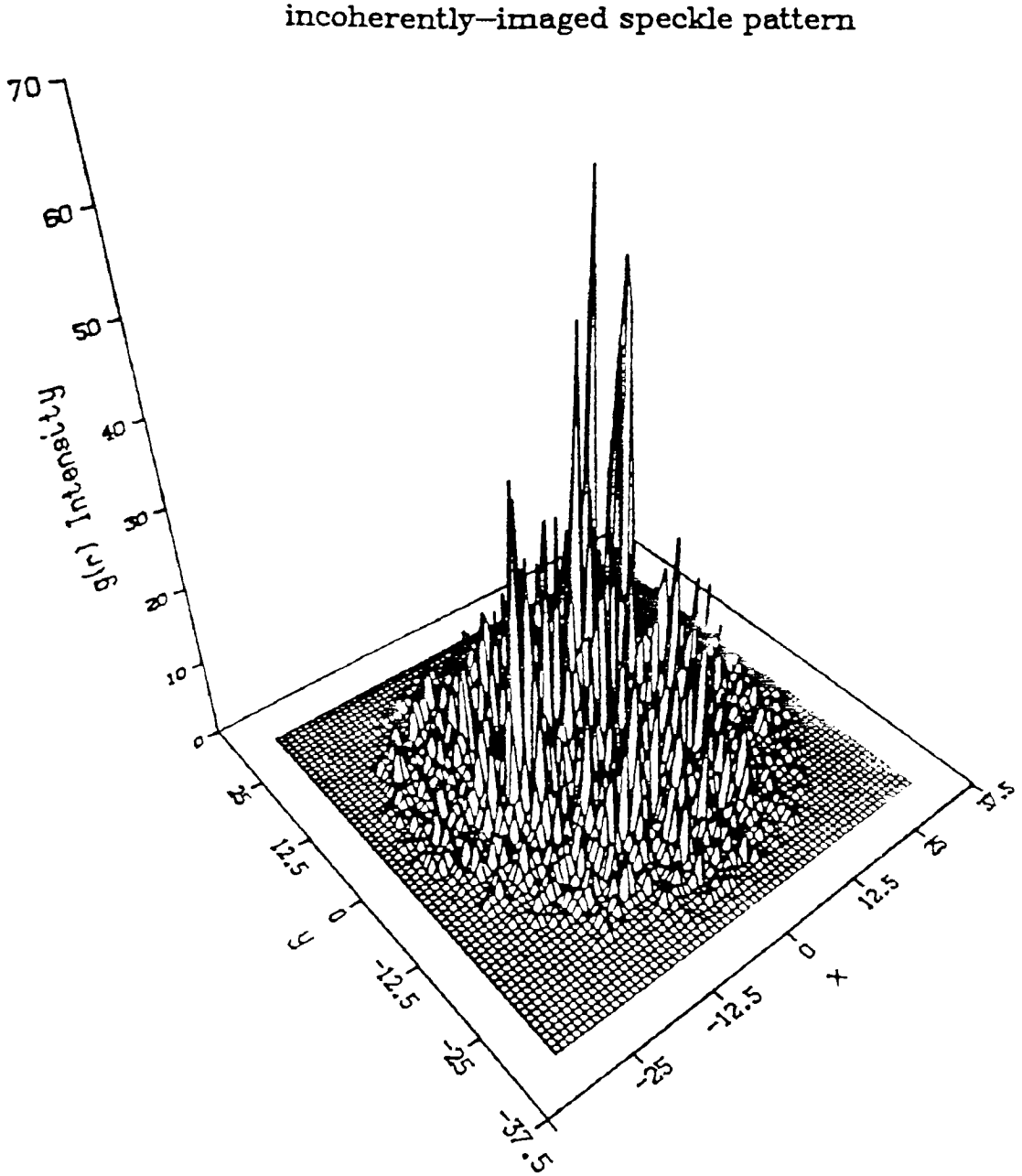

Figure 12c. Truth Object Speckled Via the TFM. Incoherent Transfer Function Used. Cylindrical Aperture (Diameter = 64 pixels)

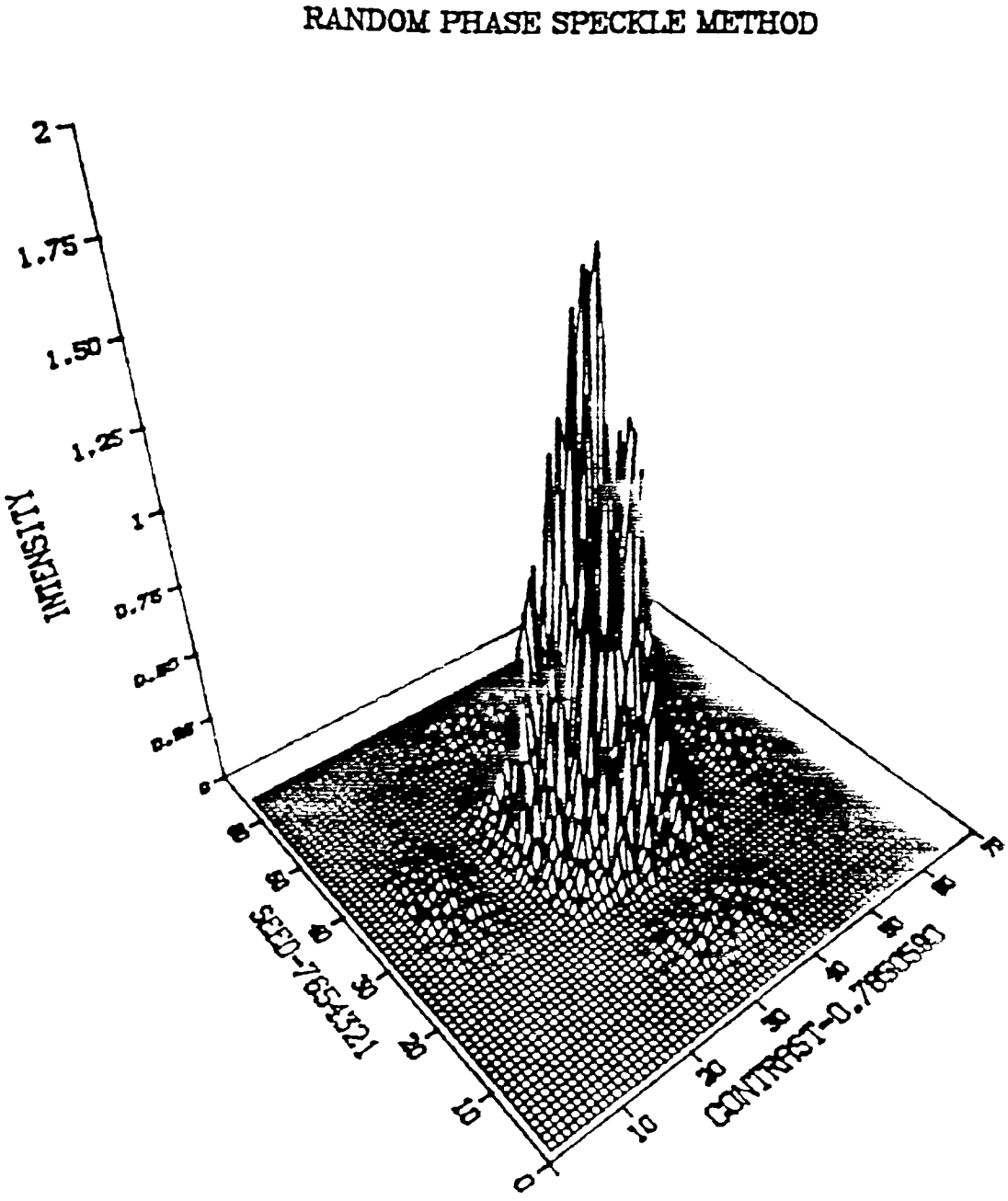

Figure 13a. Truth Object Speckled Via the RPM in Image Plane

RANDOM PHASE MODEL

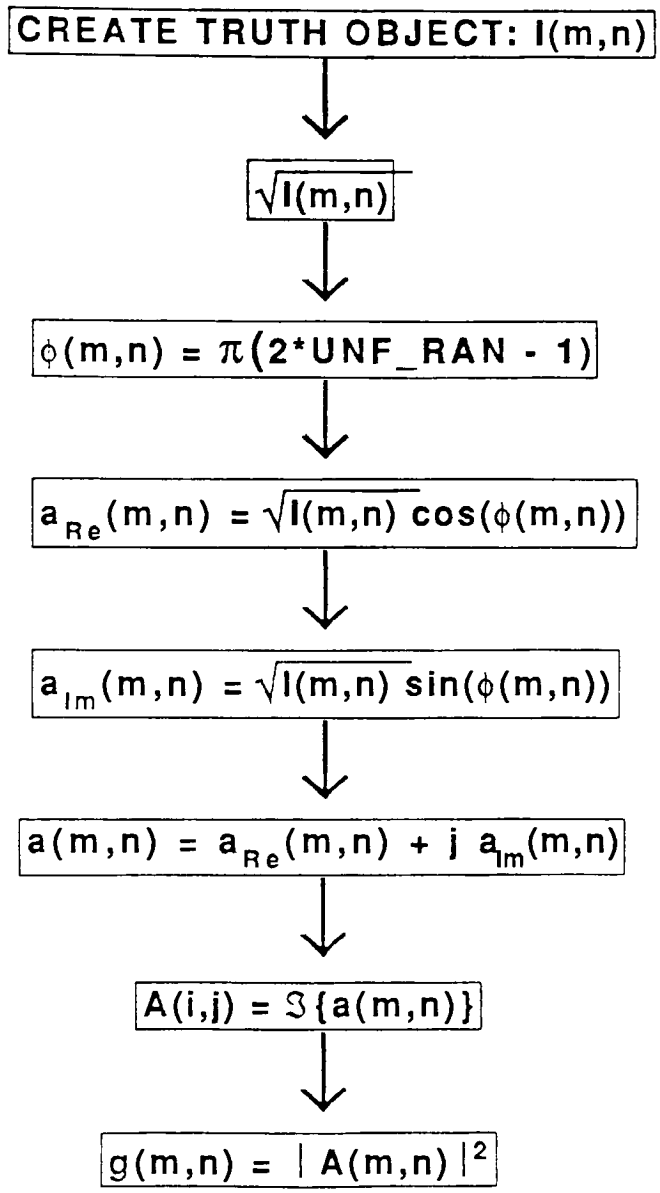

Figure 13b. Flow Diagram for the Random Phase Model

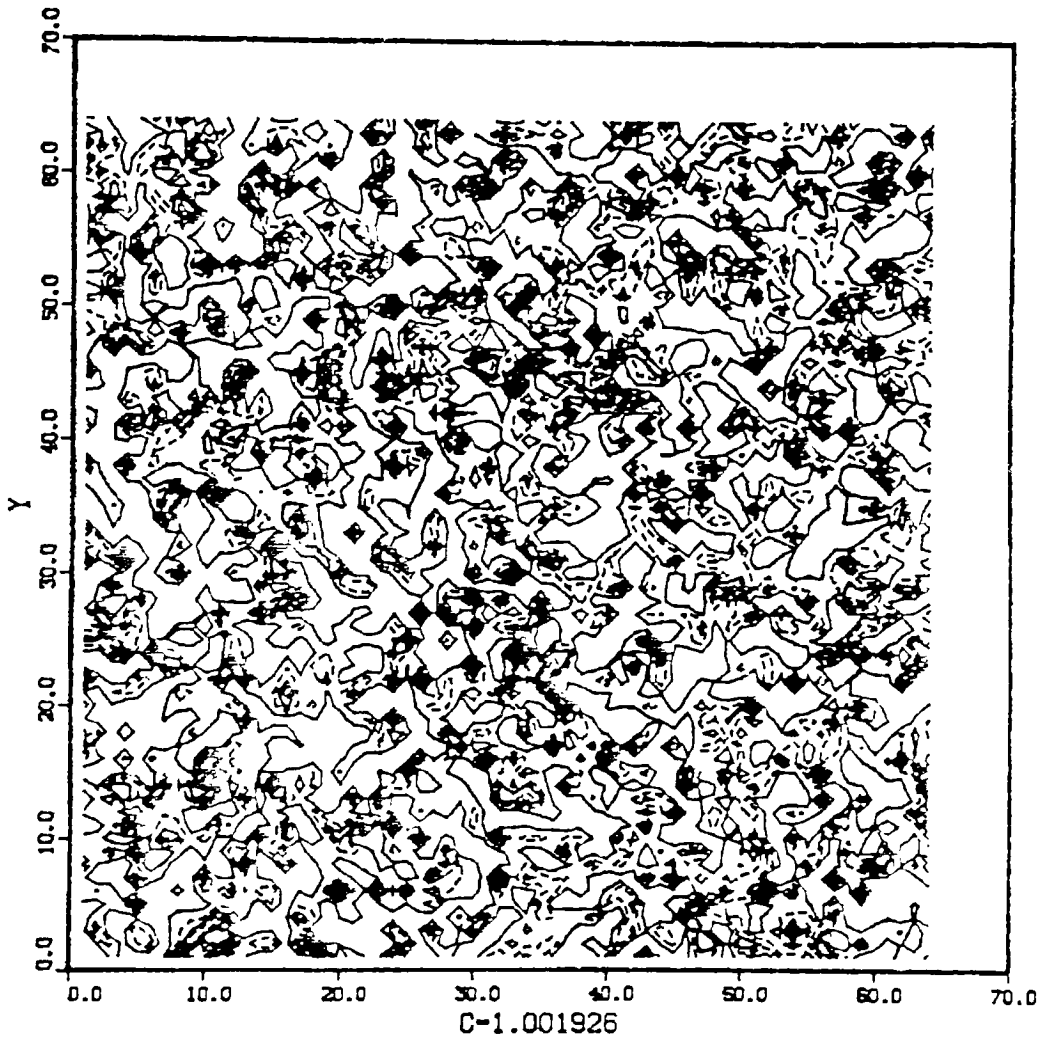

Figure 13c. Truth Object Speckled Via the RPM in the Pupil Plane

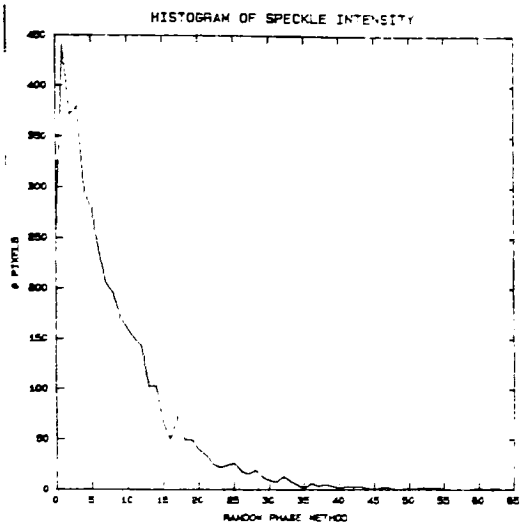

(d)

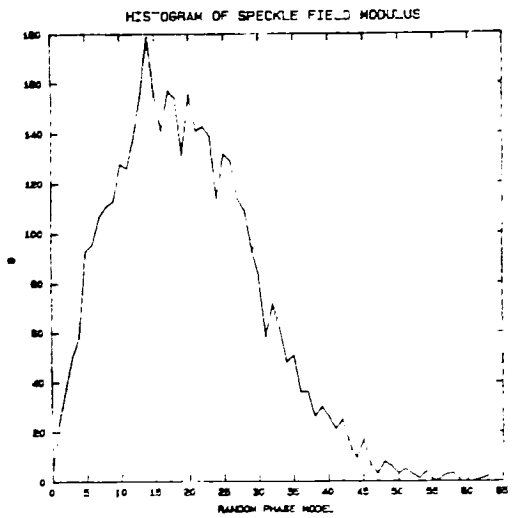

(e)

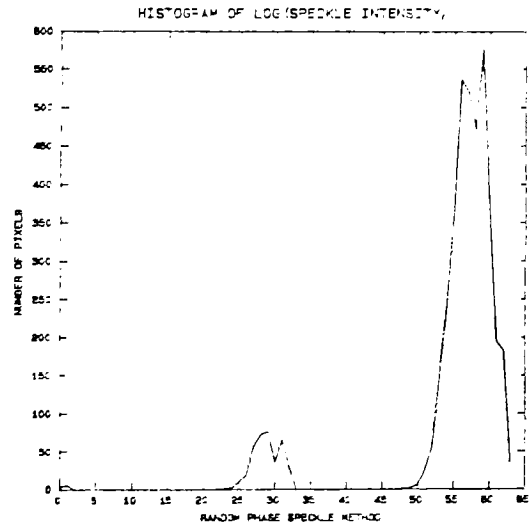

(f)

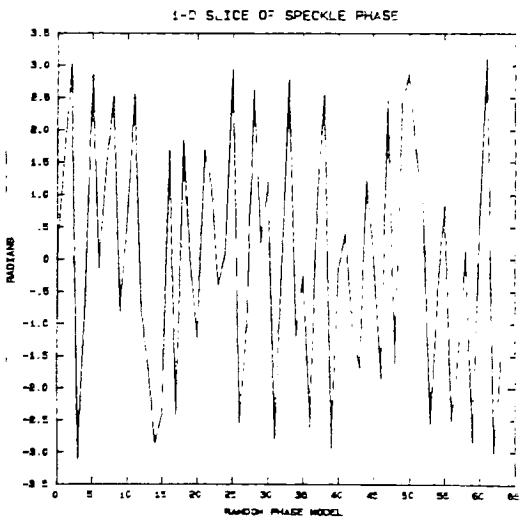

(g)

Figure 13d-g. Statistical Histograms and Phase for the RPM

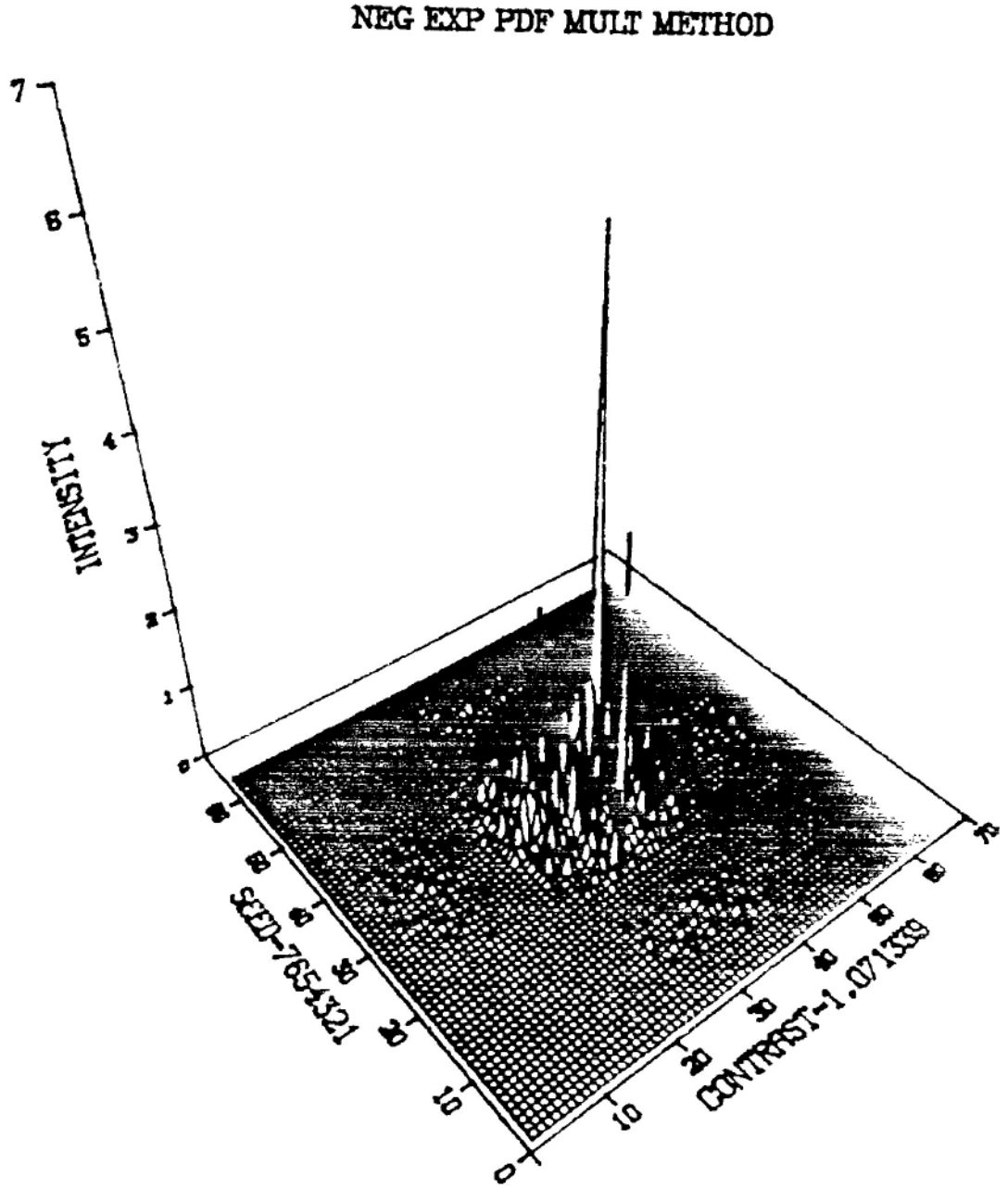

Figure 14a. Truth Object Speckled Via the NEM

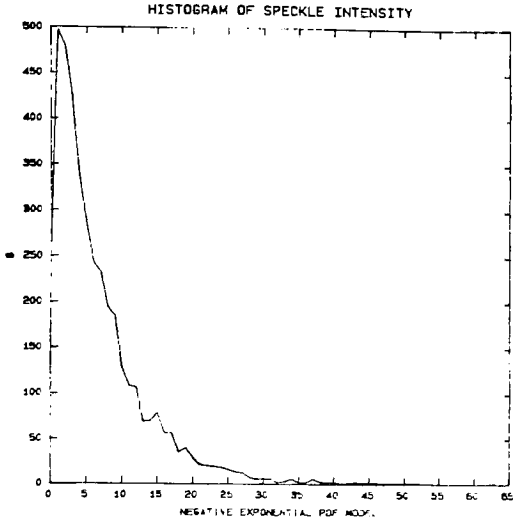

(b)

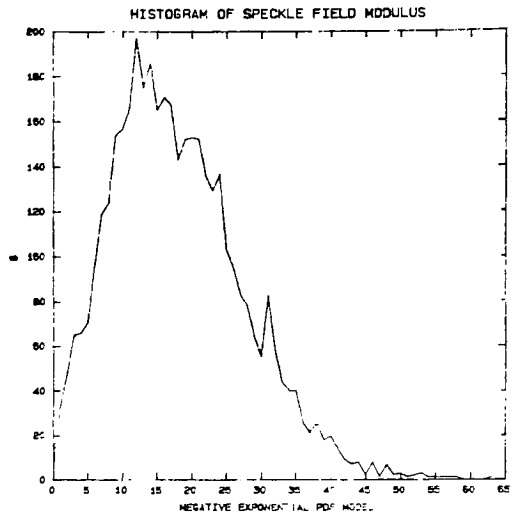

(c)

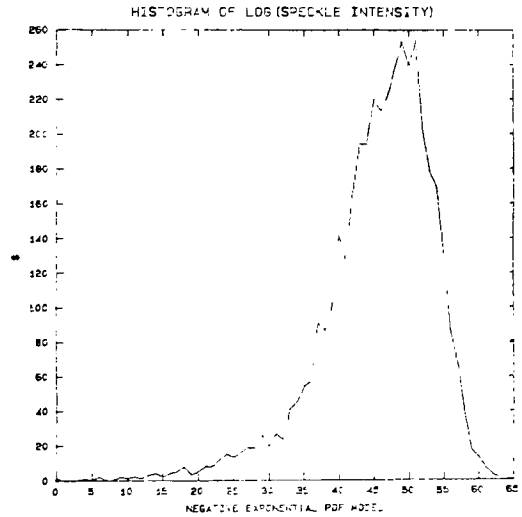

(d)

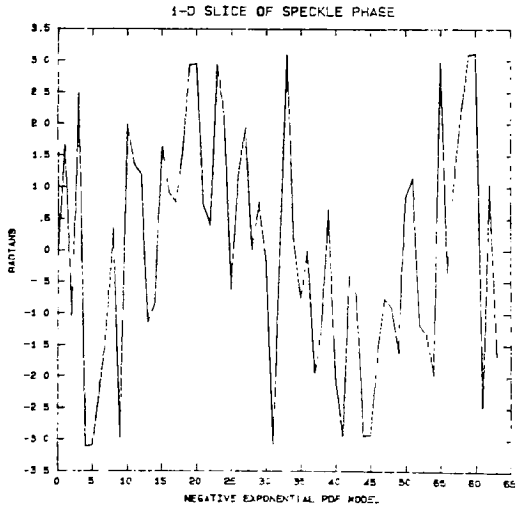

(e)

Figure 14b-e. Statistical Histograms and Phase for the NEM

Figures 15a through 15h demonstrate the AGM. Figure 15a is the AGM using a "wall" for an object (C=1.214454) and Figures 15b-e exhibit its statistics. Notice that the logarithm of the speckle intensity has a Gaussian histogram (skewness=$7.562X10^{-4}$ as it should given that the object had a completely singular intensity (ln(1)=0). Figure 15f shows the speckled $sinc^2$ using the AGM (C=1.102836). Figure 15g show its logarithm of the speckle intensity histogram and Figure 15h shows the same statistics but for the logarithm of the object intensity subtracted first (skewness=$6.56X10^{-4}$). This simply verifies that my model was implemented correctly (see Figure 7a).

From these results, it is clear that a coherently speckled object can be modeled in either the pupil or image plane. For my bispectral analysis, I will use the DDM, CWM, and the AGM for the speckle modeling. As will be shown in the 2-D reconstruction, the bispectrum works particularly well for the AGM case. Appendix A has a tabular synopsis of all of these speckling techniques.

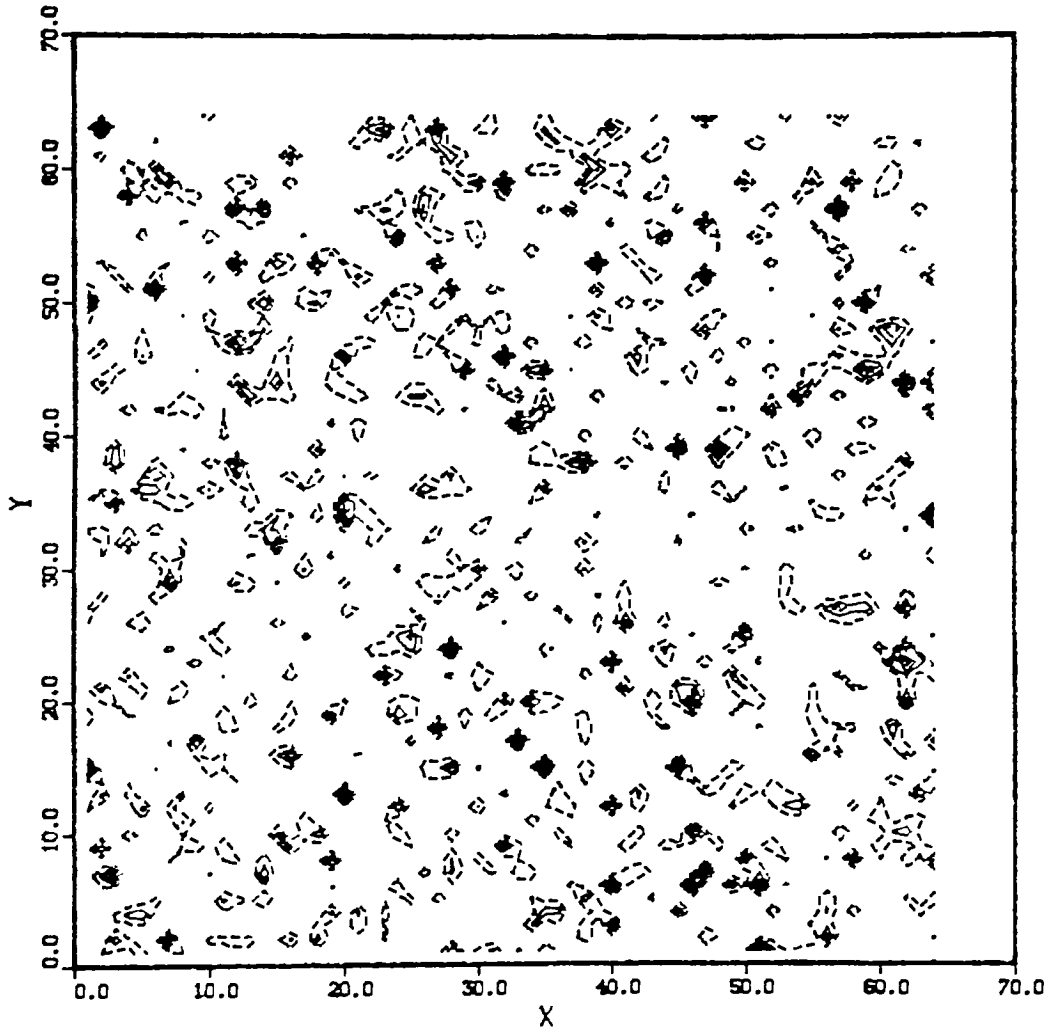

Figure 15a. Speckled "Wall" Using the AGM

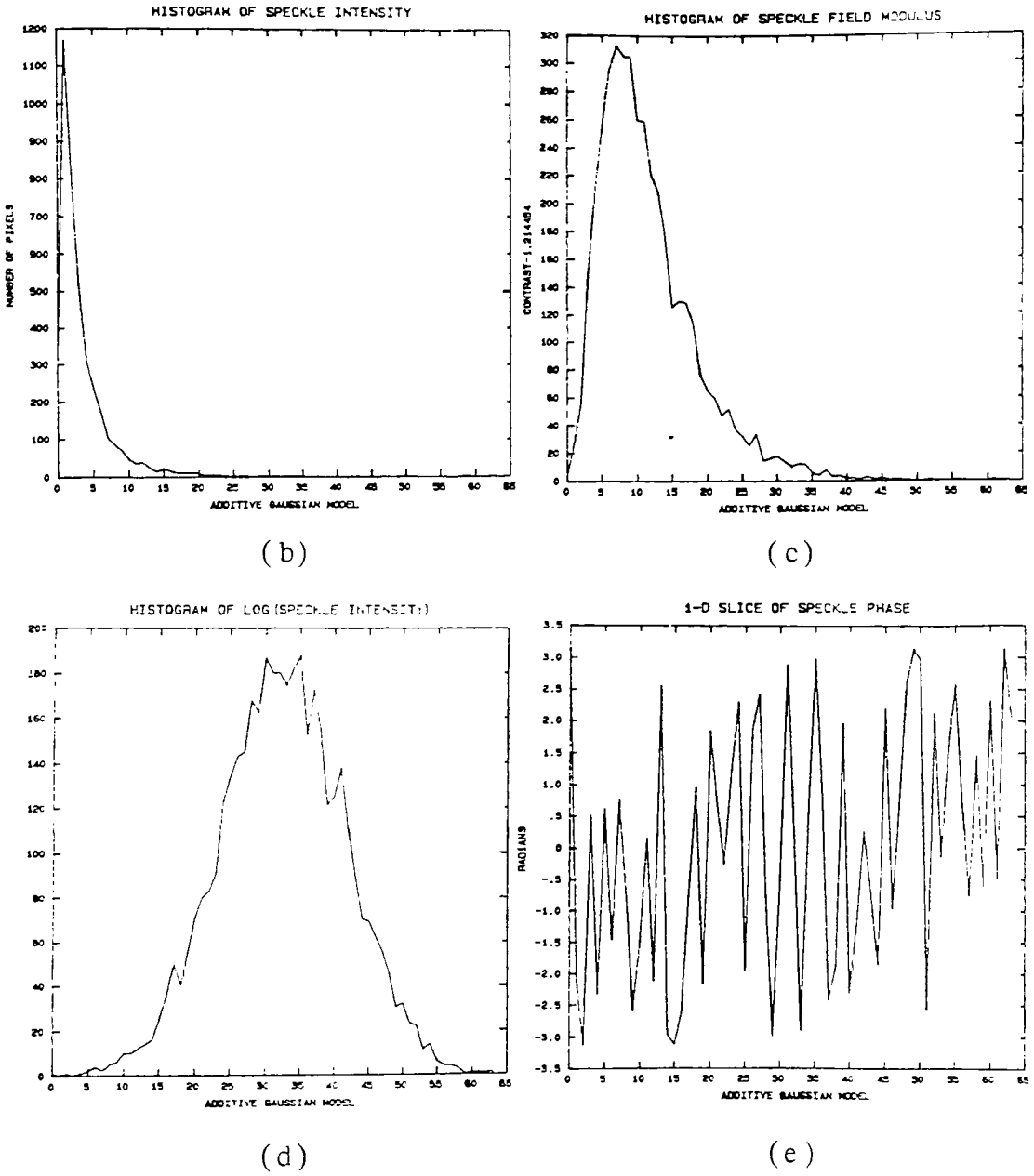

Figure 15b-e. Statistical Histogram and Phase for Speckle "Wall" Using AGM

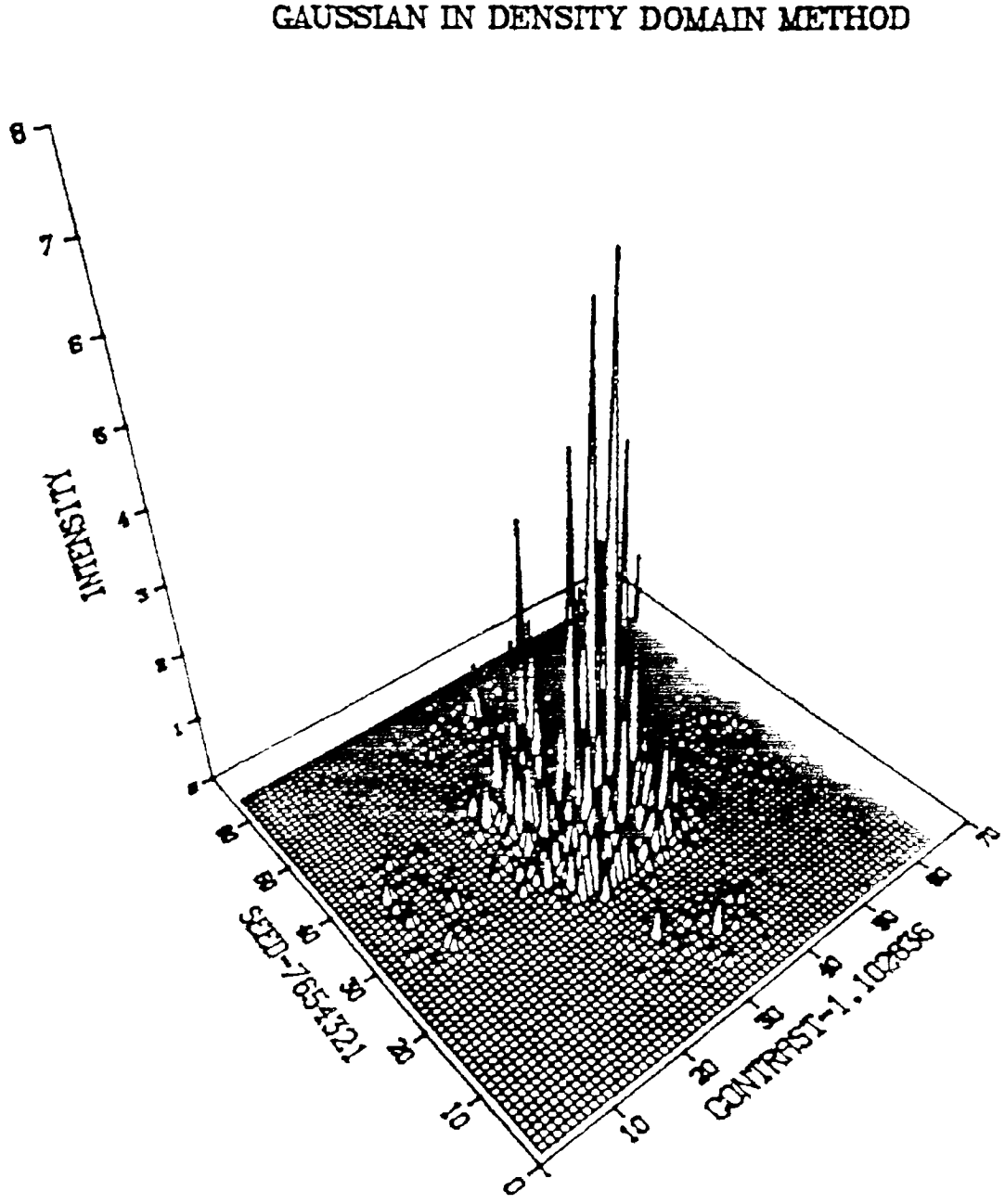

Figure 15f. Truth Object Speckled Via the AGM

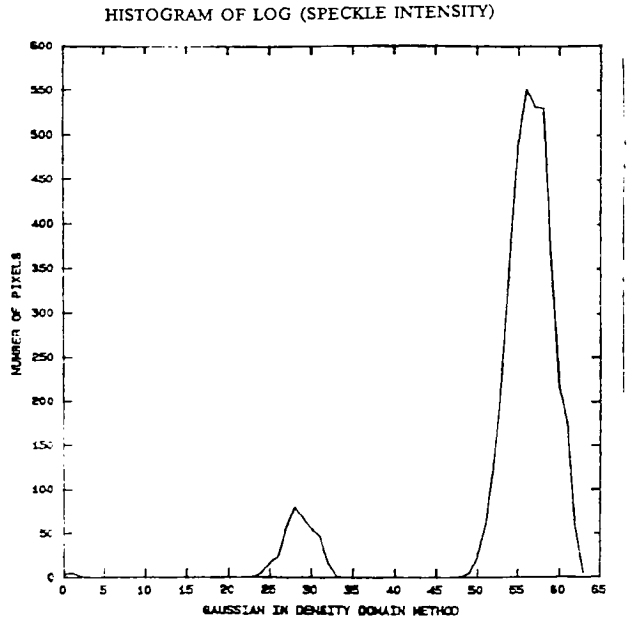

(15g)

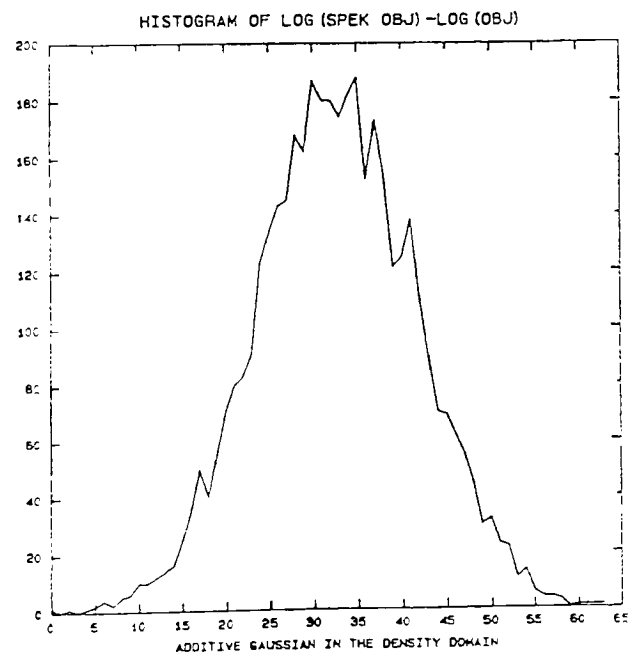

(15h)

Figure 15g-h. Truth Object Speckled Via the AGM

4.0 BISPECTRUM ESTIMATION

4.1 Overview

The definition of the bispectrum, as stated previously, is given as the Fourier transform of the triple correlation. A more rigorous definition than this is given by Nikias and Raghuveer (1987), where the bispectrum is the Fourier transform of the third order cumulant sequence of a random process. This definition satisfies a broader range of statistical criteria, using cumulants, than the correlation does. But for purposes of this thesis, the correlation definition will suffice. Having stated this in words I now relate its mathematical description, using the notation of Lohmann and Wirnitzer (1984). The triple correlation is given as:

$$i^{(3)}(x_1, x_2) = \int_{-\infty}^{\infty} i(x)\, i(x + x_1)\, i(x + x_2)\, dx \qquad (41)$$

where i(x) is a 1-D object (or a two dimensional (2-D) object with x being a 2-D vector).

The bispectrum is then formally given as:

$$I^{(3)}(f_1, f_2) = \int_{-\infty}^{\infty}\int_{-\infty}^{\infty} i(x_1, x_2) \exp\left[-2\pi j(f_1 x_1 + f_2 x_2)\right] dx_1\, dx_2 \qquad (42)$$

This can be written as (see Appendix B):

$$I^{(3)}(f_1, f_2) = I(f_1)\, I(f_2)\, I^*(f_1 + f_2) \qquad (43)$$

The bispectrum, then, becomes the triple product of the object Fourier transform over spatial frequencies f_1 and f_2. From Equation 43 it can be seen that the

bispectrum is generally complex and has redundant regions providing hexagonal support (Nikias and Raghuveer, 1987). This is shown in Figure 16 (Bartlelt, et al, 1984). Note that, from Equation 43, a 1-D Fourier object results in a 2-D bispectrum and thus, by inference, a 2-D Fourier object will give a four dimensional (4-D) bispectrum. This can be a concern for large dimensions due to the memory space required in a computer. Therefore, any algorithm which applies the bispectrum must attempt to resolve this by sampling only portions of the bispectrum, since it has redundant information built into it.

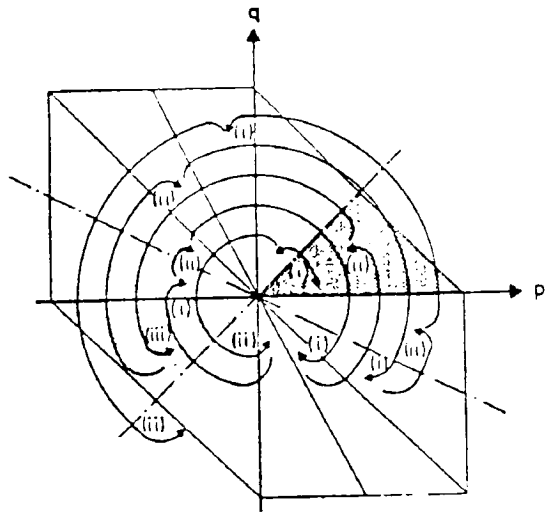

(i) $I^{(3)}(p,q) = I^{(3)}(q,p)$

(ii) $I^{(3)}(p,q) = I^{(3)}(p, -p-q)$

(iii) $I^{(3)}(p,q) = \left| I^{(3)}(-p,-q) \right|^{*}$

if i (x) is real

Figure 16. Redundant Regions of the Bispectrum

4.2 Properties

Signal processing with the bispectrum has several important advantages. Unlike the power spectrum density (PSD), Fourier phase information is retained in the bispectrum so that unique image reconstruction can occur. Fourier phase is lost in the PSD due to the complete spatial symmetry of the autocorrelation while the bispectrum's support retains this object phase. This is quite easy to see from the definition of the phase of the bispectrum (see Appendix B). This property is also useful in identifying whether a system is maximum, minimum, or mixed phase (Nikias and Raghuveer, 1987).

Another advantage of the bispectrum is that it is shift-invariant, i.e., it is insensitive to linear, translational motion. This property allows one to use ensemble averaging to reduce noise present in the image without concern for registering images. When averaging M images together, the noise decreases as the $\sqrt{M}$ (Jain and Christensen, 1980). If these images are not perfectly aligned, the resultant noise-reduced image will be blurred (Gonzalez and Wintz). Since the bispectrum is insensitive to this misregistration, ensemble averaging can be performed without this image blur if the averaging is performed in the bispectral domain. In this thesis, this property will be tested by randomly shifting the image from frame-to-frame while bispectral averaging is being performed.

Another property of the bispectrum has to do with its third order correlation. If the noise present in the image has a symmetric pdf, then its third order moment is zero in the average. This is a property of all odd-order correlations. If the noise, n(x), is signal-independent, additive and stationary, then the noisy image, j(x), can be written as(Lohmann and Wirnitzer, 1984):

$$j(x) = i(x) + n(x) \tag{44}$$

Taking the ensemble average of the triple correlation of Equation 44 gives (Lohmann and Wirnitzer, 1984; Bartelt, et al, 1984; Freeman, et al. 1988):

$$\begin{aligned} \langle j^{(3)}(x_1, x_2)\rangle &= i^{(3)}(x_1, x_2) + \langle n^{(3)}(x_1, x_2)\rangle \\ &+ \langle n(x)\rangle \left[i^{(2)}(x_1) + i^{(2)}(x_2) + i^{(2)}(x_2 - x_1) \right] \\ &+ \bar{i} \left[\langle n^{(2)}(x_1)\rangle + \langle n^{(2)}(x_2)\rangle + n^{(2)}(x_2 - x_1) \right] \end{aligned} \tag{45}$$

where:

$\langle\ \rangle$ denotes the ensemble average

$n^{(2)}(x)$ is the autocorrelation (ATC) of the noise

$n^{(3)}(x_1, x_2)$ is the triple correlation of the noise

$\bar{i}$ is the image mean

$\langle n(x)\rangle$ is the noise mean

$i^{(3)}(x_1, x_2)$ is the triple correlation of the image.

Three undesired terms exist that need to be dissolved. If the noise is assumed to be zero mean, all values multiplied by that term go to zero. Thus the ATC of the image is of no concern. If the noise has a symmetric pdf, its third order moment goes to zero and thus the $n^{(3)}(x_1, x_2)$ term vanishes. Finally, the $\bar{i}$ term can be zero if the image mean is subtracted from the image before processing, or if the

image mean is zero initially. The terms multiplied by that value are ignored if this is the case. All that is left is:

$$\langle j^{(3)}(x_1, x_2)\rangle = i^{(3)}(x_1, x_2) \tag{46}$$

From this relationship the object Fourier magnitude and phase can be recovered (via the bispectrum) and then the original object can be reconstructed. Sundaramoorthy, et al, (1990), proved this same result in the Fourier domain. They found that as long as the bispectral axes were not used in the reconstruction, unbiased estimates would be obtained for the original object (if it was in an additive noise process that had a zero bispectrum).

Two key points should be considered here before I continue. One is that the noise above is *additive* and that the noise reduction is performed in the *ensemble*. As stated previously, speckle noise is multiplicative. The task is to convert this multiplicative process into an additive one. To do this a homomorphic transformation can be taken on the speckled image. The transformation is called homomorphic because a homomorphism from the set of multiplicative numbers to an additive group of numbers has occurred. A homomorphic transformation is one in which the natural logarithm of the image intensity is taken before any further processing is performed. The multiplicative noise process then becomes additive due to this logarithmic operation. Several authors review this technique in general (Oppenheim and Schafer, 1975; Lim,1987; Arsenault and Levesque, 1984; and Gonzalez and Wintz, 1987) while others have reviewed this transformation for speckle in particular (Jain and Christensen,1980; Lim and Nawab, 1981; and Sadjadi, 1990). Arsenault and April (1976) have shown that an object in speckle noise becomes

additive and signal-independent with an approximately Gaussian pdf when undergoing the transformation of:

$$D = -\ln(I) \tag{47}$$

where D is the density (a term left over from the film grain studies) and I is the speckle intensity. Therefore, theoretically at least, performing a homomorphic transformation on Equation 34 will give me the result of Equation 44. After the homomorphic transformation is performed for each speckled image, these images should be ensemble averaged. Guenther, et al, (1978) shows that this should reduce the noise level by the $\sqrt{N}$, where N is the number of images processed. How this will be done using the bispectrum is discussed next.

4.3 Algorithms

In this section I will review the algorithms used to reconstruct multiple, speckle-degraded, jittered images. To begin I refer to the bispectrum definition of Equation 43, written here as:

$$I^{(3)}(f_1, f_2) = \left|I^{(3)}(f_1, f_2)\right| \exp\left[j\psi(f_1, f_2)\right] \tag{48}$$

This function has both magnitude and phase, broken into their respective components here as:

$$\left|I^{(3)}(f_1, f_2)\right| = \left|I(f_1)\right| \left|I(f_2)\right| \left|I^*(f_1 + f_2)\right| \tag{49}$$

$$\psi(f_1, f_2) = \phi(f_1) + \phi(f_2) - \phi(f_1 + f_2) \tag{50}$$

For a noisy sequence j(k)=i(k)+n(k), from $0 \leq k \leq N-1$, its Fourier transform is given as:

$$J(\lambda) = \sum_{n=-\infty}^{\infty} j(n) \exp\left[-j2\pi n\lambda\right] \tag{51}$$

For M images, the ensemble-averaged bispectrum of Equation 51 becomes:

$$\hat{J}^{(3)}(\lambda_1, \lambda_2) = \frac{1}{M} \sum_{I=1}^{M} J_I(\lambda_1) J_I(\lambda_2) J_I^*(\lambda_1 + \lambda_2) \tag{52}$$

where $\hat{J}^{(3)}(\lambda_1, \lambda_2)$ is the bispectrum estimate of the noisy image. The ultimate goal is to obtain a bispectrum estimate $\hat{J}^{(3)}$ that is as close as possible to the image bispectrum $I^{(3)}(\lambda_1, \lambda_2)$, the Fourier transform of Equation 46. Once this is attained image recovery can be performed by the following algorithms.

4.3.1 One-Dimensional Algorithm

For 1-D images I use a different algorithm each for the magnitude and the phase reconstruction. The magnitude algorithm is from Sundaramoorthy, et al, (1990) while the phase algorithm is from Bartelt, et al, (1984). Matsuoka and Ulrych (1984) discuss several other phase algorithms that could be used for 1-D images (seismic wavelets) but the recursive algorithm of Bartelt appears to be sufficient. I will first develop the 1-D algorithm for a 1-D sequence from $0 \leq m.n \leq N-1$, letting B(m,n) denote $I^{(3)}(\lambda_1, \lambda_2)$ and H denote I. With these substitutions I get:

$$B(m,n) = H(m)H(n)H^*(m+n) \tag{53}$$

where B(m,n) is the bispectrum of H (the Fourier transform of the 1-D sequence). Letting m=1, Equation 53 becomes:

$$B(1,n) = H(1)H(n)H^*(1+n) \tag{54}$$

Since the object is assumed to be real its Fourier transform is Hermitian, i.e., $f(x) = f^*(-x)$ (Gaskill). Hermitian means that the complex function has a real component which is even ($e(x) = e(-x)$) and an imaginary component which is odd ($o(x)=-o(-x)$). This implies I only have to sample the bispectrum from Equation 54 for $1 \le n \le \frac{N}{2} - 1$ and then I can later extend the reconstructed object from these samples for $\frac{N}{2}$ to N-1. The value of H(0) is the image mean (Gonzalez and Wintz). If this value is zero, or the mean is subtracted from the image before Fourier transformation, this term could cause magnitude reconstruction problems, since many magnitude algorithms have this term as a divisor (see Bartelt, 1984).

Once the bispectrum values of Equation 54 have been calculated and summed for M images, I can reconstruct the Fourier magnitude and phase of the original object. For the magnitude, I simply write Equation 54 in terms of its magnitude, letting n=j-1, as (for real objects):

$$|H(j)| = \frac{|B(1, j-1)|}{|H(1)|\,|H(j-1)|} \tag{55}$$

where the value of j goes from 2 to $\frac{N}{2}$. For values of $j > \frac{N}{2}$, $|H(j)| = |H(N-j)|$.

Notice that I have the $|H(1)|$ term as a constant to determine before I can recur-

sively find the other values of $|H(n)|$. This value is given from Sundaramoorthy, et al, as:

$$|H(1)| = \sqrt[6]{\frac{|B(1,1)|^3 \; |B(1,3)|}{|B(1,2)| \quad |B(2,2)|}} \tag{56}$$

Note that an additional bispectrum term has arisen in this formulation. Therefore the constant B(2,2) must be calculated and summed during the calculation of the other bispecturm terms. From Equation 53 this becomes:

$$B(2,2) = H(2)^2 H^*(4) \tag{57}$$

From this I can find its magnitude and use its value in the recursive routine (B(2,2) is not needed in the phase recursion routine). Since this technique requires only $\frac{N}{2}$ samples of the bispectrum along the m=1 line and the B(2,2) sample (for an image of size N), considerable savings can be had both in memory allocation and computation time.

The phase portion of the bispectrum reconstruction is also recursive. The calculated values of the bispectrum phase are an extension of Equation 50 used in Equation 54, written as:

$$\psi(1,n) = \phi(1) + \phi(n) - \phi(1+n) \tag{58}$$

where, as before, ψ is the bispectrum phase and ϕ is the object phase. Letting i = n−1, these values are calculated only from $1 \le i \le \frac{N}{2}$. I can rewrite Equation 58 to determine the values of ϕ as:

$$\phi(i) = -\Psi(1, i-1) + \phi(1) + \phi(i-1) \tag{59}$$

where: $$\phi(1) = \frac{2}{N} \sum_{n=1}^{\frac{N}{2}-1} \psi(1, n) \tag{60a}$$

$$\phi(i) = -\phi(N-i) \text{ for } i \geq \frac{N}{2} + 1 \tag{60b}$$

Values for both the magnitude and the phase for $n \geq \frac{N}{2}+1$ to N–1 can be found by taking advantage of the Hermitian property of the Fourier object. The value of $\phi(\frac{N}{2})$ is set initially at zero since it does not affect the reconstruction but merely the placement of the reconstructed object (Matsuoka and Ulrych, 1984; Bartelt, 1984). The final values of $|H(n)|$ and $\phi(n)$ can then be combined using Euler's relationship and the inverse Fourier transform taken to obtain the reconstructed object.

4.3.2 Two-Dimensional Algorithm

The 1–D algorithm developed previously worked extremely well on all types of noise, as well as speckle (see Results section) but, being a 1–D algorithm, it did not extend well to 2–D images. By extension I mean continuing to use this 1–D approach on 2–D images by first "raster–scanning", or peeling, the image before obtaining its bispectrum. If the 2–D image was noise–free, this technique worked perfectly for jittered, image reconstruction. All 2–D objects of any extent, constraint, or phase type could be reconstructed with this method. Once a noise was added, though, even in small amounts, reconstruction would not occur. Since noise

essentially creates phase errors in the object phase (Marron, et al, 1990), these phase errors are propagated and therefore increased when scanning an image recursively over its NXN extent. This is because you have given the phase errors a greater amount of data to accumulate in as you scan the array as opposed to a 1XN image.

The 2-D magnitude reconstruction algorithm I used is from Dianat and Raghuveer (1990). Their approach is developed as follows. Write Equation 53 for 2-D images as:

$$B(i,j;m,n) = H(i,j)H(m,n)H^*(i+m,j+n) \tag{61}$$

where the B(i,j;m,n) is the 4-D bispectrum of the 2-D Fourier object H for pixels m,n,i,j. To simplify to a 2-D problem, let i = m, j = n, to get, only for 2-D subplane:

$$B(m,n) = H(m,n)^2\ H^*(2m, 2n) \tag{62}$$

Taking the natural logarithm of the magnitude of both sides of Equation 61 gives:

$$\ln\left[\left|B(m,n)\right|\right] = 2\ln\left[\left|H(m,n)\right|\right] + \ln\left[\left|H(2m, 2n)\right|\right] \tag{63}$$

By describing the above equation in terms of its discrete Fourier transform (DFT, see Equation 51) and equating like coefficients on both sides, the following relationships can be seen as (where the $\sim$ term denotes the DFT of the natural logarithm of the magnitude):

1. For m,n odd:

$$\tilde{H}(m,n) = \frac{1}{2}\,\tilde{B}(m,n) \tag{64}$$

2. For $\frac{m}{2}$ or $\frac{n}{2}$ odd:

$$\begin{aligned}\tilde{H}(m,n) = \frac{1}{2}\,\tilde{B}(m,n) - \frac{1}{2}\,\tilde{H}\left(\frac{m}{2},\frac{n}{2}\right) - \frac{1}{2}\,\tilde{H}\left(\frac{m}{2},\frac{n}{2}+\frac{N}{2}\right) \\ - \frac{1}{2}\,\tilde{H}\left(\frac{m}{2}+\frac{N}{2},\frac{n}{2}+\frac{N}{2}\right) - \frac{1}{2}\,\tilde{H}\left(\frac{m}{2}+\frac{N}{2},\frac{n}{2}\right)\end{aligned} \tag{65}$$

3. Repeat Step 2 recursively for cases when $\frac{m}{2^L}$ or $\frac{n}{2^L}$ is odd for L = 2,3,....., $\log_2(N)-1$.

4. Finally, compute:

$$\tilde{H}(0,0) = \frac{1}{3}\left[\tilde{B}(0,0) - \tilde{H}\left(0,\frac{N}{2}\right) - \tilde{H}\left(\frac{N}{2},0\right) - \tilde{H}\left(\frac{N}{2},\frac{N}{2}\right)\right] \tag{66}$$

Once I have calculated all values of $\tilde{H}(m,n)$ recursively from the bispectrum using the above relationships, I exponentiate this value to obtain the Fourier magnitude $|H(m,n)|$. I have found this algorithm to work practically flawlessly for magnitude reconstruction. As will be discussed in detail later, it is the 2-D phase that will determine the true shape of the reconstructed object. The above routine also can be extended to the phase but it is not as robust in phase recovery as the magnitude algorithm is. Thus, for phase reconstruction, I used a 2-D recursive routine similar to the 1-D in development but with some added calculations.

The two-dimensional, recursive, phase reconstruction algorithm is a 2-D extension of the Lii-Rosenblatt technique described by Matsuoka and Ulrych (1984). This algorithm requires the H(0,1) and H(1,0) subplanes as a minimum because these subplanes represent the lowest spatial frequencies in the 2-D object. This being the case, I let i=0, j=1 in Equation 61 to get:

$$B(m,n) = H(0,1)H(m,n)H^*(m,n+1) \tag{67}$$

Similarly, for i=1, j=0 I get:

$$B(m,n) = H(1,0)H(m,n)H^*(m+1,n) \tag{68}$$

Finally, I need to calculate a single bispectrum constant to complete the calculated values necessary to reconstruct the image. This value represents the limit of the subplanes given above that I will need to sample:

$$B\left(\frac{N}{2},0;\ 0,\frac{N}{2}\right) = H\left(\frac{N}{2},0\right) H\left(0,\frac{N}{2}\right) H^*\left(\frac{N}{2},\frac{N}{2}\right) \tag{69}$$

To calculate the Fourier phase I use the following relationships, once I have obtained the bispectrum for $2 \le m,n \le \frac{N}{2}-1$:

1. Using ψ calculated from Equation 67 for m=0, $2 \le n \le \frac{N}{2}-1$,

$$\phi(0,n) = \phi(0.1) + \phi(0,n-1) - \psi(0,n-1) \tag{70}$$

where: $$\phi(1.0) = \frac{2}{N} \sum_{m=1}^{\frac{N}{2}-1} \psi(0,n)$$

2. Using ψ calculated from Equation 68 for n=0, $2 \leq m \leq \frac{N}{2}-1$,

$$\phi(m,0) = \phi(1,0) + \phi(m-1,0) - \psi(m-1,0) \tag{71}$$

where: $$\phi(1,0) = \frac{2}{N} \sum_{m=1}^{\frac{N}{2}-1} \psi(m,0)$$

3. Using Equation 70 for $1 \leq m,n \leq \frac{N}{2}-1$,

$$\phi(0,n+\tfrac{N}{2}) = -\phi(0,\tfrac{N}{2}-n) \tag{72}$$

4. Using Equation 71 for $1 \leq m,n \leq \frac{N}{2}-1$,

$$\phi(m+N/2) = -\phi(N/2-m,0) \tag{73}$$

5. Using ψ calculated from Equation 67 for $1 \leq m \leq N-1$, $1 \leq n \leq \frac{N}{2}$.

$$\phi(m,n) = \phi(0,1) + \phi(m,n-1) - \psi(m,n) \tag{74a}$$

$$\phi(m,n+\tfrac{N}{2}) = -\phi(N-m,\tfrac{N}{2}-n) \tag{74b}$$

6. Finally, the following constant values, which affect the position of the object, are set at:

$\phi(0,0) = 0$

$\phi(\frac{N}{2},0) = 0$

$\phi(0,\frac{N}{2}) = 0$ (or π if $B(\frac{N}{2},0;0,\frac{N}{2})$ is less than zero).

As one can see from this, finding the phase recursively for 2-D images is a bit more involved than for 1-D. Once both the Fourier magnitude and phase have been determined, I combine them and inverse Fourier transform them to get the object. Examples of both 1-D and 2-D image reconstruction will be found in the next section.

5.0 RESULTS

In this section I report my findings from the computer simulations I have performed on shift-invariant image reconstruction of speckle-degraded images using the bispectrum. I have separated the results into two sections: 1) non-speckled, and 2) speckled. This is because of certain results I obtained from the algorithms used above that were totally unrelated to the speckle problem.

In Appendix C, I have given an overall flowchart of the 2-D reconstruction algorithm used for jittered, speckled images. It is directly applicable to both unspeckled images and all of the 1-D cases. The pieces of the algorithm that make up the entire program have been described previously.

When I began this thesis my first question was: "Is the bispectrum robust enough to handle speckled images?" The bispectrum has recently been used for tonal noise and additive Gaussian noise (Sundaramoorthy, et al, 1990) as well as photon-limited background noise with SNR < 1 (Newman and Van Vracken, 1989). The bispectrum has been used in the last few years (see Ayers, et al, 1988; Bartelt, et al, 1984; Lohmann, et al, 1983; and Freeman, et al, 1988) to retrieve astronomical objects from atmospheric speckle (described by Dainty (1971, 1973) and Labeyrie (1970)). Marathay (1986) and Sato, et al, (1978) have investigated methods to physically perform correlations to help retrieve objects. Thus, the recent interest in bispectrum estimation to reconstruct objects in noise led to this thesis. The concern for coherent speckle is that, by definition, its phase is a modulo 2π random phase,

white noise process. Is this too big of a challenge for a phase retrieval routine such as the bispectrum?

Another question was: "Can ensemble averaging be performed on multiple, shifted, and possibly blurred images in noise without image blurring in the ensemble occurring as a result?" This problem can occur when imaging an object moving against a uniform background that is recorded by videotape. The same image is taken over many frames (at the standard video rate of 30 frames per second) and trying to register these perfectly without introducing blurring is a formidable task. Thus, the shift-invariant nature of bispectrum estimation makes it an excellent candidate to perform this function.

Therefore, this thesis was proposed as a conceptual study of image reconstruction of speckled images. Since ensemble averaging of the speckled images is the MLE of the noise-free object, performing this in the bispectral domain while jittering the object in the spatial domain should test its shift-invariant capabilities as well as its phase-retrieval capabilities.

5.1 Non-Speckled

When I began this task I did not foresee that I would have problems reconstructing a noise-free object and, in most cases, I did not. There are certain conditions that can occur that can either distort the reconstructed object or preclude its reconstruction at all and I will discuss those conditions next. These problems were found by thoroughly exercising the algorithms for various types of constrained objects in

various extents and viewing the results. The biggest problem was phase distortion of the reconstructed object and I will review that next.

5.1.1 Phase Distortion Problem

Bispectrum estimation results in a linear phase shift being introduced into the reconstructed object, given as $H(\lambda)\exp[-j2\pi\alpha\lambda]$, where $H(\lambda)$ is the Fourier domain representation of the reconstructed object and $\exp[-j2\pi\alpha\lambda]$ is the linear phase shift (α is a real constant). This phase shift can be seen in the reconstructed objects of the following figures.

Figure 17a is the reconstructed version of Figure 9a. Figure 17b is a 2-D contour plot of Figure 9b while Figure 17c is the recentered object using a program I wrote that centers the image by wrapping it around given the amount of shift desired in both the x and y direction. Notice that the reconstructed values go negative. This is an artifact of the 2-D bispectrum reconstruction. Figure 18a is a 1-D slice of the object in Figure 26a and the reconstructed object is in 18b. The reconstruction there is exact except for the phase shift. This phase shift acts as a filter that merely introduces a shifting of the object in the spatial domain. The 1-D tribar target of Figure 19a did not show a phase shift upon reconstruction (Figure 19b), probably because α was zero so the phase shift was zero. To explain this I will use a linear systems approach (Gaskill). For an object, $f(x)$, being convolved with a filter, $h(x)$, I can write (where (*)) denotes the convolution operator):

$$g(x) = f(x) * h(x) \tag{75}$$

and its Fourier transform relationship is (Gaskill):

$$G(\lambda) = F(\lambda)H(\lambda) \tag{76}$$

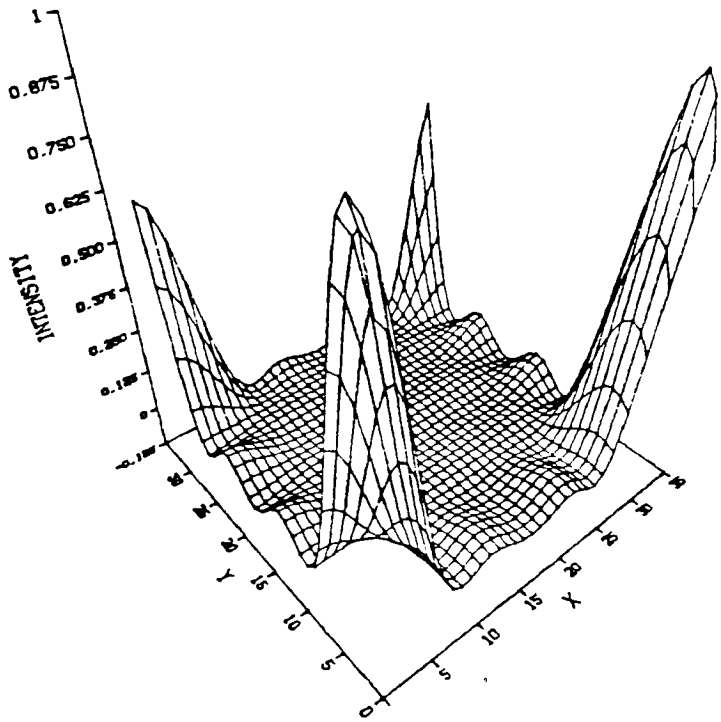

Figure 17a. Three-Dimensional Plot of Bispectrally-Reconstructed $Sinc^2(X/16,Y/16)$

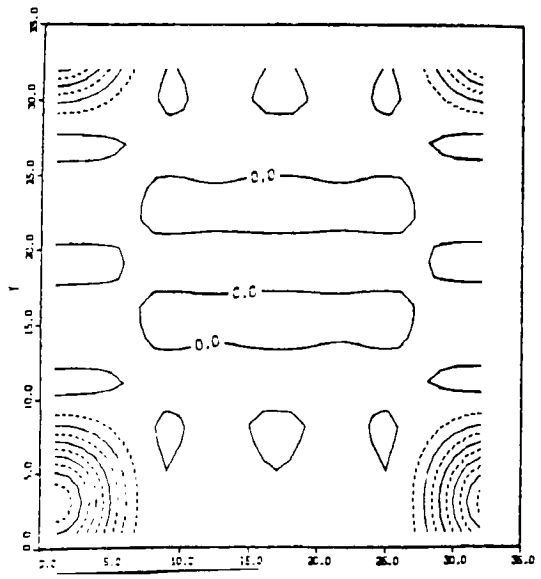

17b. Two-Dimensional Contour of (a)

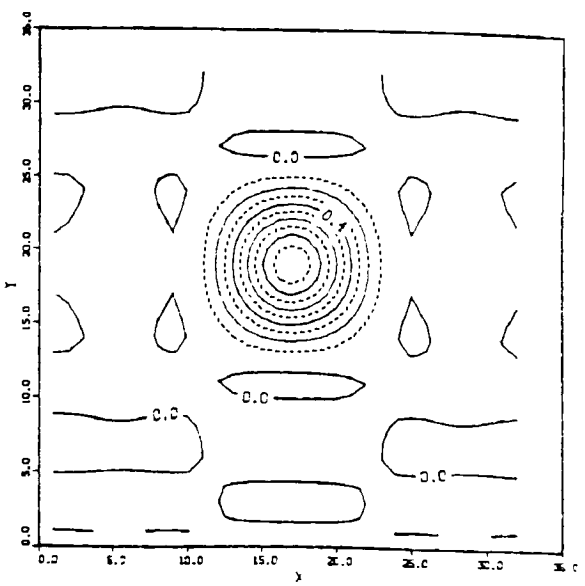

17c. Recentered Version of (b)

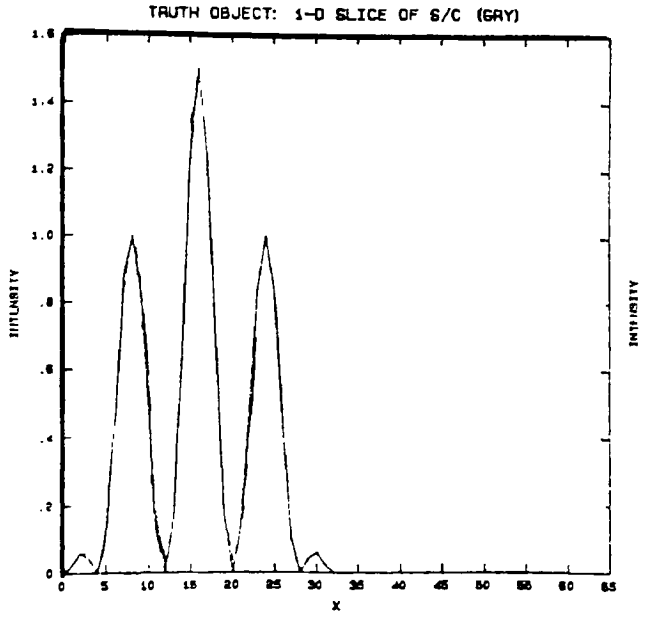

Figure 18a. One-Dimensional Truth Object

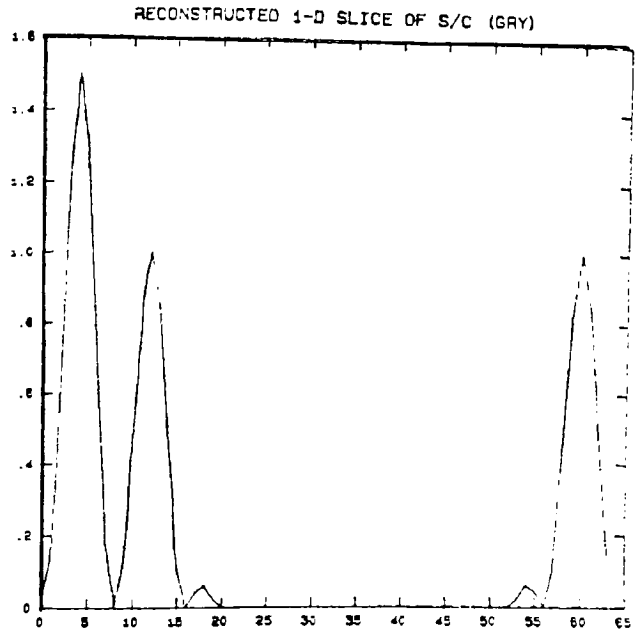

Figure 18b. Bispectrally Reconstructed Version of (a)

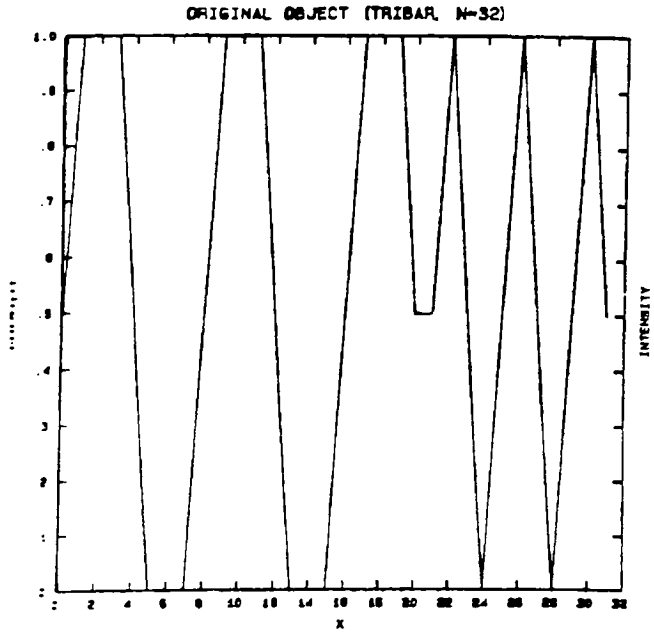

Figure 19a. One-dimensional Truth Object

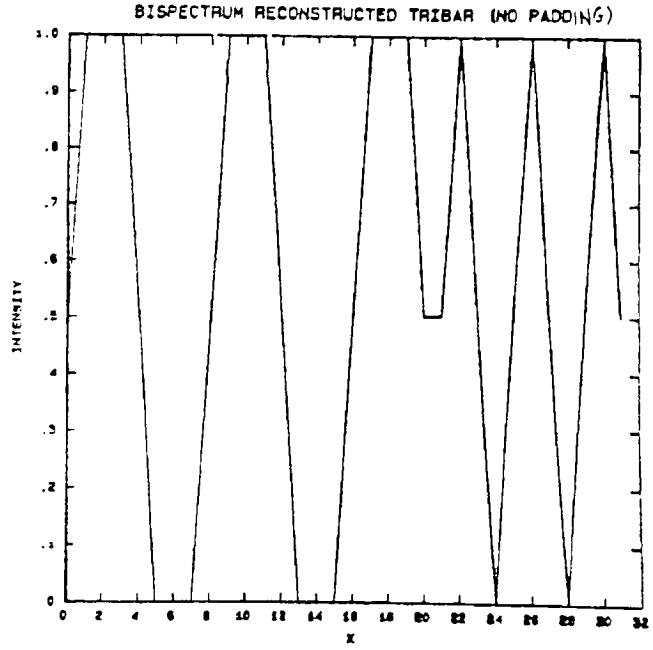

Figure 19b. Bispectrally Reconstructed Version of (a)

As we have seen, each Fourier quantity has both magnitude and phase since the Fourier expression is, in general, complex. Thus, I can write Equation 76 as:

$$G(\lambda) = |F(\lambda)||H(\lambda)|\exp\left[-j\{\Phi_F(\lambda) + \Phi_H(\lambda)\}\right] \tag{77}$$

But for a phase filter, $|H(\lambda)| = 1$ and Equation 76 is written as:

$$G(\lambda) = F(\lambda)\exp\left[-j\Phi_H(\lambda)\right] \tag{78}$$

If $\Phi_H(\lambda) = 2\pi\alpha\lambda$, then the output function, g(x) would merely be a shifted version of the input, since, by definition, $h(x) = \delta(x - \alpha)$ in Equation 75 (where δ is the Dirac delta function (Papoulis)):

$$g(x) = f(x) * \delta(x - \alpha) = f(x - \alpha) \tag{79}$$

There is no phase distortion, then, if the phase transfer function is a linear function of λ. Also, if $\Phi_H(\lambda)$ is a constant no phase distortion will occur (Gaskill). For example, if $\Phi_H(\lambda) = \frac{\pi}{2}$, the real-valued input becomes an imaginary-valued output. Similarly, for $\Phi_H(\lambda) = n2\pi$ (n is an integer), g(x) = f(x) and for $\Phi_H(\lambda) = (2n+1)\pi$, g(x) = -f(x). The 1-D tribar target of Figure 18a did not show a phase shift upon reconstruction probably because of the spatial frequency of the tribar was such that $\Phi_H(\lambda) = n2\pi$.

The importance of phase information cannot be overstated when reconstructing an object. In general, the magnitude gives you information regarding the *strengths* of the signal but the phase gives you information about the *structure* of the signal. Reconstructing an object merely from its Fourier magnitude is similar to taking the autocorrelation of the object (Goodman, 1985). This is the result of the square-law

detection aspect of image recording. As shown above, phase records the **location** of the image whereas the magnitude does not. A simple example of this is seen by the following three objects where (Dainty and Fienup):

$f(x,y)$ is the original object

$f(x - x_0, y - y_0)$ is the object shifted by x_0, x_0

$-f(x - x_0, y - y_0$ is the object shifted and reflected about origin.

All three objects have the same Fourier modulus but all 3 are not located at the same position or orientation. The phase problem becomes, then, as posed by Bates and McDonnell, does there exist more than one object belonging to the set of all possibilities for the phase? If the phase can be retained exactly, there is no ambiguity in the object reconstruction (Oppenheim, et al, 1982).

An illustration that compares the relative importance of phase versus magnitude for image reconstruction is given by Oppenheim and Lim (1981). They provide the example of the reconstruction of the atomic structure of a L–tyrosine HCL crystal image from its exact phase data. They compare three succeedingly worse cases for the magnitude: 1) magnitude of one; 2) magnitude equal to an average of several different L–tyrosine HCL atoms; and 3) magnitude from a totally different atom! In all cases the original L–tyrosine HCL atomic structure was reproduced from the correct phase but erroneous magnitude information.

For further proof of the importance of phase in reconstructing an object, I performed my own experiment using the truth objects of Figure 20a ("battleship") and Figure 20b ("Lena"). I combined the battleship's phase with Lena's magnitude and obtained Figure 21a. Similarly, I combined Lena's phase with the battleship's magnitude and created Figure 21b. Clearly, the phase is key when reconstructing an image.

Returning to the phase filter, if the recovered phase is distorted, the reconstructed object will be distorted. Phase distortion occurs when the "phase-filter" aspects of the operation cause the spectral components of the original signal to be misplaced from their original spacing (i.e., the amount of shift of the spectral components is not linear with increasing frequency (Gaskill)). When phase distortion occurs, you do not have the simple, shifted, delta function convolution described in Equation79 for integer values of α. This relationship is merely a special case of the more general result:

$$g(x) = f(x) * \mathrm{sinc}(x-\alpha) \tag{80}$$

where $\mathrm{sinc}(x) = \frac{\sin(\pi x)}{\pi x}$ (see Gaskill) and a delta function results at the limit (see Papoulis, p. 280-281). If $|\alpha| \leq \frac{1}{2}$ (Dianat and Raghuveer, 1990) then noninteger values of the phase filter exist and thus nonlinear increases in the phase shift occur. For values of $\alpha > \frac{1}{2}$ up to multiple integer values, the shift is merely a π or 2π phase shift and further distortion does not occur. The reconstructed object appears to be blurred by a convolution with a sinc function. Examples of this are seen in Figures 22 through 26.

Figure 20a. "Battleship" Used for Magnitude/Phase Comparison

Figure 20b. "Lena"

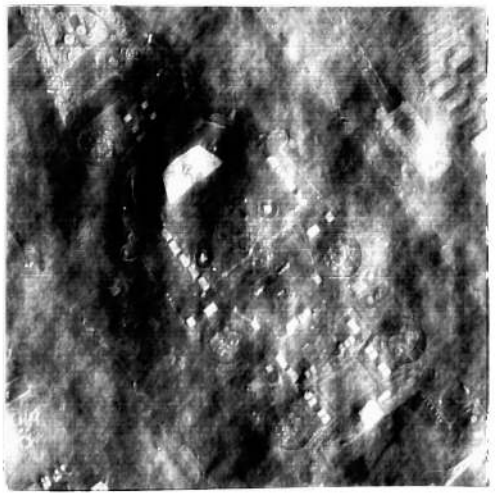

Figure 21a. Reconstructed Object Using "Battleship" Phase and "Lena" Magnitude

Figure 21b. Reconstructed Object Using "Lena" Phase and "Battleship" Maginitude

Figure 22a is the same tribar as in Figure 19a except that now it is zero-padded. Its reconstructed image is in Figure 22b. Notice that this image exhibits the phase shifting **and** the sinc blurring (which causes the negative-valued artifacts seen, for example, in Figure 17). For the 1-D case I removed the sinc blurring with data windows, which I will discuss shortly.

For 2-D images, the sinc blurring was much worse. I tried several different phase reconstruction algorithms (Dianat and Raghuveer, 1990; Swami and Giannakis, 1988) before settling on the one described previously and it still shows sinc blurring for certain constrained objects. For example, Figure 23a is a $\mathrm{tri}\left(\frac{x}{8},\frac{y}{8}\right)$ truth object reconstructed in Figure 23b. Notice the severe sinc blurring of the object. I now change the constraint of the object to be $\mathrm{tri}\left(\frac{x}{7},\frac{y}{7}\right)$ and the reconstructed object of Figure 24a is exact, save for the introduced phase shift. My shift-image program then recenters the object for viewing (Figure 24b).

Not only is object constraint a problem but also the object shape can cause sinc blurring in the reconstructed image. Figure 25a is what I call a "binary" spacecraft because its gray levels change value abruptly. Figure 25b is the reconstructed object. Notice that the sinc blurring has actually distorted the object and makes it appear noisy. Even for smoothly varying objects, such as my "gray" spacecraft of Figure 26a (so-called because there are several gray levels in the image that vary smoothly), you can see a ripple of sinc blurring in the reconstructed object (Figure 26b).

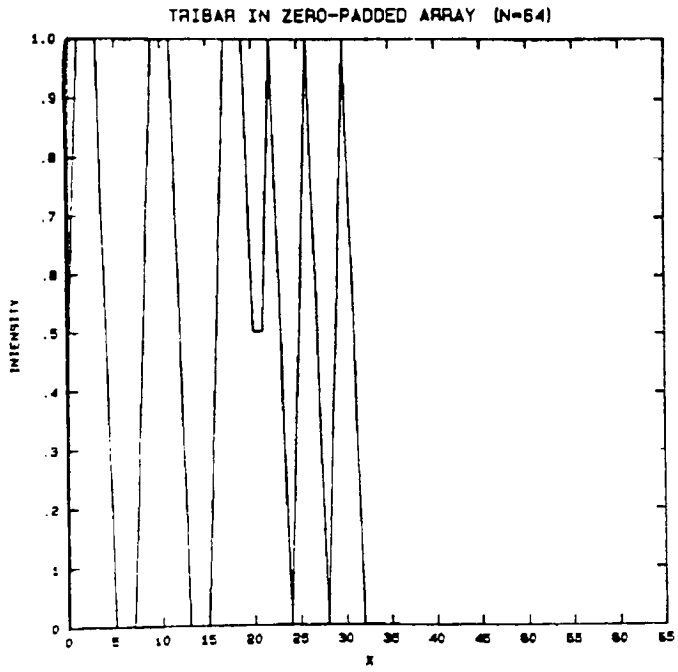

Figure 22a. Original Object

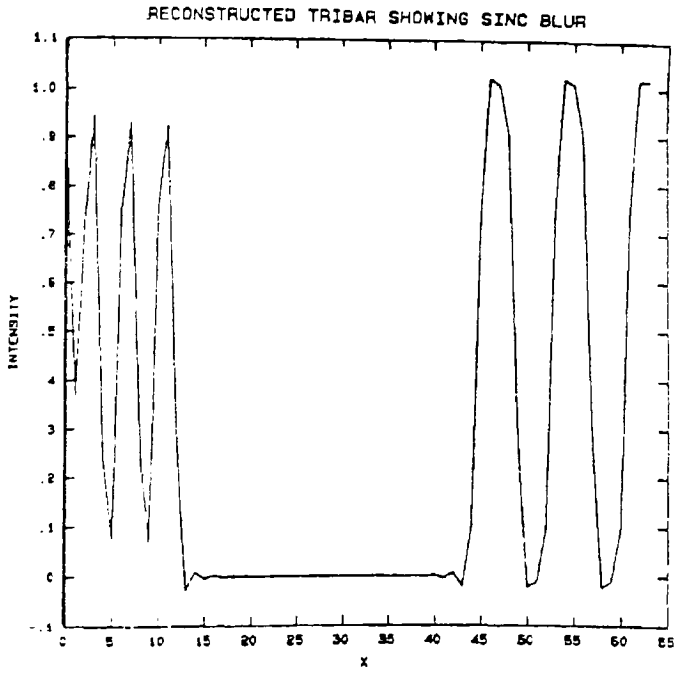

Figure 22b. Bispectrally Reconstructed Version of (a)

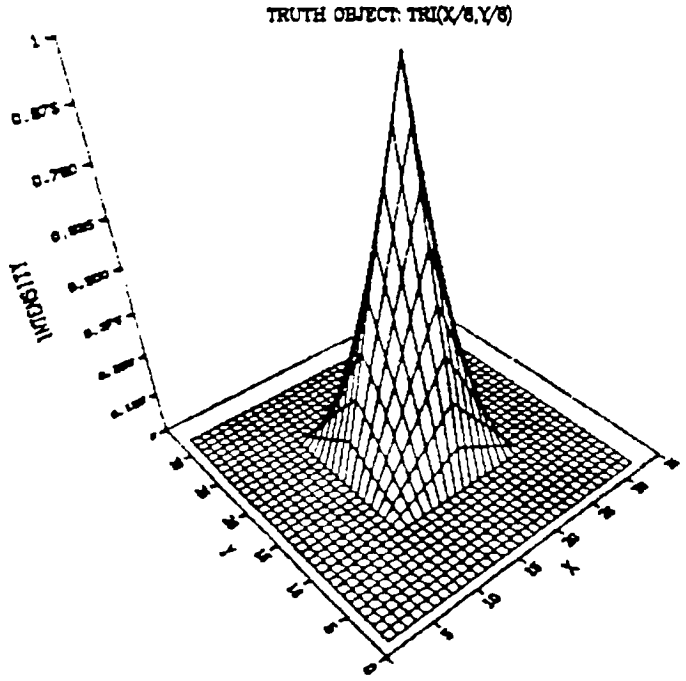

Figure 23a. Original Object

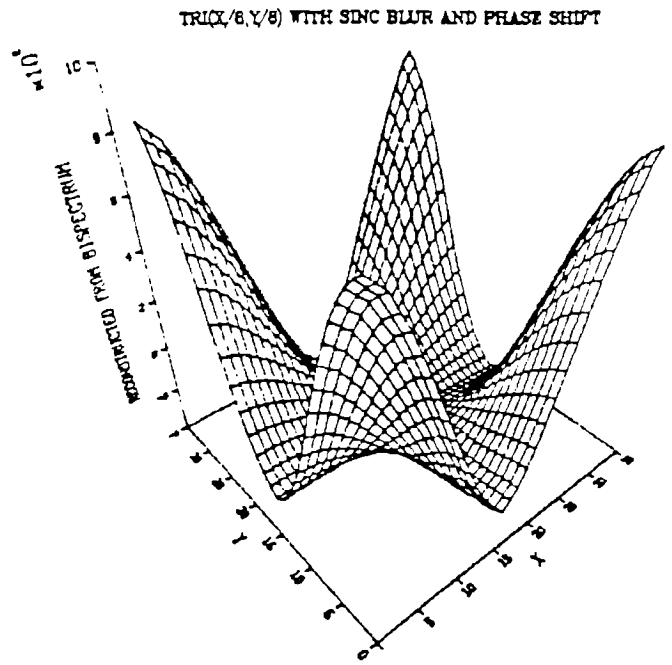

Figure 23b. Bispectrally Reconstructed Version of (a)

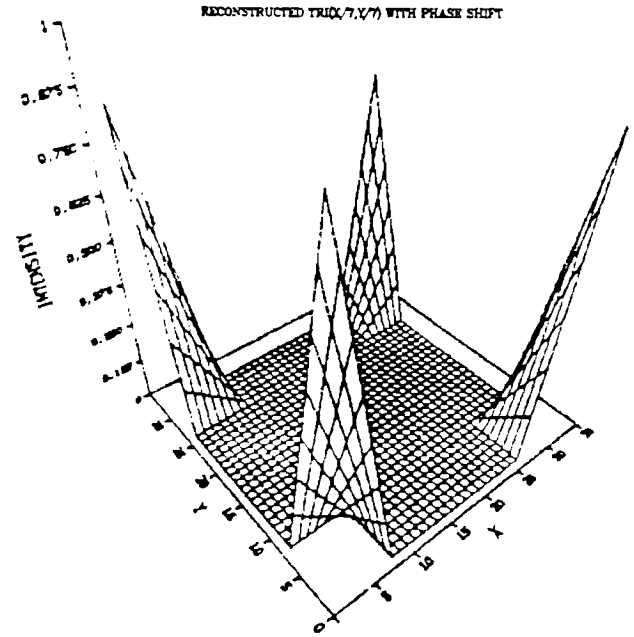

Figure 24a. Bispectrally Reconstructed Tri (X/7, Y/7)

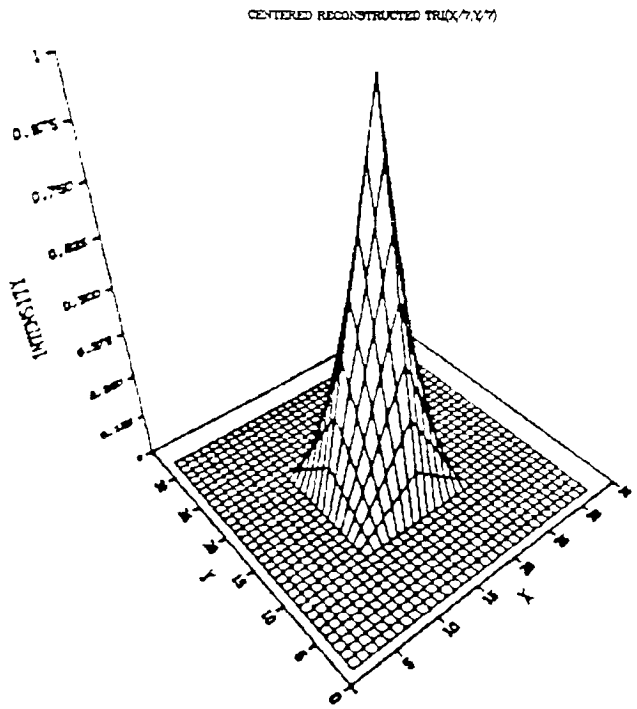

Figure 24b. Centered Version of (a)

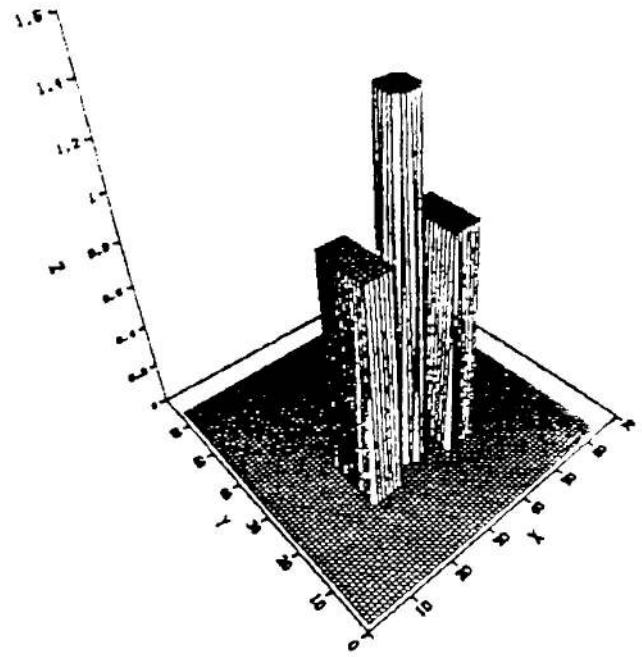

Figure 25a. Original Objects

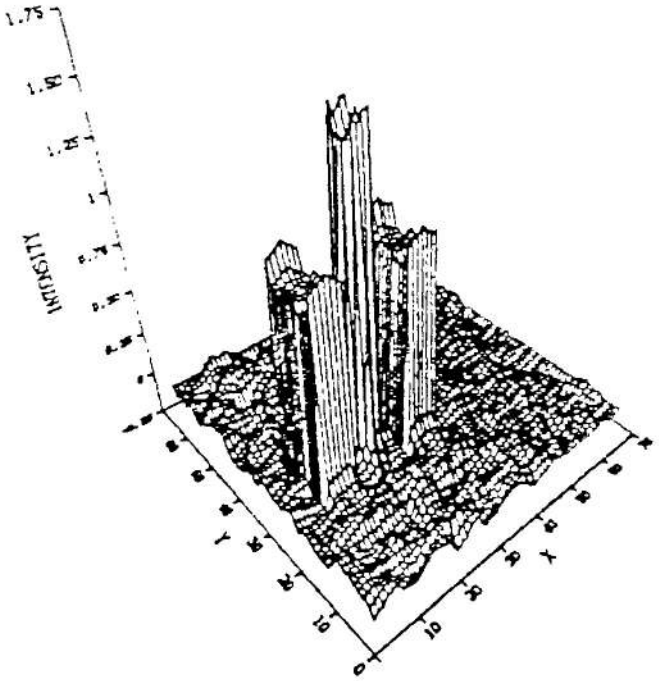

Figure 25b. Bispectrally Reconstructed Version of (a)

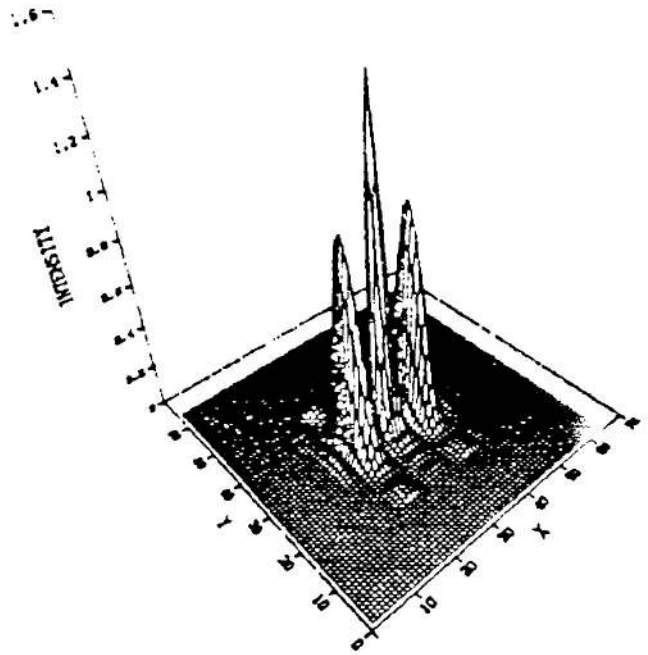

Figure 26a. Original Object

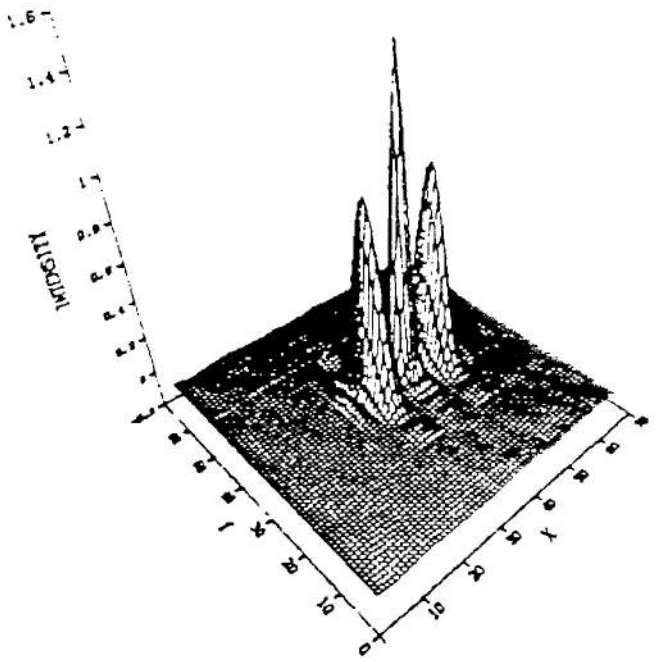

Figure 26b. Bispectrally Reconstructed Versions of (a)

One way to avoid the sinc blurring in the 2-D case was to use the 1-D algorithm and raster-scan the image before calculating its bispectrum. Figures 27a shows the binary spacecraft, its jittered representation is in Figure 27b from and the reconstructed object is in Figure 27c. Notice that there is no sinc blurring of the reconstructed image (I have recentered it after image reconstruction). No noise was present so there was no reconstruction problems when applying the 1-D raster-scan method to the 2-D image.

5.1.2 Windowing the Data

In the 1-D case certain bispectrum reconstructions resulted not only in sinc blurring but also in incomplete reconstructions, i.e., it would lead to an indeterminate condition (divide by zero). For the 1-D case, I believed these occurrences were happening because of errors in sampling the spectrum. This was because I noticed that whenever I zero-padded an array, the reconstructed object often had sinc blurring or it would not reconstruct at all. To overcome this, I decided to use data windows and they worked as advertised.

To review, data windows are used to relieve leakage or "ringing" artifacts when spectrum data is aperiodically sampled. Data windows help by forcing the sampled spectra to have a period of N extent (where N is the length of the data record) even though the object itself may have an aperiodic spectra. The formulas used for the data windows were taken from Stearns and David. In particular, I used the Bartlett (triangular) and the tapered rectangular data windows.

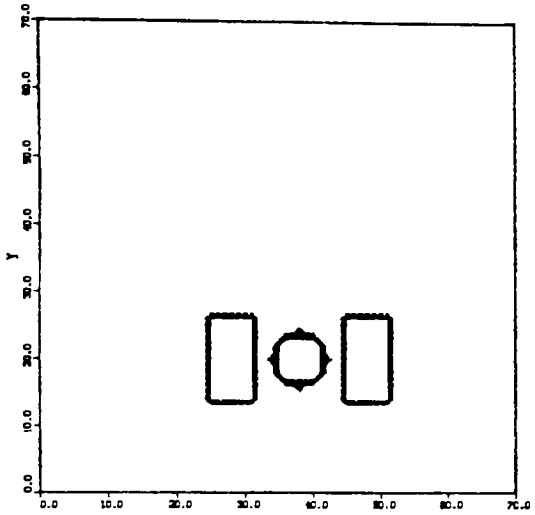

Figure 27a. Original Object

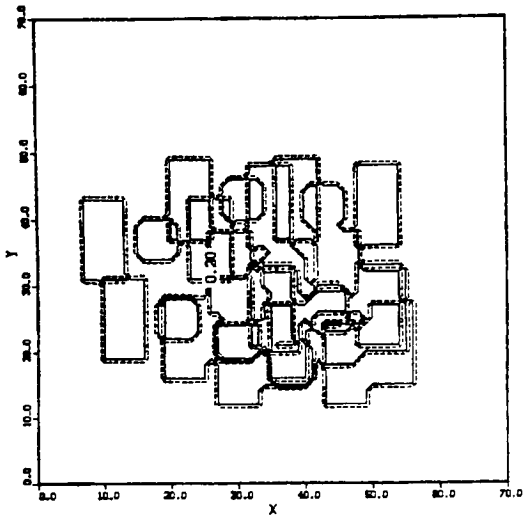

Figure 27b. Representative Object Jittered Randomly In The Field Of View For 10 Frames–No Noise

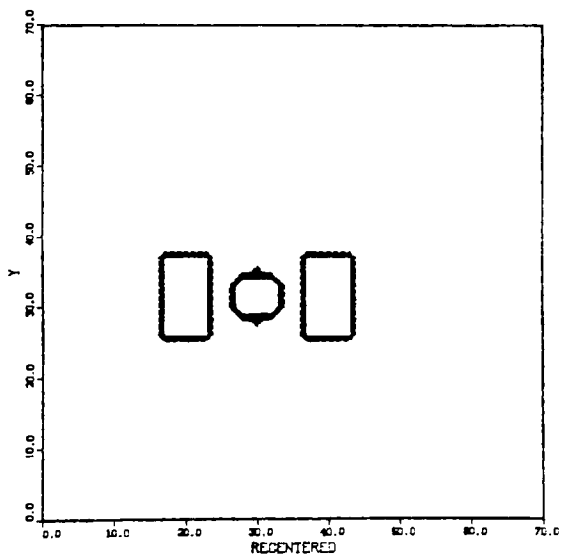

Figure 27c. Bispectrally Reconstructed Version of (a)

Figure 28 is an example of using a tapered rectangular window on the object in Figure 22a before calculating its bispectrum. Compare this result to that of Figure 22b. This implies to me that the sinc blurring in the 1-D case is actually ringing due to aperiodic sampling and not the same phenomenon seen in the 2-D reconstruction.

Figure 29a is an example of an object that would not reconstruct with the 1-D algorithm unless a data window was used. By using a tapered rectangular window, though, I obtained the reconstructed object of Figure 29b. I noticed that if a certain type of object is constrained to some factor of 2 submultiple of N $\left(\frac{N}{2}, \frac{N}{4}, \frac{N}{8}, \text{etc.}\right)$, then it would not reconstruct at all, either. Figure 30a is an example of this object and Figure 30b is its reconstructed shape after windowing by a Bartlett window. In all cases where an indeterminate reconstruction arose, data windowing allowed for its reconstruction (though the window function is visible in the reconstruction).

Finally, in the 1-D case, objects placed in very large data records (1X256, 512, 1024, etc.) would not reconstruct but give an indeterminate condition unless data windows were used.

I attempted to use data windowing in the 2-D reconstruction but was never successful in removing the sinc blur. Thus, I conclude that the cause of the sinc blur is more fundamental in the 2-D case then mere aperiodic sampling errors. It appears that, since my 2-D phase reconstruction algorithm only samples the two lowest spatial frequency bispectral subplanes [(1,0),(0,1)], I have bandlimited the result to these lower spatial frequencies. Higher spatial frequencies present in the recon-

structed image would give me sharper edges and not the sinc-blurred edges I am getting now.

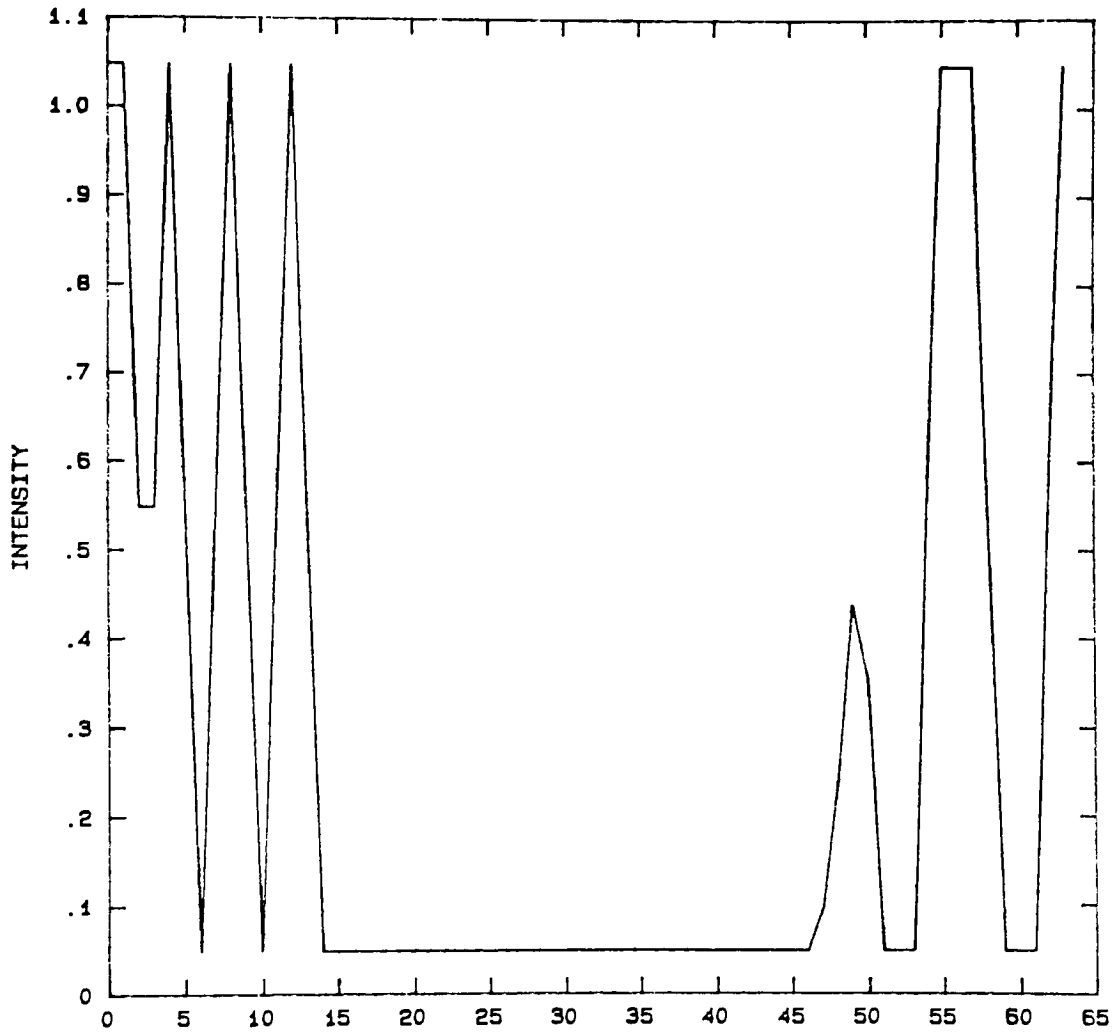

Figure 28. Bispectrally Reconstructed Padded Tribar with Data Window

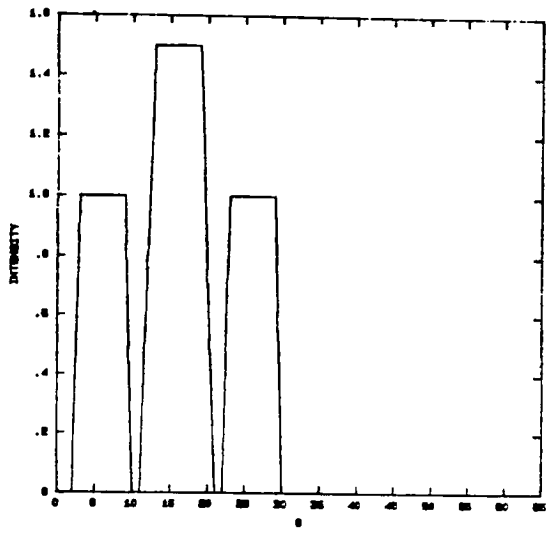

Figure 29a. Original Object

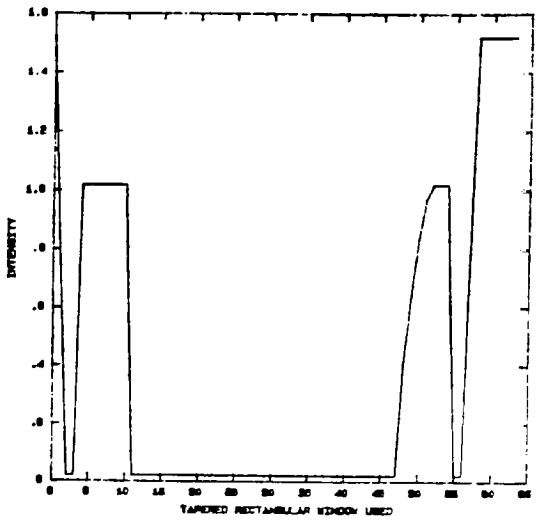

Figure 29b. Bispectral Reconstruction of (a) Using a Data Window

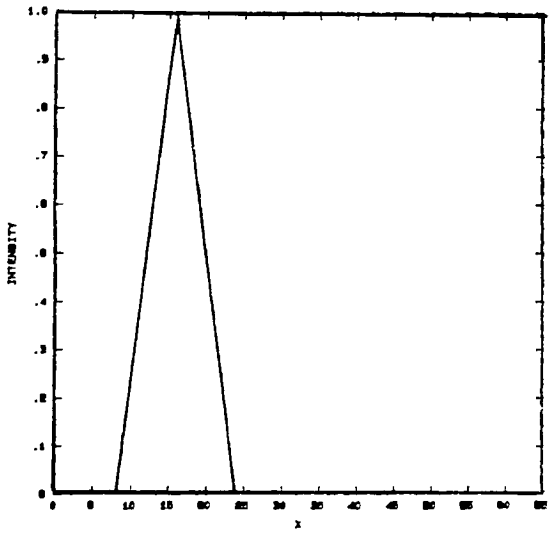

Figure 30a. Original Object

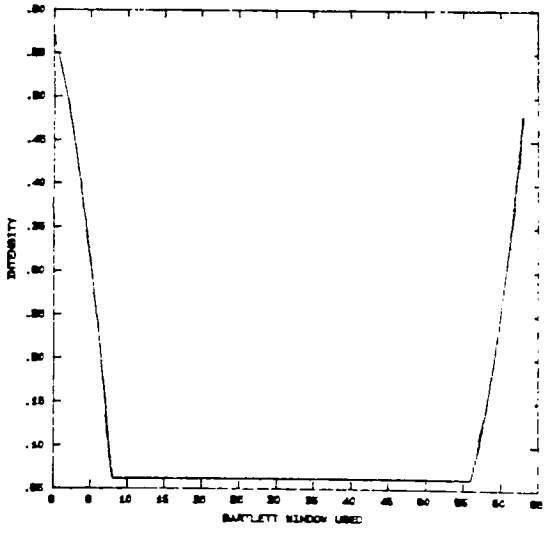

Figure 30b. Bispectral Reconstruction of (a) Using a Data Window

5.2 Speckled

To begin the speckled section I should review at the outset the flow of the processing that I performed to reconstruct a speckled object. Before I do that I will briefly discuss it. The overall methodology will be, in general, the same whether using the1-D or 2-D bispectrum algorithm.

The truth object is created and stored in an array that does not change. For a selected number of images, M, each one is speckled independently using one of the speckle algorithms. The speckled object varies from frame-to-frame by using a different random number seed to create the speckle for each frame. I then randomly jitter the speckled object in x and y for each frame. This models image capture. I then perform a homomorphic transformation before I Fourier transform the image. I then calculate the bispectrum of this function and sum it with previously calculated values. Once all images have been summed, I normalize the resultant function and calculate the Fourier magnitude and phase from their respective 1-D or 2-D algorithms. Combining these quantities and inverse transforming, then exponentiating that result, gives the final answer. A median filter is included, if desired. See Appendix C for the flow diagram of this entire procedure.

As noted previously several times, the MLE of an undegraded version of the speckled image is the ensemble average of the multiple speckled images. To find the MLE of the undegraded image using multiple observations of the multiplicative noise model, I can write:

$$g_k(m,n) = I(m,n)\,u_k(m,n) \tag{81}$$

where the values take the same meaning as Equation 34 except that it is the k^{th} estimate for N observations (k=1,2,3.....,N). Performing the homomorphic transformation, I get:

$$\ln (g_k(m,n)) = \ln (I(m,n)) + \ln (u_k(m,n)) \tag{82}$$

From Raghuveer, let these values equal, respectively,:

$$Z_k = \theta + n_k \tag{83}$$

To find the MLE, I want to maximize the probability that the N observations produce the original object. For N independent observations I can write:

$$p(\underline{z}|\theta) = p(z_1|\theta)\,p(z_2|\theta)\,p(z_3|\theta)\,.....\,p(z_N|\theta) \tag{84}$$

where $\underline{z}$ is a vector. Looking only at one observation, I can express it in terms of $n_1 = z_1 - \theta$ as:

$$p(z_1|\theta) = p(n_1) = p(z_1 - \theta) \tag{85}$$

From the pdf for the logarithm of the intensity, I can be write:

$$p(z_1 - \theta) = \exp\left[-(z_1 - \theta) - \exp\left[-(z_1 - \theta)\right]\right] \tag{86}$$

therefore, for all N observations, taking the logarithm of Equation 86 gives:

$$\ln (p(z_k - \theta)) = \sum_{k=1}^{N} \left(-(z_k - \theta) - \exp\left[-(z_k - \theta)\right]\right) \tag{87}$$

$$\ln(p(z_k - \theta)) = \sum_{k=1}^{N} z_k + N\theta - \sum_{k=1}^{N} \exp\left[-(z_k - \theta)\right] \tag{88}$$

differentiating this with respect to θ and setting it equal to zero gives:

$$N = \exp[\theta] \sum_{k=1}^{N} \exp[-z_k] \tag{89}$$

returning to the original definitions, I can substitute in for θ and z_k and divide by N to get:

$$I(m, n) = \frac{1}{N} \sum_{k=1}^{N} g_k(m, n) \tag{90}$$

Thus, averaging N observations of the noisy image will provide the MLE of the degraded image. This result is similar to the result given by Lim and Nawab (1981) except they kept the noise expression in the non-logarithmic domain during the proof.

To see what this implies for image reconstruction, notice the speckled version of a sinc^2 seen in Figures 31a and b, both in 2-D and 1-D, respectively. Figures 32a and b are the resultant images after 150, independently-speckled images were ensemble averaged. Notice that you do not reconstruct the image to obtain Figure 9 but, hopefully, to see what the object was in the first place! This is a result of the severe image degradation caused by the fully-developed speckle.

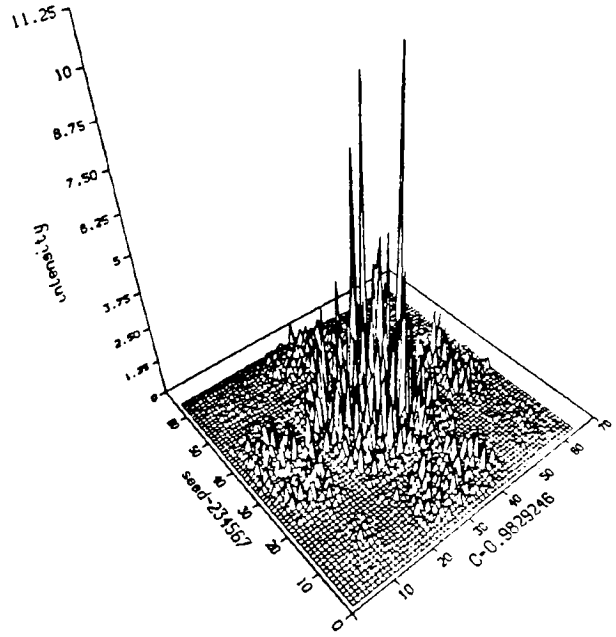

Figure 31a. Three-Dimensional Plot of Speckled $Sinc^2(X/16,Y/16)$

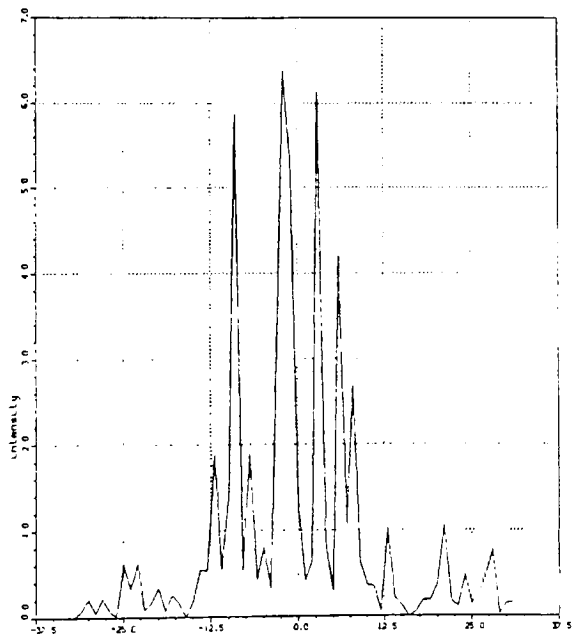

Figure 31b. One-Dimensional Slice of (a) DDM Used

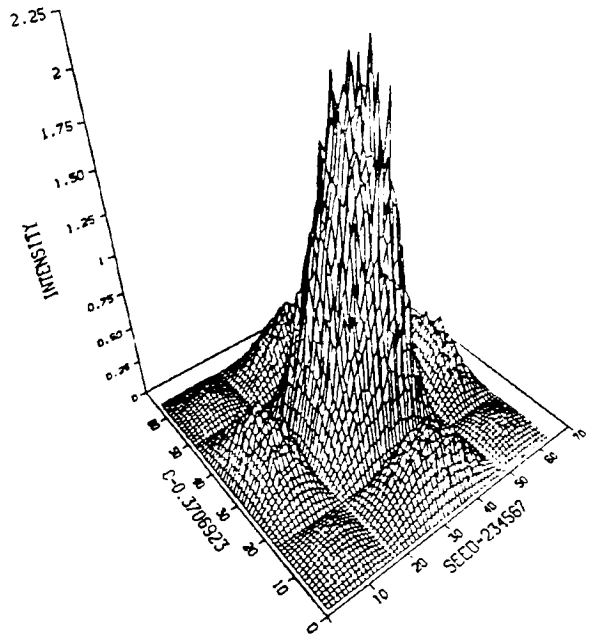

Figure 32a. Ensemble-Averaged Version of Figure 31a After 150 Frames

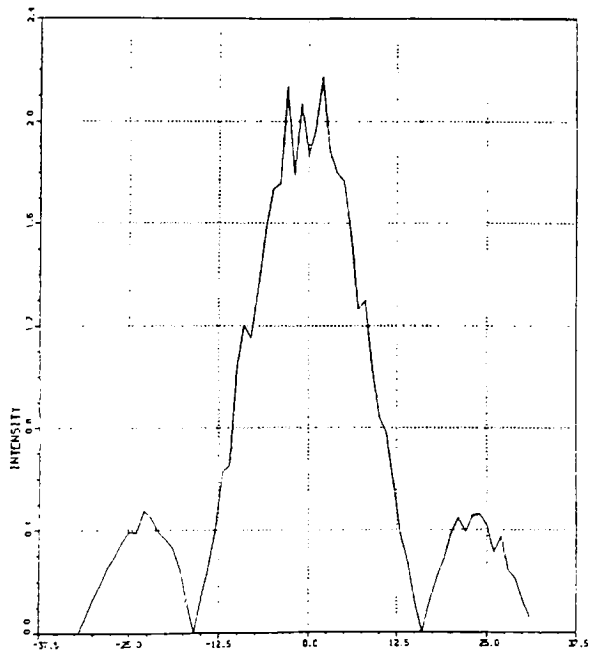

Figure 32b. One-Dimensional Slice of (a)

5.2.1 One-Dimensional Examples

The first example used showing image reconstruction is found in Figures 33a-g. Figure 33a is the truth object and Figure 33b is a typical speckled object before the bispectrum routine begins. The DDM was used to speckle the object. Figure 33c is the ensemble averaged reconstruction of the jittered images and Figure 33d is the reconstructed object after 200 images were bispectrum averaged. Figure 33e is the object after a 1X3 median filter has passed over the reconstructed image. Figure 33f is the reconstructed object if no homomorphic transformation is taken. As one can see, no object reconstruction will occur for speckled objects unless the natural logarithm is taken first. Figure 33g is the reconstructed object after only 30 images were bispectrum averaged, showing how rapidly bispectral averaging can converge to a solution.

One reason the bispectrum rapidly converges to a solution is shown in Figures 34a-c. Figure 34a is the natural logarithm of a $\text{sinc}^2(x/8)$ function. Wherever the real function goes to zero I set its density domain representation to -150. Figure 34b is the log of the speckle intensity shown in Figure 33b. Notice how the noise now appears to "ride" on top of the function, essentially improving the SNR of the resultant image. Figure 34c is the bispectrally averaged estimate of the speckled image prior to exponentiation (which then gives Figure 33d). Notice how the noise has smoothed considerably.

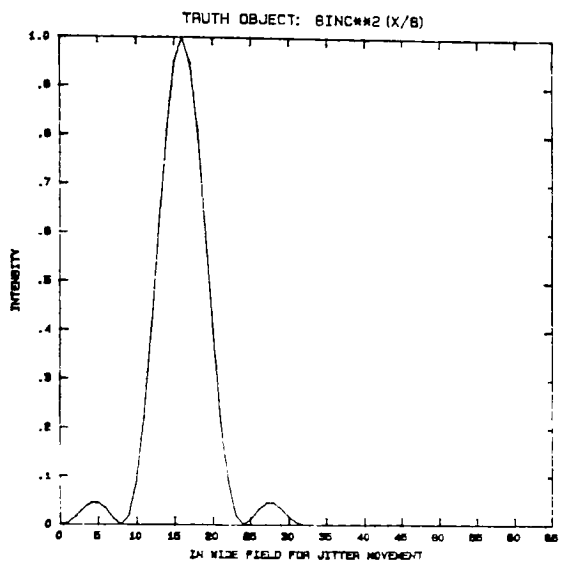

(a)

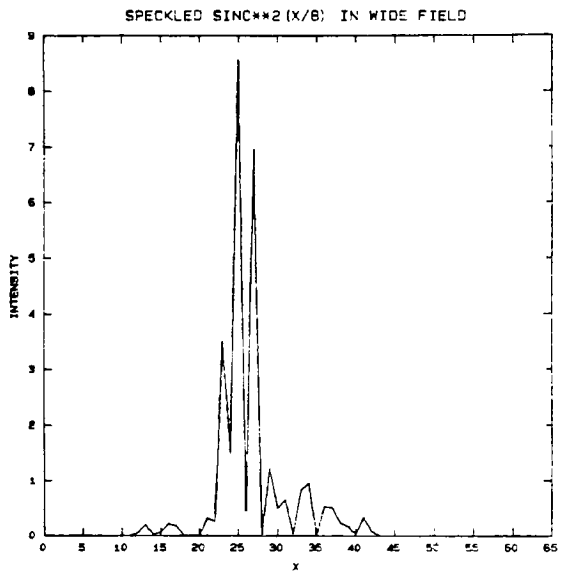

(b)

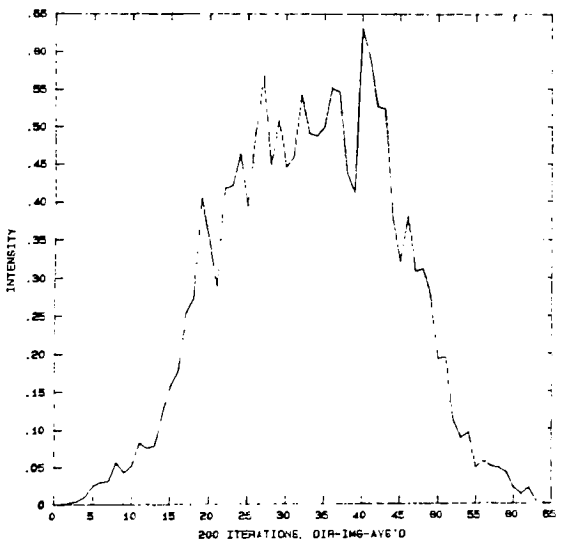

(c)

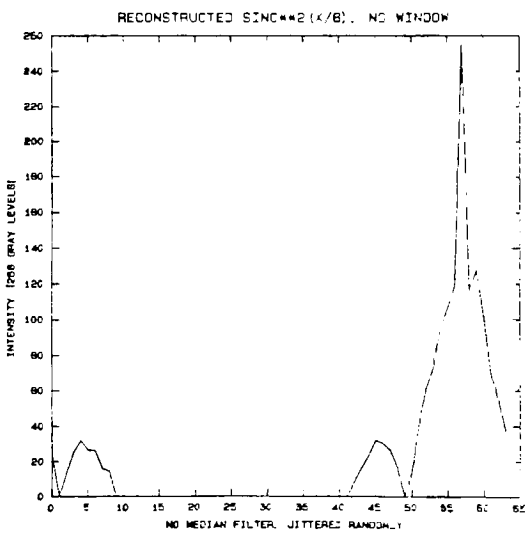

(d)

Figure 33a-d. Example of Bispectral Averaging of Jittered, Speckled Objects

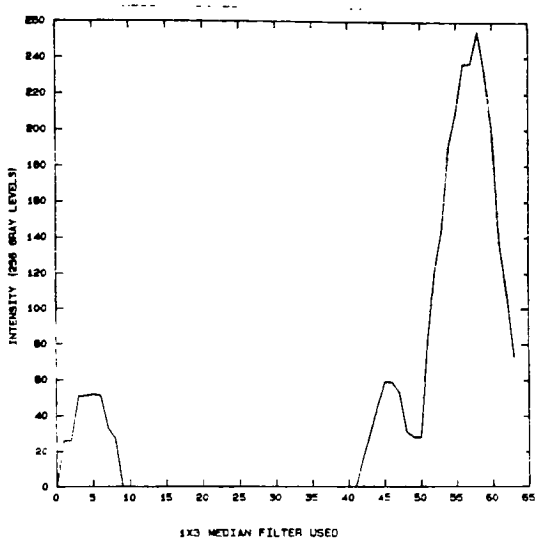

(e)

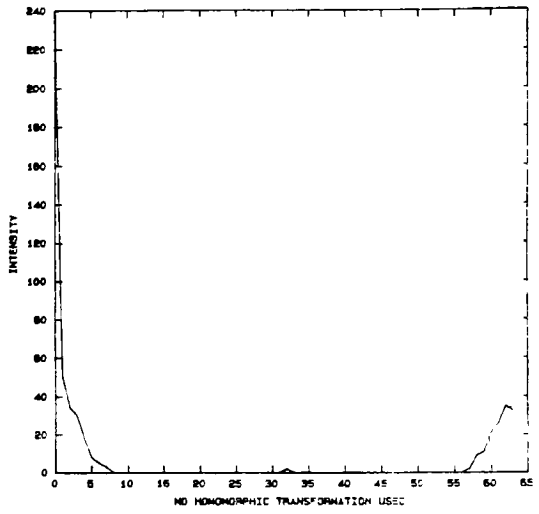

(f)

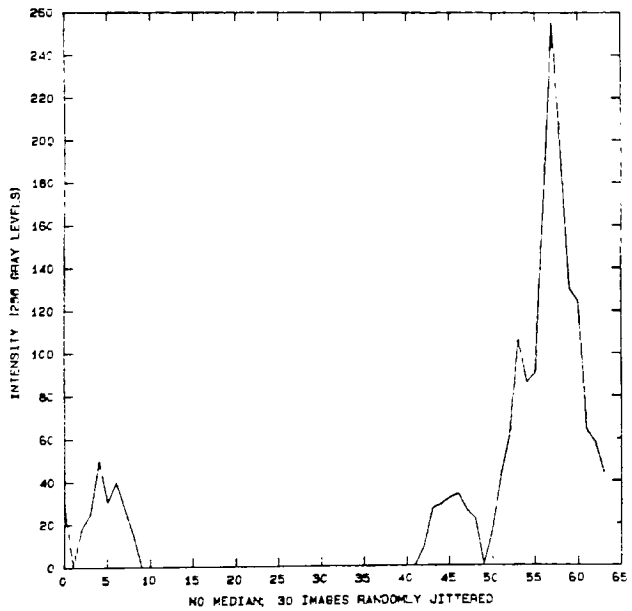

(g)

Figure 33e-g. Example of Bispectral Averaging of Jittered, Speckled Objects (Cont'd)

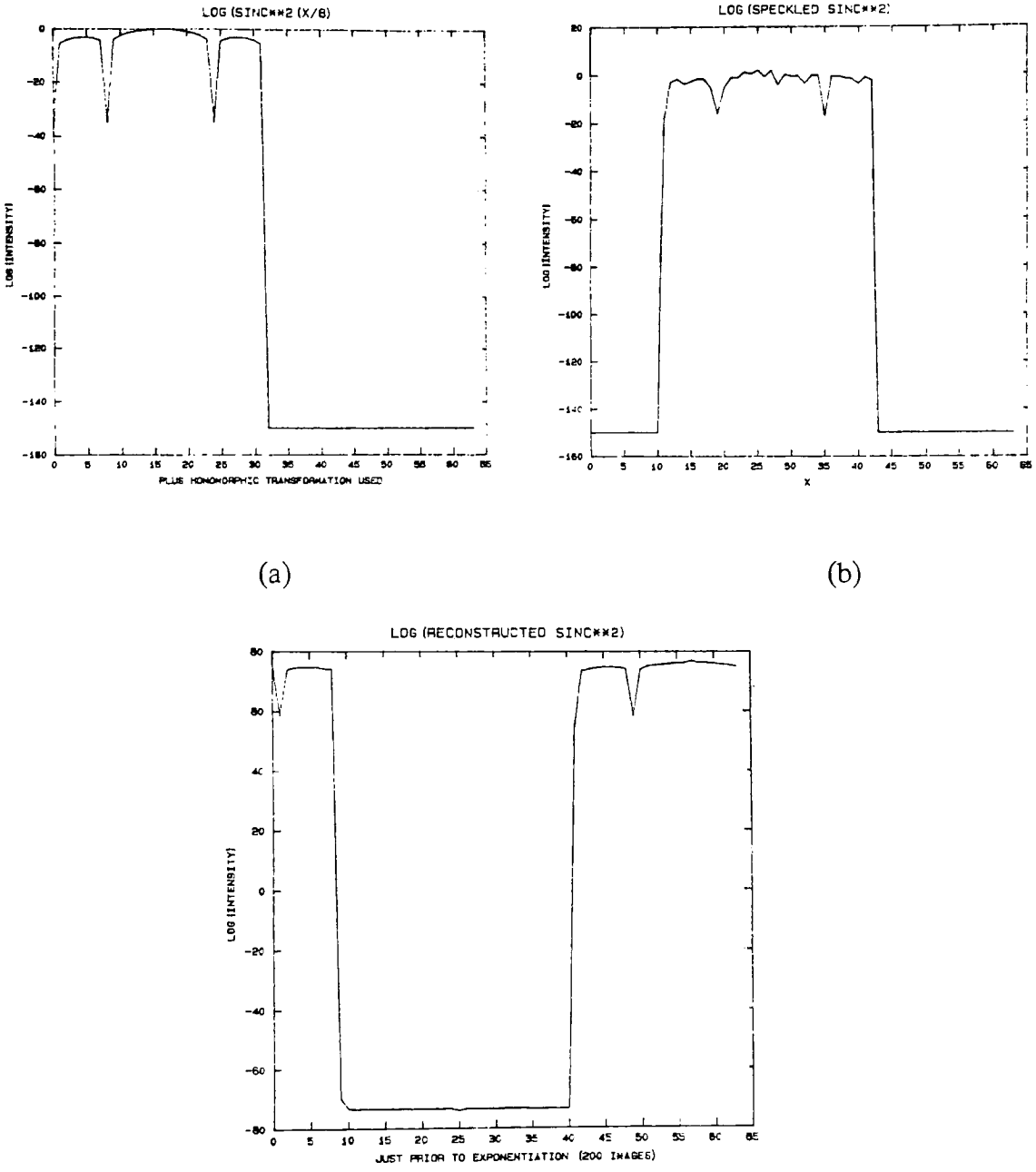

Figure 34a-c. Result of Bispectral Averaging an Object in its Logarithmic Domain

Another reason the bispectrum can handle speckled images is seen in Figures 35a–f. I use the same $sinc^2$ again but with no zero padding so as to view the results better. I show the logarithmic representation but I also include the Fourier transform of the log of the speckle intensity (Figure 35f). Compare this to Figure 35e. Thus, the bispectrum, which uses the function in Figure 35f to obtain its values, basically sees a very close approximation of the original object when processing in this domain (the Fourier of the log domain).

The next three sets of Figures use a tri(x) object to describe three key points. Figures 36a–f show a non-jittered object with its bispectrally-averaged rendition. Notice that, even using the ensemble average (Figure 36c) I only get a form of the tri back. Figure 36d is what a 1X3 median filter would do if used directly on Figure 36b. Figures 36e–f are the bispectrally reconstructed image without and with the median filter, respectively.

The next set of Figures (37a–e) are of a tri that is jittered randomly in a wider field 200 times. Since averaging is done in the bispectral domain, the shifting is ignored by the bispectrum and reconstruction occurs (Figures 37c–d). Figure 37e shows the result if no homomorphic transformation occurs.

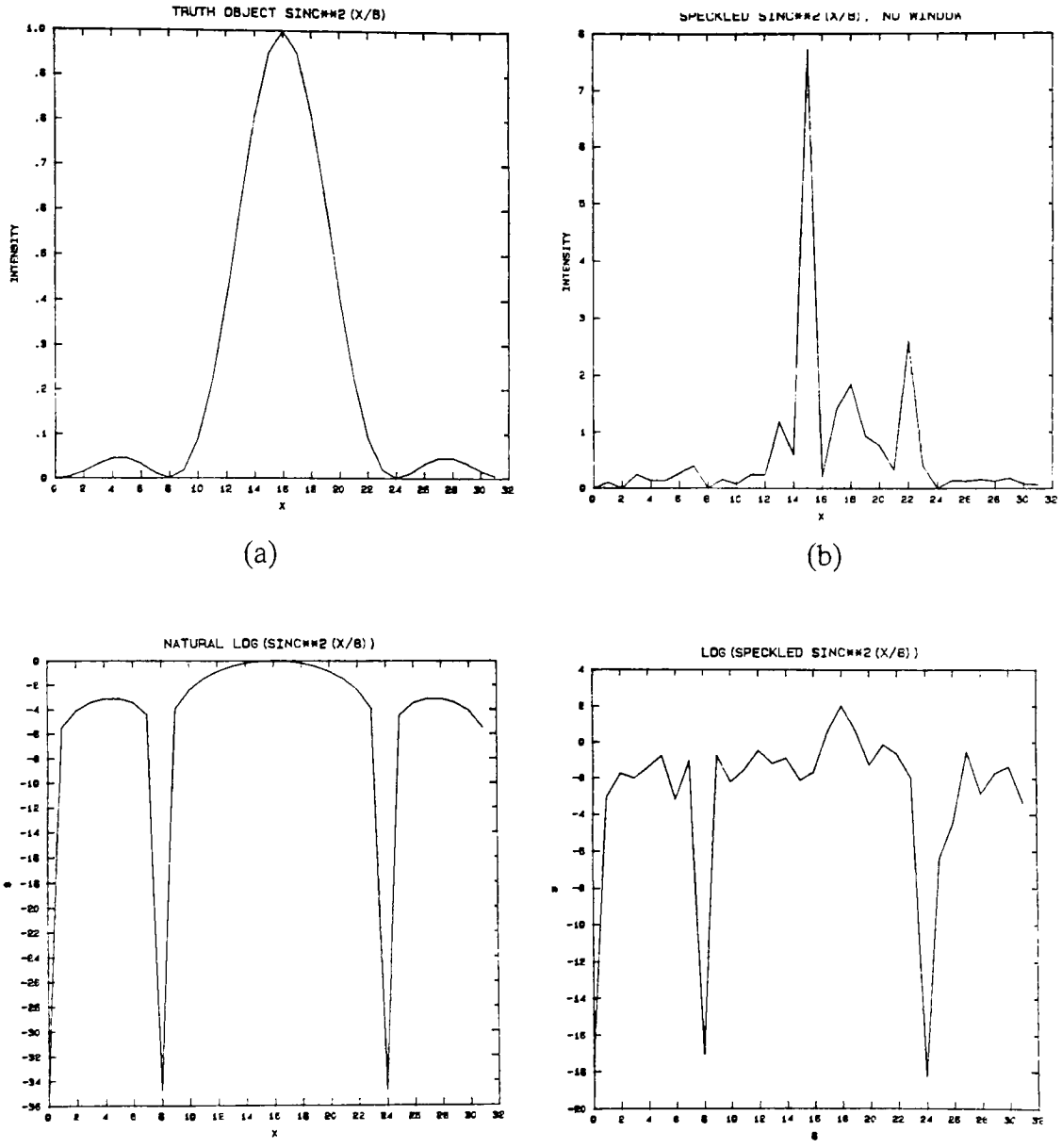

Figure 35a-d. Comparison of the Fourier Representation of a Speckled Object with its Unspeckled Version

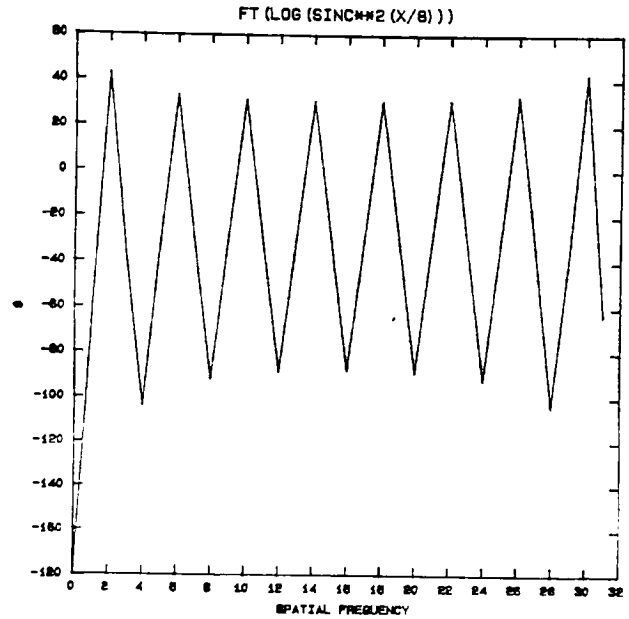

(e)

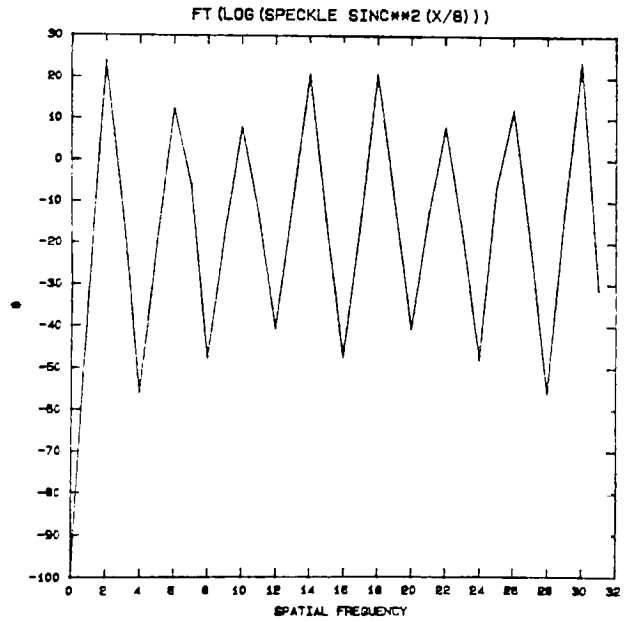

(f)

Figure 35e-f. Comparison of the Fourier Representation of a Speckled Object with its Unspeckled Version (Cont'd)

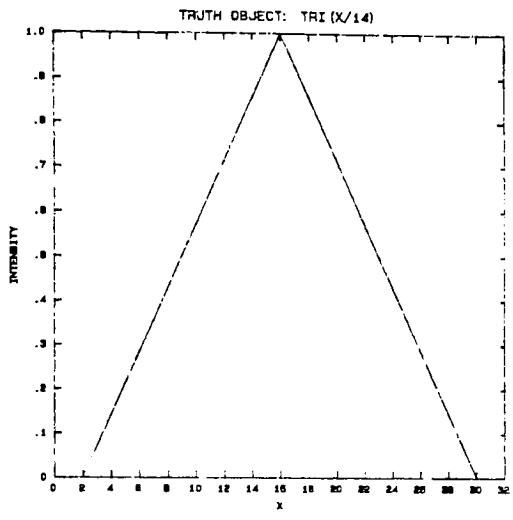

(a)

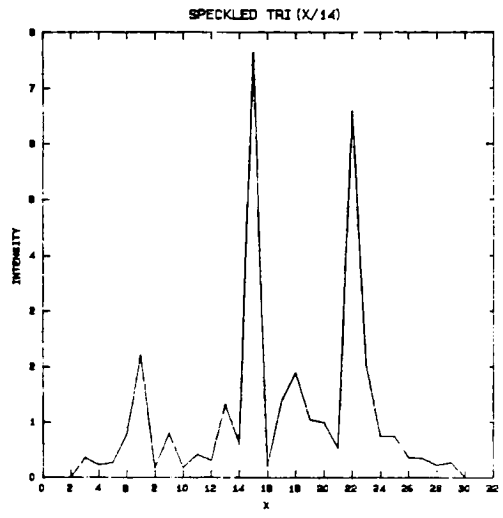

(b)

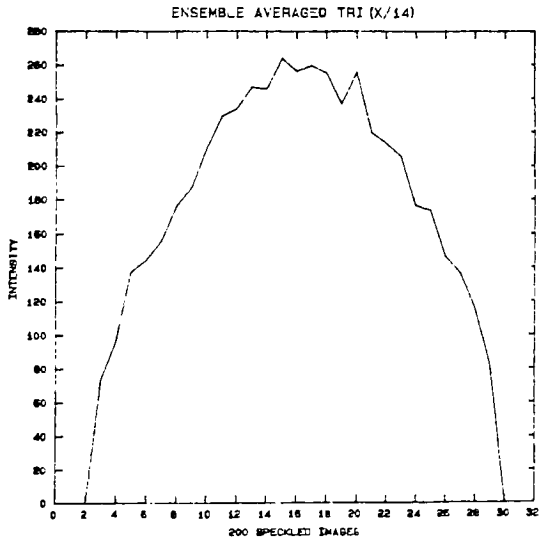

(c)

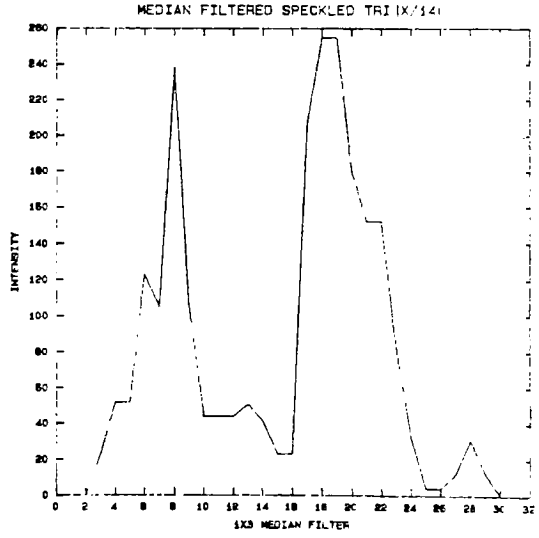

(d)

Figure 36a-d. Example of Bispectral Averaging of Speckled Object

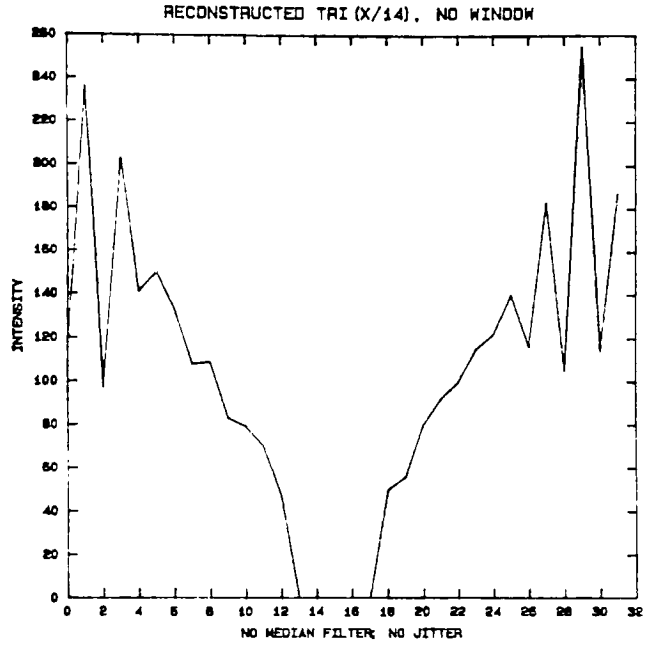

(e)

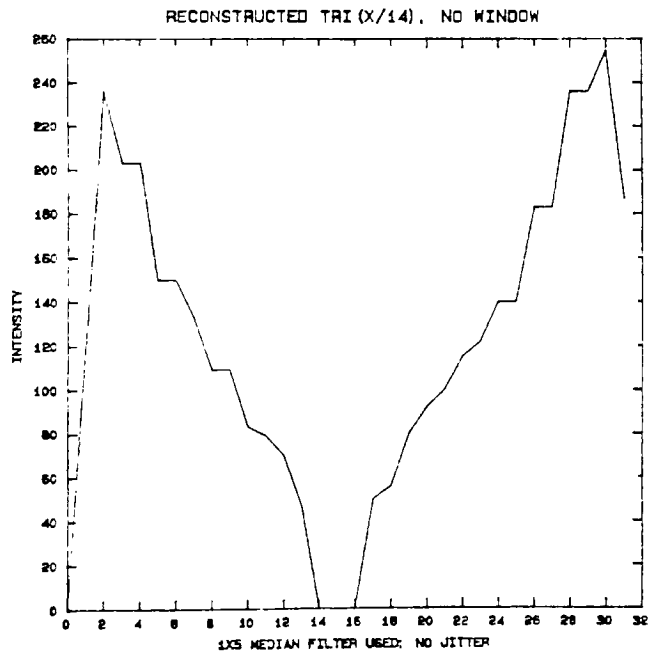

(f)

Figure 36e-f. Example of Bispectral Averaging of Speckled Object (Cont'd)

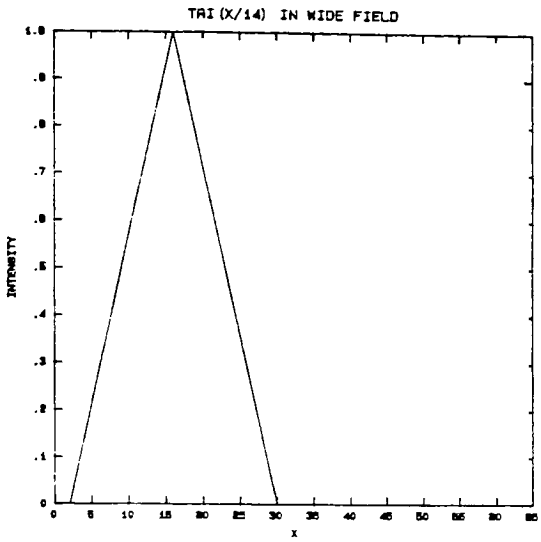

(a)

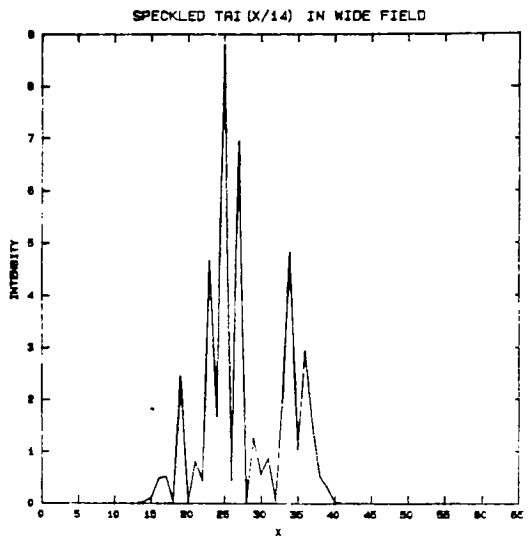

(b)

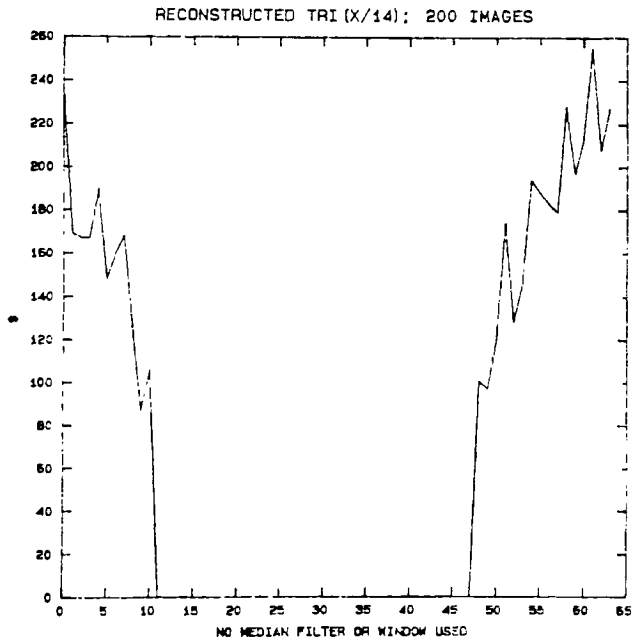

(c)

Figure 37a-c. Example of Bispectral Averaging of Jittered, Speckled Object

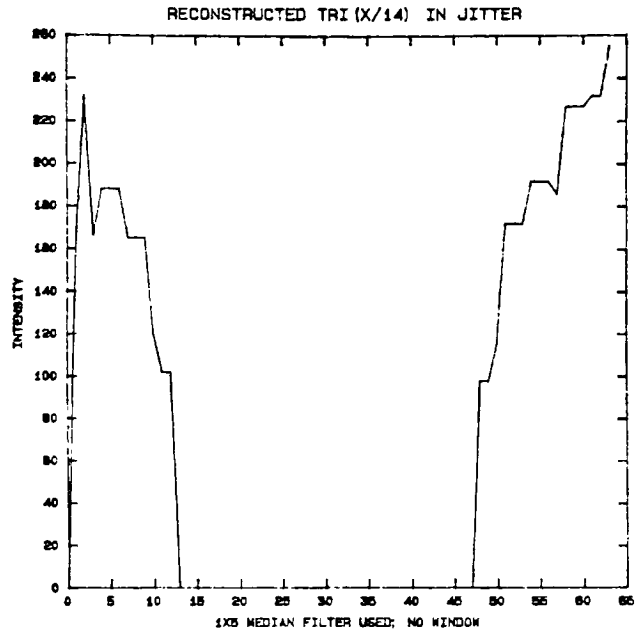

(d)

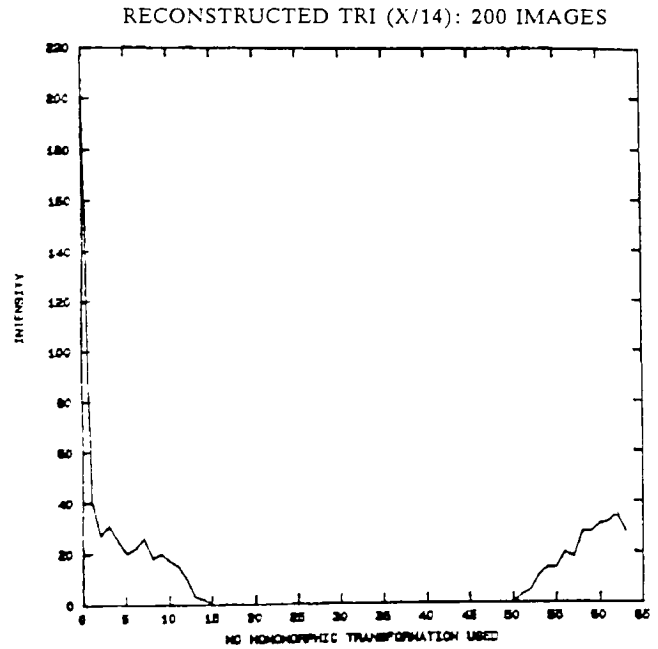

(e)

Figure 37d-e. Example of Bispectral Averaging of Jittered, Speckled Object (Cont'd)

The third set of Figures (38a–e) show why bispectral averaging works for the tri. The log of the speckled tri (Figure 38b) has such an improved SNR (visually) than the speckled version. After averaging (Figure 38c), the noise is considerably smoothed. Figure 38d is the Fourier transform of the log of the tri. Compare this to Figure 38e: there is no difference! For the scale factors used, the noise is practically nonexistent in this domain. This is what the bispectrum sees when it is being calculated.

Finally, Figures 39 and 40 are speckled and reconstructed versions of Figures 18a and 22a, respectively. Notice how well we can discriminate the form of these objects which was lost in the speckle (see Korwar and Pierce, (1981) for a discussion of this loss of discrimination) after bispectral averaging.

5.2.2 Two-Dimensional Examples

I was so pleased with the results of the 1-D algorithm that I decided to extend it to 2-D images. To do this, I would raster-scan the 2-D image, after jittering and speckling, to reconstruct the object. Before attempting this, though, I tested the 1-D algorithm on Figure 41a, which is the object "E" jittered in a "smearing" action (Figure 41b). Figure 41c is the result: perfect reconstruction!

I then tried it on a very small amount of additive Gaussian noise. It is so small (variance ± 0.003 about the image) that you can barely see it on a 3-D plot (Figure 42a). After 32 iterations, an "E" results that is slightly distorted (Figure 42b). By 150 iterations, the noise is gone and the original image results (though it is phase-shifted) (Figure 42c).

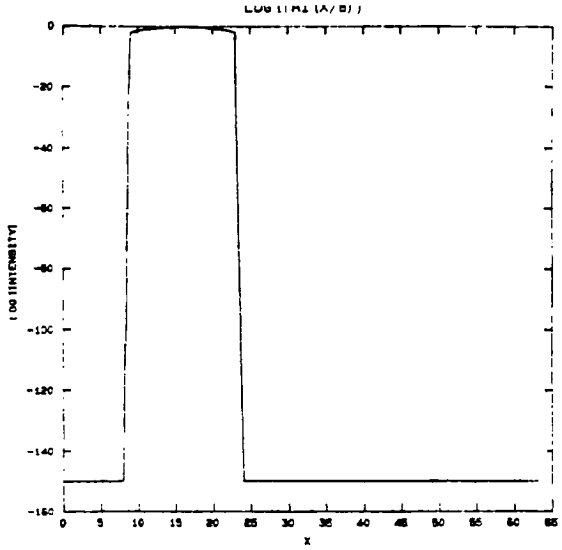

(a)

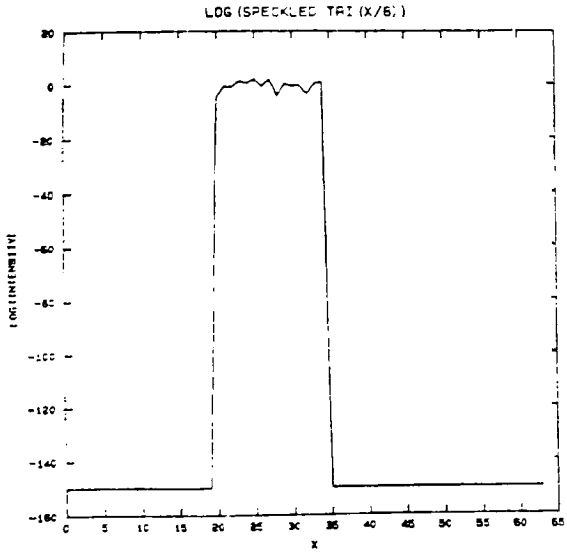

(b)

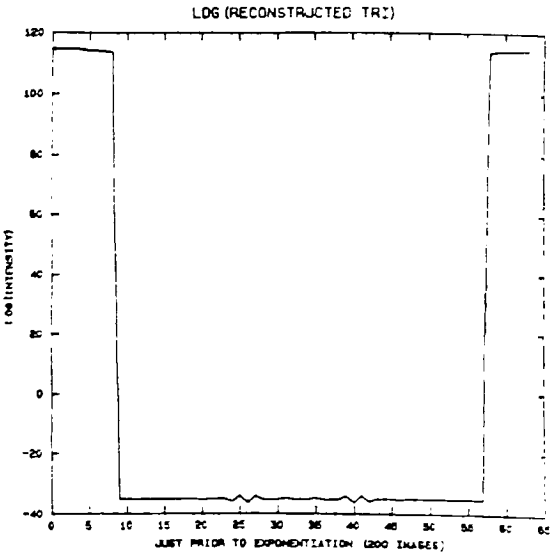

(c)

Figure 38a-c. Bispectral Reconstruction in Logarithmic Domain and Fourier Comparison of Speckled Object with Original Version

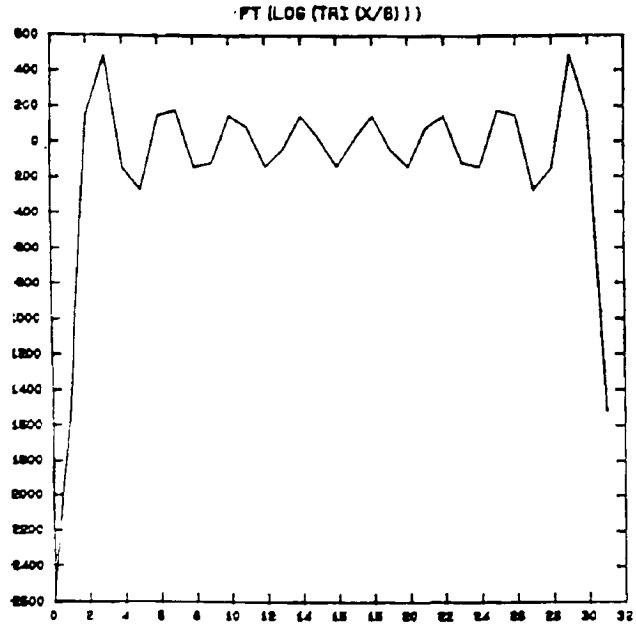

(d)

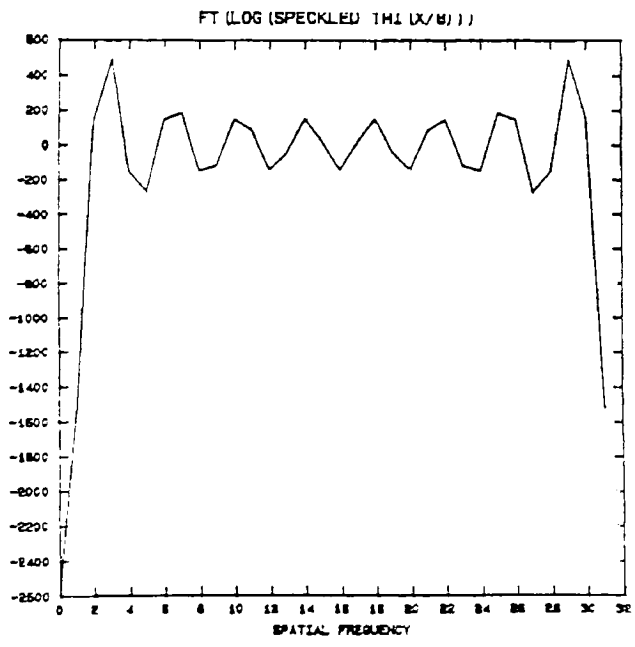

(e)

Figure 38d-e. Bispectral Reconstruction in Logarithmic Domain and Fourier Comparison of Speckled Object with Original Version (Cont'd)

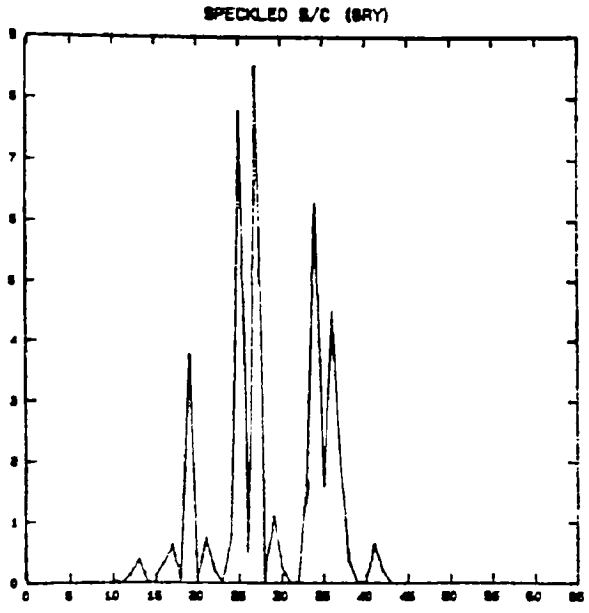

(a)

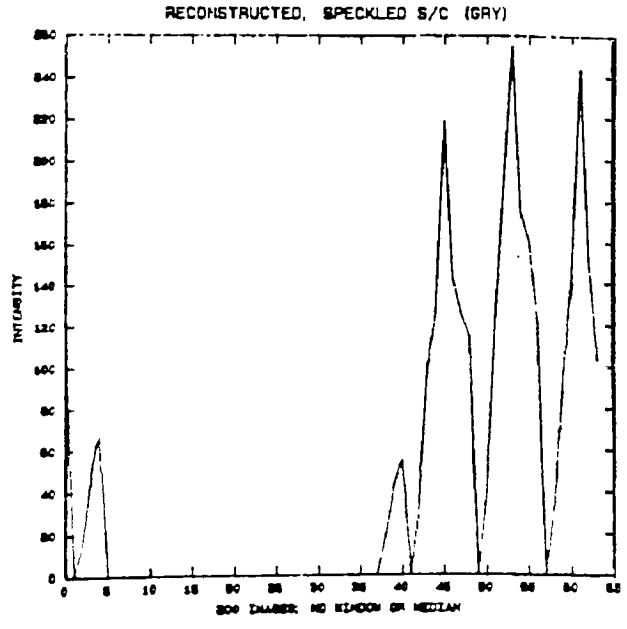

(b)

Figure 39a-b. Bispectral Reconstruction of Speckled Object

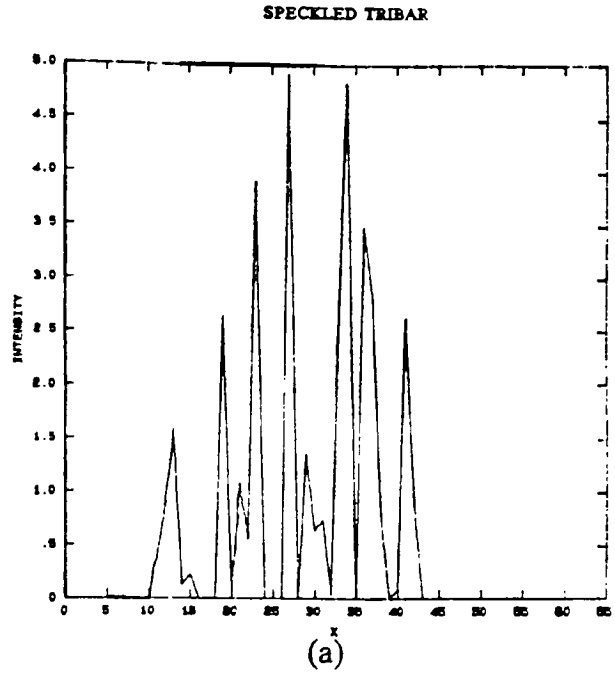

(a)

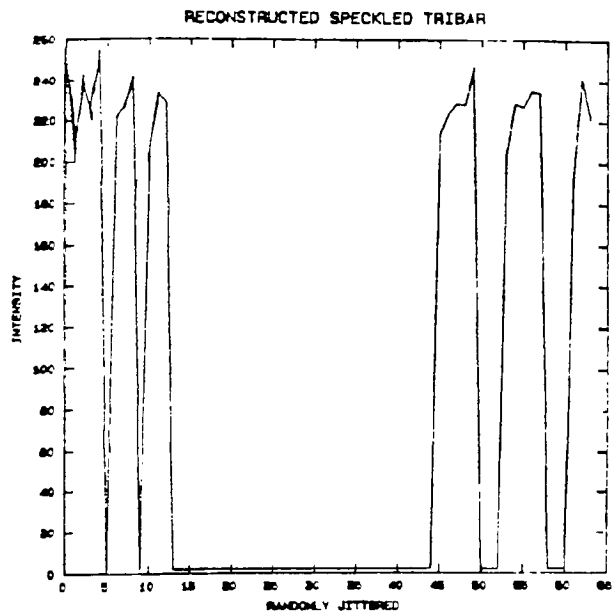

(b)

Figure 40a-b. Bispectral Reconstruction of Speckled Object

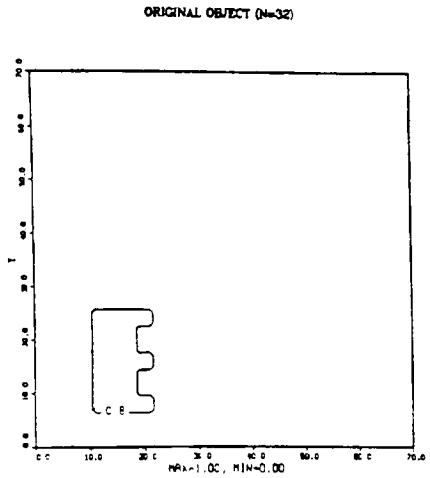

(a)

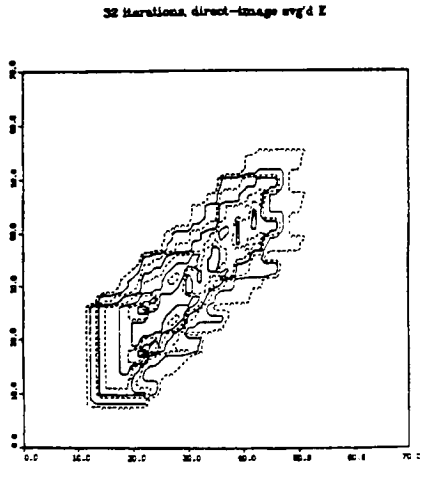

(b)

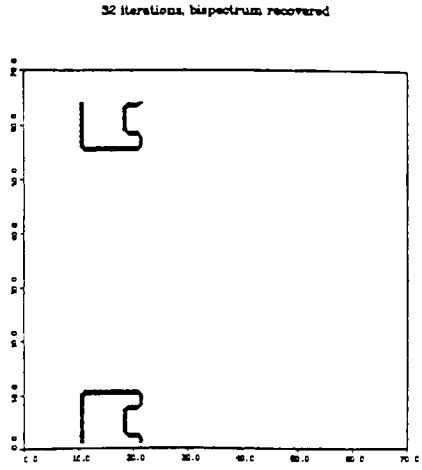

(c)

Figure 41a-c. Bispectral Reconstruction of 2-D Object Using 1-D Algorithm - No Noise

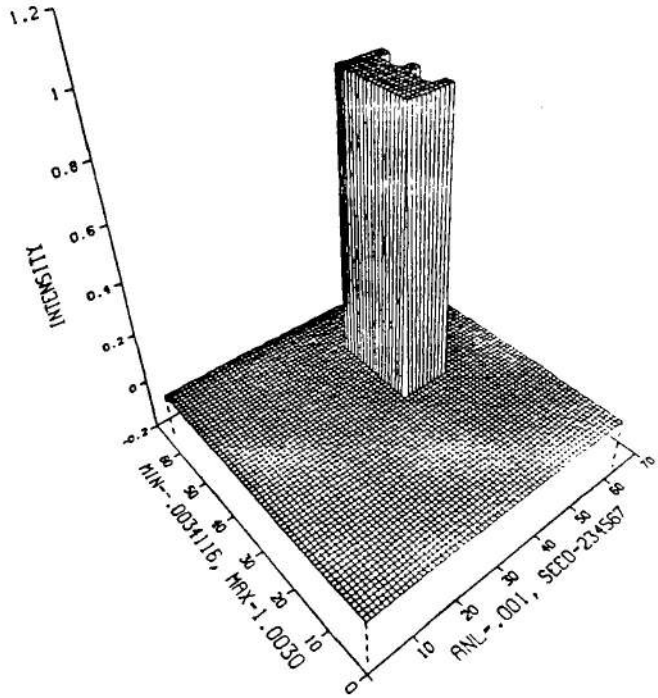

(a)

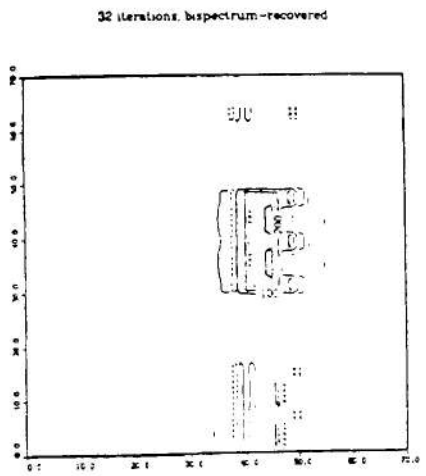

(b)

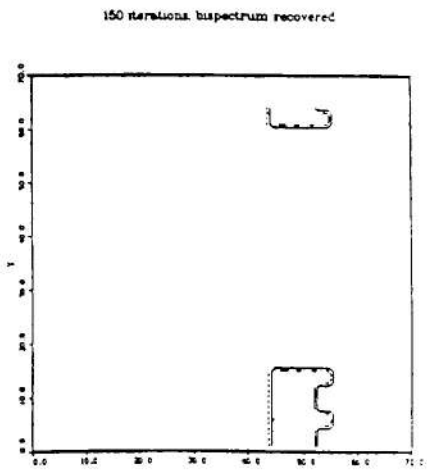

(c)

Figure 42a-c. Bispectral Reconstruction of 2-D Object Using 1-D Algorithm - Additive Gaussian Noise (Variance = 0.001)

I next increased the variance of the zero mean, additive Gaussian noise to 10X the previous value to see the results. Figure 43b is the result: unrecognizable reconstruction! When noise was present, a 2-D extension of the 1-D algorithm was not possible. This is due to the phase errors propagating throughout the reconstruction algorithm from the recursion formula used. Larger noise means larger phase errors.

Obviously, speckle was an even worse problem than this so I had to find a 2-D algorithm to work on 2-D images. That 2-D algorithm, developed previously in this thesis, was used on these 2-D images.

Figure 44a is the speckled version of Figure 27a using the CWM with a contrast of 1.053862. Figure 44b shows 30 speckled images ensemble-averaged together. Figure 44c is the reconstructed object after 30 images were bispectrally averaged, and Figure 44d is the same image but with a median filter passed over the image.

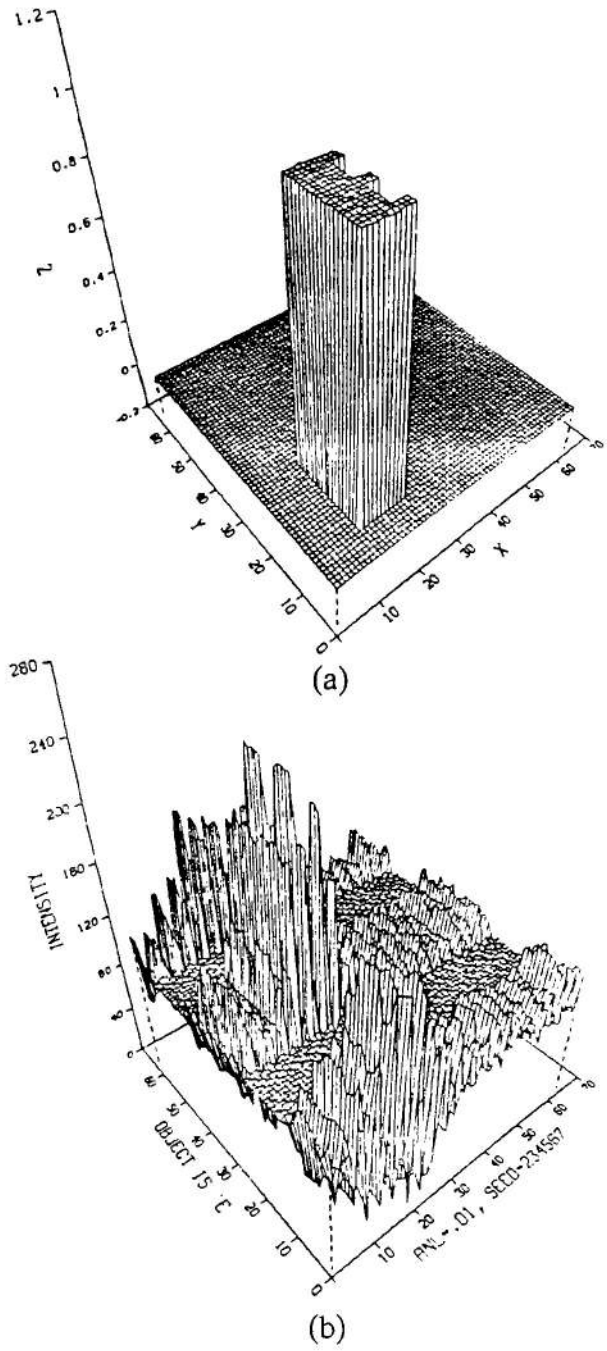

Figure 43a-b. Bispectral Reconstruction of 2-D Object Using 1-D Algorithm - Additive Gaussian Noise (Variance = 0.01)

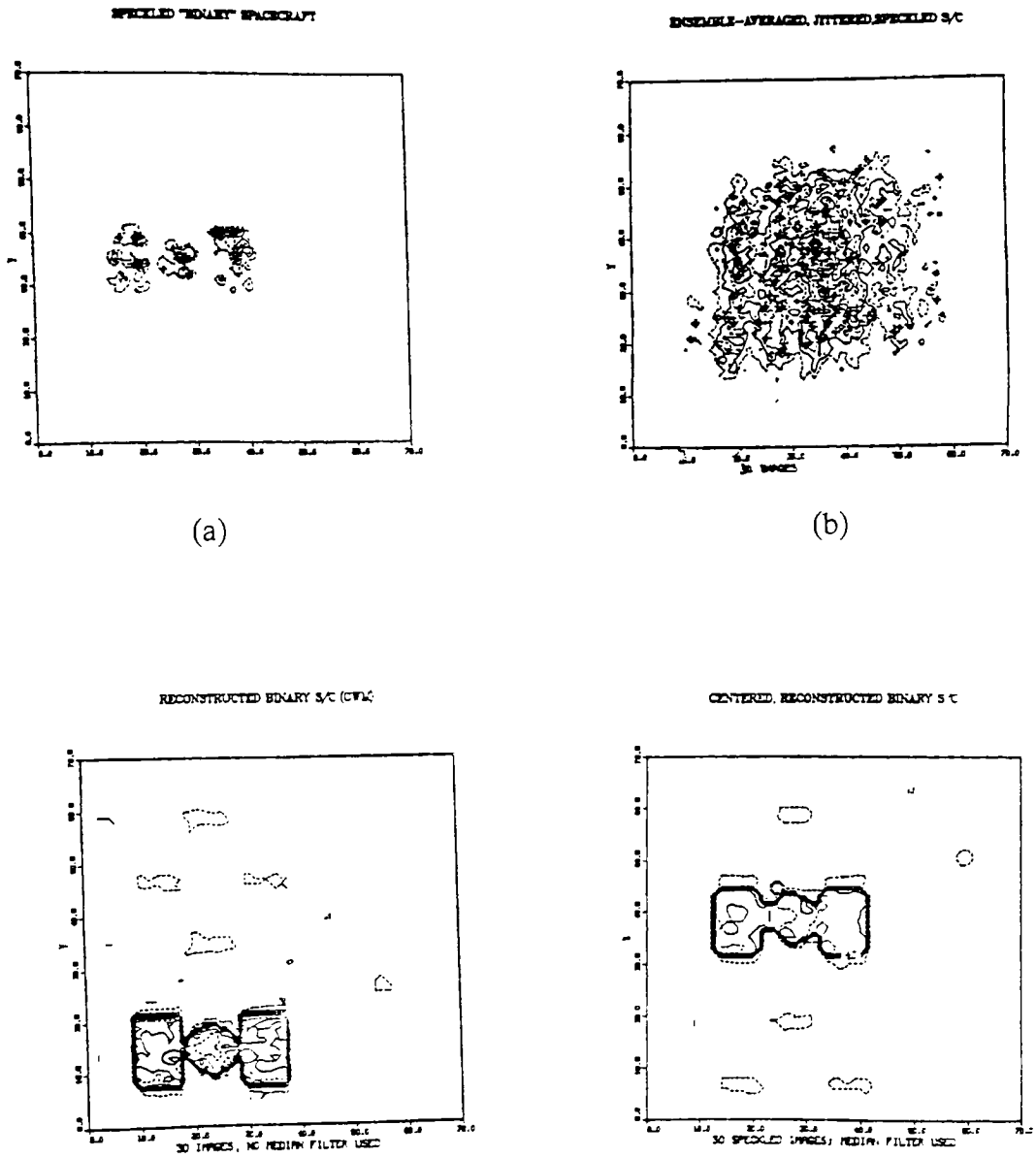

Figure 44a-d. Bispectral Reconstruction Using 2-D Algorithm. Object Speckled Via CWM

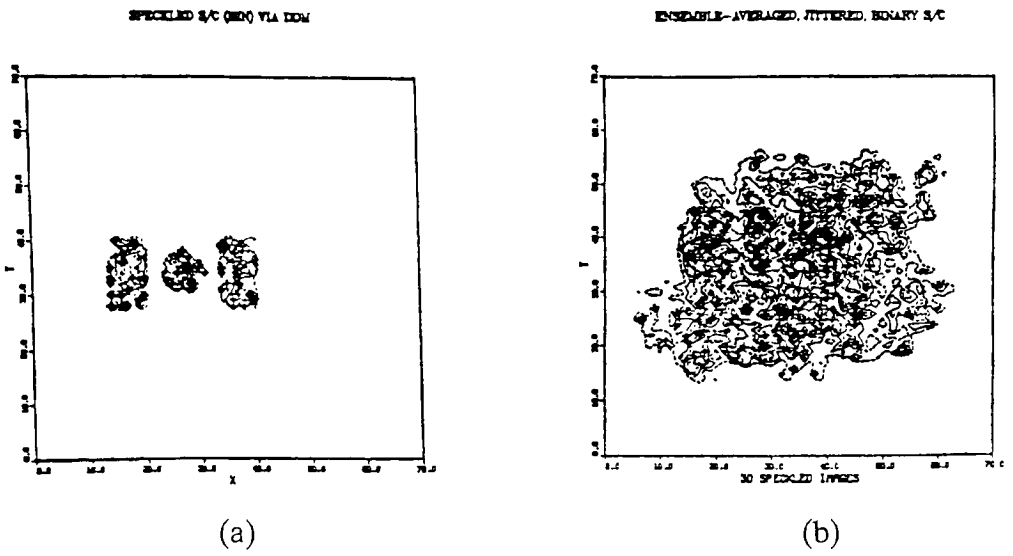

(a) (b)

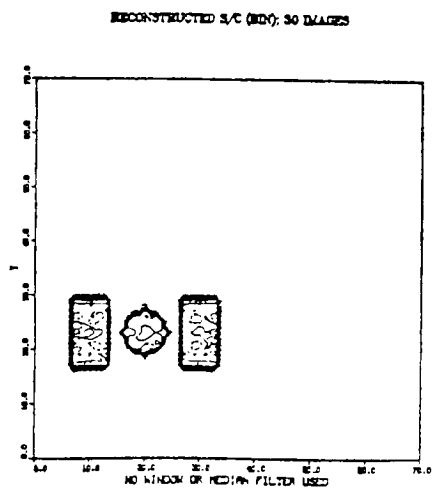

(c)

Figure 45a-c. Bispectral Reconstruction Using 2-D Algorithm. DDM Used to Speckle Object

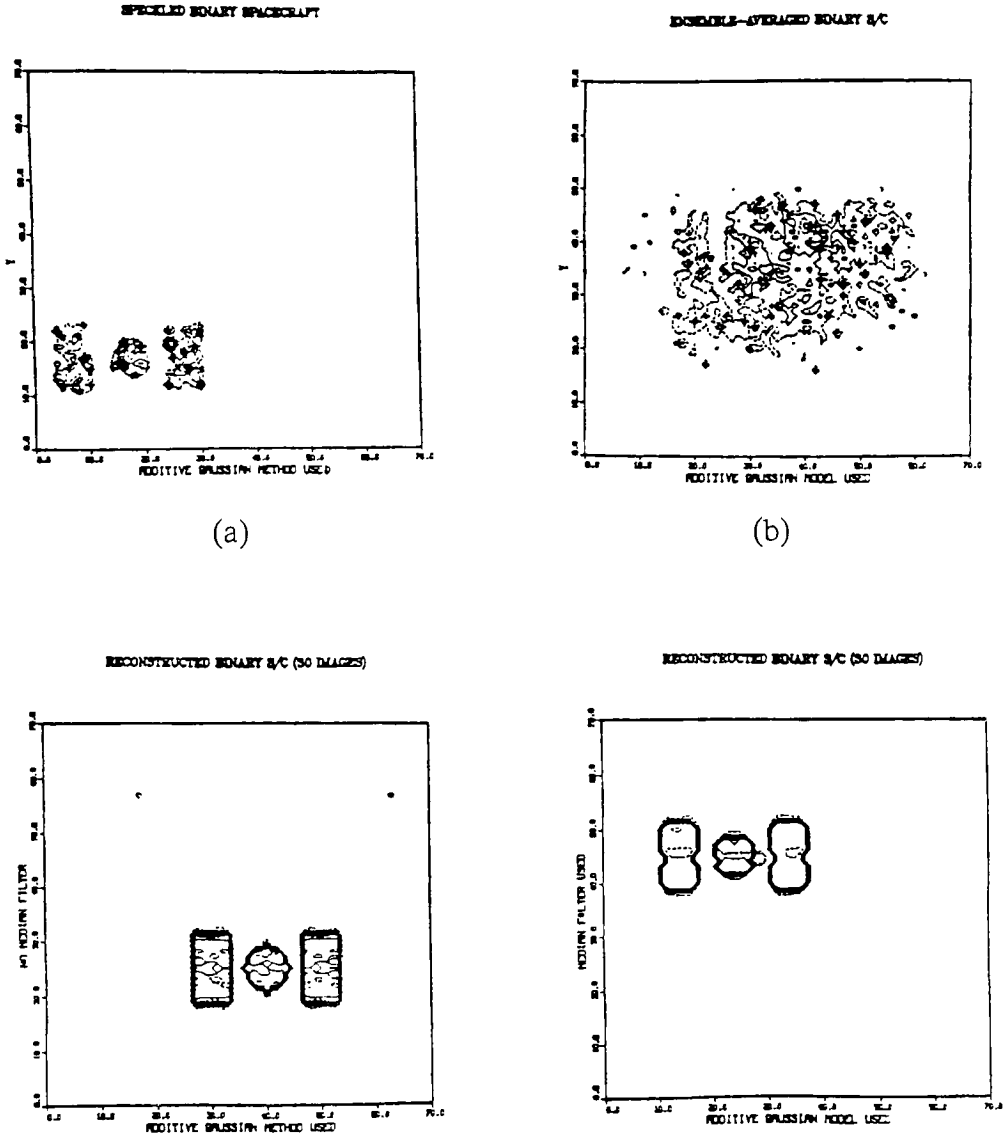

Figure 46a-d. Bispectral Reconstruction Using 2-D Algorithm. AGM Used to Speckle Object

Figure 47 is the reconstructed spacecraft from 30 speckled images using a correlation technique I devised to keep track of the shift of the object from frame-to-frame. Basically, I use the first speckled image as a reference with which I correlate all of the following images. Since speckle is wideband, random noise, their correlations have a distinct peak when they overlap during the correlation procedure. I keep track of this peak's location and align the images with the reference image so that ensemble averaging can be performed. The 2-D contour plot shows a gradual sloping toward the center of each object structure and the edges are a bit blurred. No homomorphic transformation is taken with this method.

A very important point has to be made here. When using the bispectrum to estimate a speckled object, the logarithm **must** be taken prior to the estimation. This was seen in the 1-D case and Figure 48 is the proof in the 2-D case for a speckled binary spacecraft.

In using the homomorphic transformation, I also discovered that care must be taken prior to exponentiation to obtain optimum results. In some cases, the reconstructed Fourier object had values that would cause an arithmetic overflow if not normalized by some constant. The choice of this constant also was an integral part of the quality of the reconstruction. Different objects required different normalizing factors and the choice was purely subjective based on what the reconstructed object needed to enhance its appearance, i.e, edges. Since the goal of speckle-image reconstruction is the return of the object form destroyed by the speckle, this is the only necessary metric by which to base the decision on the choice of the normalizing factor.

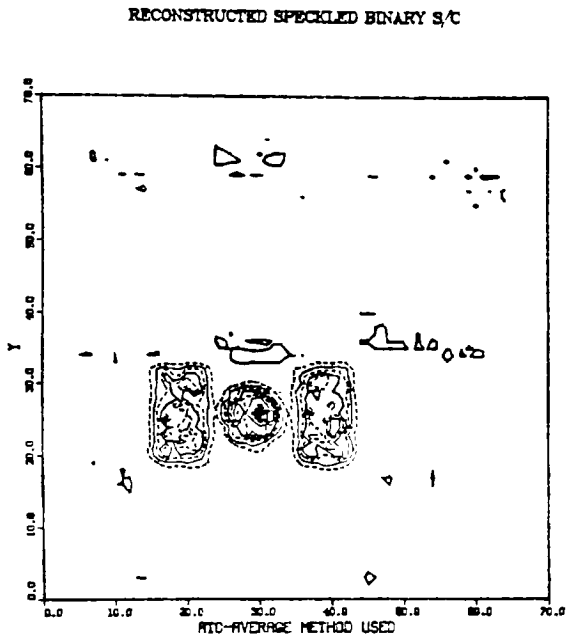

Figure 47. Autocorrelation-Averaged Reconstruction

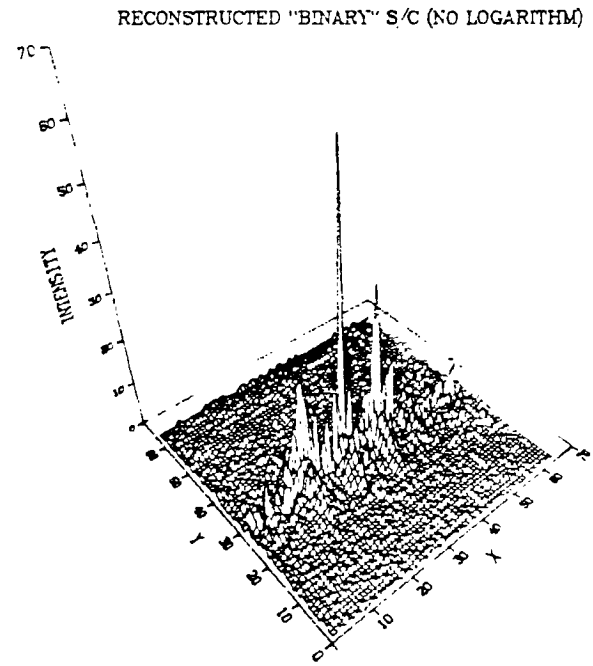

Figure 48. Bispectral Reconstruction of Speckled Object without Logarithmic Transformation

5.3 Conclusions

This thesis has shown that, conceptually, bispectrum estimation is robust enough to recover speckle-degraded images when a homomorphic transformation is taken and the objects are averaged in the bispectrum. This is especially true in the 1-D case, where any object could be reconstructed from any form of the speckle model. The necessary object conditions were that: 1) it had to stay consistently within the field of view of the array when jittering and, 2) even though it could change position within the field of view, it could not change orientation.

The phase recovery problems with the 2-D case were not totally resolved. Phase unwrapping was thought to be a solution but trying to unwrap a 2-D object's phase to obtain a unique solution in 2-D is difficult, especially if the phase changes by modulo 2π every pixel! A 2-D object has phase terms going in the x and y directions; phase unwrapping in one direction may not be what is needed in the other direction at each m,n pixel location. This is because phase unwrapping attempts to impose continuity on the phase function to remove any ambiguities present in the phase (Fiddy and Stark). One ambiguity that arises is from the introduced phase shift of the reconstructed bispectrum. If I could write the reconstructed estimate as an integer phase shift then I would get (after Kaveh and Soumekh):

$$\hat{F}(\lambda\,\zeta) = F(\lambda\,\zeta)\exp[j2\pi n] = |F(\lambda\,\zeta)|\exp\left[j(\Phi_F(\lambda\,\zeta) + 2\pi n)\right] \quad (91)$$

The argument of $\hat{F}(\lambda,\zeta)$ for the phase, then, is given by:

$$\mathrm{ARG}\left\{\hat{F}(\lambda,\zeta)\right\} = 2\pi n + \arctan\left(\frac{\mathrm{Im}(F(\lambda,\zeta))}{\mathrm{Re}(F(\lambda,\zeta))}\right) \quad (92)$$

The ambiguity for the value of the integer, n, is no problem since $\Phi_F(\lambda,\zeta)$ and $\Phi_F(\lambda,\zeta) + 2\pi n$ give the same function for the given modulus, $|F(\lambda,\zeta)|$. The term $2\pi n$ carries no information thus no physical means exist to determine it anyway (Takajo and Takahashi, 1988). But if I take the logarithm of the function, $F(\lambda,\zeta)$, we need to know n. This can be seen from the logarithm of the complex function, $\hat{F}(\lambda,\zeta)$, which is written as:

$$\ln\left(\hat{F}(\lambda,\zeta)\right) = \ln\left(|F(\lambda,\zeta)|\right) + j\left(2\pi n + \arctan\left(\frac{\mathrm{Im}(F(\lambda,\zeta))}{\mathrm{Re}(F(\lambda,\zeta))}\right)\right) \quad (93)$$

Note that the log of the reconstructed object has the same real part as the log of the real object but it has an imaginary part that differs by integrals of 2π. The logarithm of the spectrum is no longer unique, as in the real object's case, due to this phase ambiguity. Phase unwrapping becomes a process whereby we attempt to retrieve this term.

Finally, phase can be described physically as the wavefront surface of a propagating complex wave field. If the amplitude of the propagating wave is zero at any point, its phase is indeterminate. Moving about that point causes a phase change of 2π (1 wavelength) implying wavefront dislocations (Fiddy and Stark). Since speckle is caused by modulo 2π phase excursions, there are as many wavefront dislocations as there are speckles. Phase unwrapping in this case would be indeterminate since the chance of obtaining an unambiguous phase unwrap would be slim.

In summation, this thesis was an attempt to apply spectral techniques to remove multiplicative noise from an object jittered against a uniform background in both one and two dimensions. It was also an exercise in determining the utility of the bispectrum as a signal processing tool. The homomorphic transformation creates a situation where you have a signal plus noise and this noise is small compared to the signal in the bispectral domain. Averaging in this domain allows us to obtain an estimate of the original object. Finally, this thesis attempts to review speckle theory and then model it in different fashions to fully understand the mechanisms behind coherent speckle. Further work could attempt to use actual speckled images and also increase the robustness of the 2-D phase reconstruction routine. One could also look at using additional enhancement routines (aside from the median filter used in this thesis) as post-processing techniques to improve image reconstruction.

6.0 APPENDICES

Appendix A
Tabular Synopsis Of Speckle Models

Model	Description	Assumptions	Transfer Function?
DDM	Circular, complex Gaussian r.v. with zero mean, i.i.d. real and imaginary components created as field. Magnitude squared for speckle intensity.	Large number of surface scatterers; no multiple scattering; no depolarization upon reflection.	NO-assumed embedded in incoherent image.
TFM	Speckle field as in DDM, then Fourier transformed for propagation. Coherent transfer function multiplied by this and then inverse transformed before magnitude squaring.	Coherent optical system can resolve all details in object.	YES-user defined. A key player in ultimate object appearance and statistics.
CWM	Speckle field as in DDM. Complex spatial window of equal strengths correlates complex field. Magnitude squaring result gives intensity.	High quality optics would correlate the speckle locally.	YES-in the form of a 3X3, 5X5, etc. spatial window. Window acts as averaging filter.
RPM	Modulo 2π random phase created from uniform random number generator. This used with image field via Euler's notation to create speckle field, then magnitude squared to give speckle intensity. Can be imaged or pupil-plane speckle.	Object surface is rough on the order of the wavelength of the incident coherent source, up to multiples of 2π until coherence length of source is reached.	YES-is optional but would be implemented similar to TFM once speckle field has been created.
NEM	Noise function created that has a negative exponential pdf. This is then multiplied by the incoherent image of the truth object.	Speckle noise is a signal-dependent and multiplicative noise process.	NO-field statistics are never derived.
AGM	Zero mean, unity variance, Gaussian noise added to the logarithm of the object intensity.	Log of multiple speckle intensity is approximately Gaussian.	NO-field statistics are never derived.

Appendix B
Bispectrum Fourier Expression

This appendix is proof of Equation 43 in the text. Rewriting Equation 42, the bispectrum is given as the Fourier transform of the triple correlation:

$$I^{(3)}(f_1, f_2) = \int_{-\infty}^{\infty}\int_{-\infty}^{\infty} i^{(3)}(x_1, x_2)\, \exp\left[-2\pi j(f_1 x_1 + f_2 x_2)\right]\, dx_1\, dx_2 \qquad \text{(B1)}$$

where: $$i^{(3)}(x_1, x_2) = \int_{-\infty}^{\infty} i(x)\, i(x + x_1)\, i(x + x_2)\, dx \qquad \text{(B2)}$$

is the triple correlation of the spatial image i(x) and x is a 2-D vector. Substituting B2 into B1 gives the bispectrum definition in terms of the real object, i(x) and its shifted versions, $i(x + x_1)$ and $i(x + x_2)$ as:

$$I^{(3)}(f_1, f_2) = \int_{-\infty}^{\infty}\int_{-\infty}^{\infty}\int_{-\infty}^{\infty} i(x)\, i(x + x_1)\, i(x + x_2)\, \exp\left[-2\pi j(f_1 x_1 + f_2 x_2)\right]\, dx\, dx_1\, dx_2 \qquad \text{(B3)}$$

let $\beta = (x + x_1)$, $\alpha = (x + x_2)$, therefore $d\beta = dx_1$ and $d\alpha = dx_2$ since x is constant and $(x_1 + x_2)$ are the shifted, changing values. Substitute these into B3 above to get:

$$I^{(3)}(f_1, f_2) = \int_{-\infty}^{\infty}\int_{-\infty}^{\infty}\int_{-\infty}^{\infty} i(x)\, i(\beta)\, i(\alpha)\, \exp\left[-2\pi j(f_1(\beta - x) + f_2(\alpha - x))\right] dx\, d\beta d\alpha \qquad \text{(B4)}$$

Collecting terms, noting that $\int_{-\infty}^{\infty} f(x) \exp\left[-j2\pi\zeta x\right] = F(\zeta)$ is the continuous definition of the Fourier transform of f(x) (Gaskill), I get:

$$I^{(3)}(f_1, f_2) = \int_{-\infty}^{\infty} i(x)dx \int_{-\infty}^{\infty} i(\beta) \exp\left[-j2\pi f_1 \beta\right] d\beta \int_{-\infty}^{\infty} i(\alpha) \exp\left[-j2\pi f_2 \alpha\right] d\alpha \exp\left[j2\pi f_1 x\right] \exp\left[j2\pi f_2 x\right] \tag{B5}$$

$$I^{(3)}(f_1, f_2) = \int_{-\infty}^{\infty} i(x)dx \exp\left[j2\pi x(f_1 + f_2)\right] I(f_1) I(f_2) \tag{B6}$$

Expanding the exponential term in Equation B6 into its Euler's notation, $\exp[-j\theta] = \cos(\theta) - j\sin(\theta)$, I can write the Fourier transform definition in terms of its real and imaginary components, respectively, as $F(\zeta) = F_{Re}(\zeta) - jF_{Im}(\zeta)$. Thus, I can write Equation B6 as:

$$I^{(3)}(f_1, f_2) = I(f_1) I(f_2)\left[I_{Re}(f_1 + f_2) + j\, I_{Im}(f_1 + f_2)\right] \tag{B7}$$

Noting that $F^{*}(\zeta) = \int_{-\infty}^{\infty} f(x) \exp\left[j2\pi\zeta x\right]$ Equation B7 then becomes:

$$I^{(3)}(f_1, f_2) = I(f_1) I(f_2) I^{*}(f_1 + f_2) \tag{B8}$$

From this expression I can simply write the bispectrum magnitude and phase relationships as functions of the object's Fourier representation as ($|\ I\ |$ is the object magnitude and ϕ is the object phase):

$$I^{(3)}(f_1, f_2) = |I^{(3)}(f_1, f_2)| \exp[\ j\psi\ (f_1, f_2)] \tag{B9}$$

where: $$|I^{(3)}(f_1, f_2)| = |\ I(f_1)|\ |I(f_2)|\ |I(-f_1 - f_2)| \tag{B10a}$$

$$\psi\ (f_1, f_2) = \phi(f_1) + \phi(f_2) - \phi(f_1 + f_2) \tag{B10b}$$

To compare this result with the power spectrum density (PSD), which is the Fourier transform of the autocorrelation, it is defined as:

$$I^{(2)}(f_1) = |\ I^{(2)}(f_1)|\ \exp\ [j\psi\ (f_1)] \tag{B11}$$

where: $$|I^{(2)}(f_1)| = |\ I(f_1)|\ |I(-f_1)| = |\ I(f_1)|^2 \tag{B12a}$$

$$\psi(f_1) = \phi(f_1) - \phi(f_1) = 0 \tag{B12b}$$

The PSD gives us magnitude information regarding the object but phase is lost.

Appendix C
Bispectrum Reconstruction Algorithm Flowchart

This top level block diagram gives the logic flow of how the algorithm was implemented to perform shift-invariant, speckle-degraded image reconstruction. The details of each block are in the text.

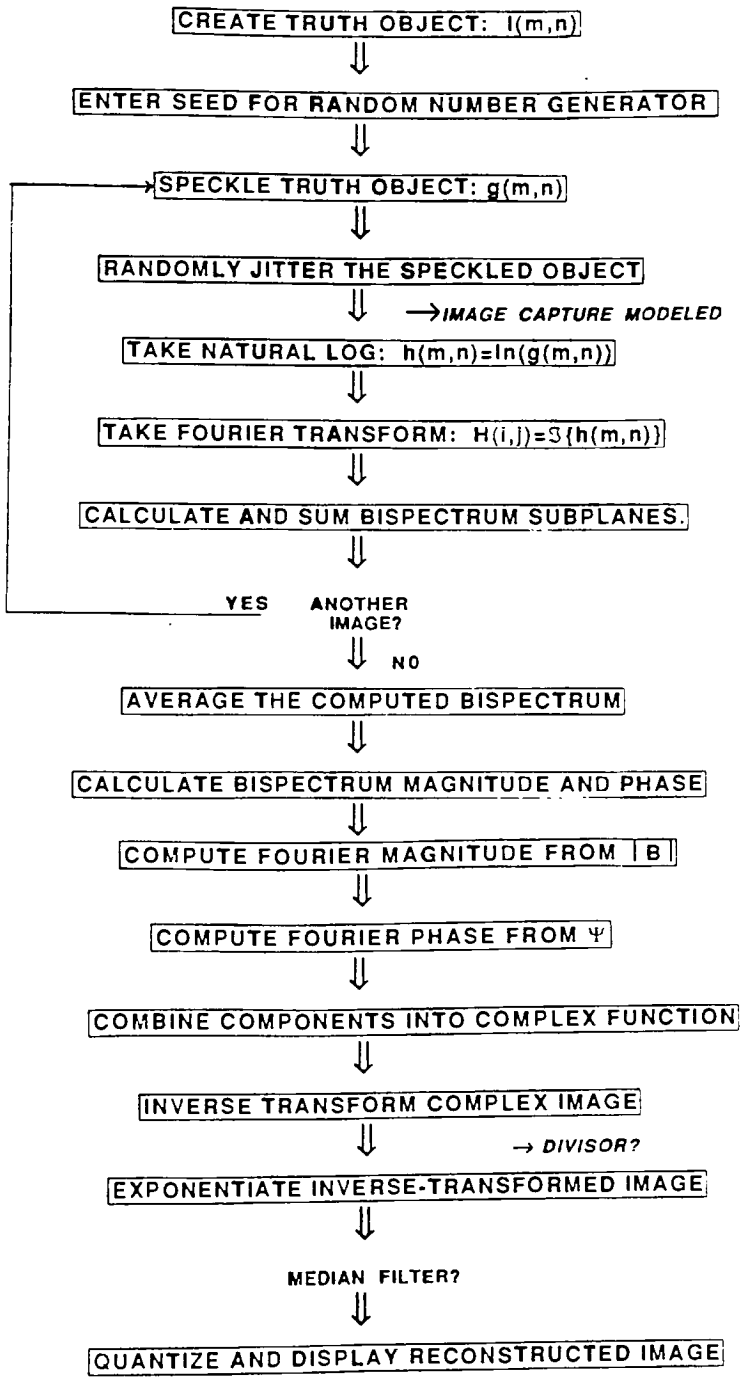

Figure C-1. 2-D Image Reconstruction Overview

7.0 REFERENCES

April, G. and H.H. Arsenault, "Nonstationary image-plane speckle statistics", Journal of the Optical Society of America (JOSA) -A, 1 (7), pp. 738-741, 1984.

Arsenault, H.H. and G. April, "Properties of speckle integrated with a finite aperture and logarithmically transformed", JOSA 66 (11), pp. 1160-1163, 1976.

Arsenault, H. H. and M. Levesque, "Combined homomorphic and local statistics processing of restoration of images degraded by signal-dependent noise", Applied Optics, 23 (6), pp. 845-850, 1984.

Arsenault, H. H. and G. April, "Information content of images degraded by speckle noise", Optical Engineering, 25 (5), pp. 662-667, 1986.

Ayers, G.R., M.J. Northcott, and J.C. Dainty, "Knox-Thompson and triple correlation imaging through the atmospheric turbulence", JOSA-A,5(7), pp. 963-985, 1988.

Bartelt, H., A. W Lohmann, and B. Wirnitzer, "Phase and amplitude recovery from bispectra", Applied Optics, 23 (18), pp. 3121-3129, 1984.

Bates, R.H.T. and M.J. McDonnell, Image Restoration and Recovery. Clarendon Press, Oxford, 1986.

Beckmann, P. and A. Spizzichino, The Scattering of Electromagnetic Waves from Rough Surfaces, Pergamon Press, Oxford, 1963.

Bendat, J. S. and A. G. Piersol, Random Data, Analysis and Measurement Procedures, 2nd Ed., John Wiley & Sons, NY, 1986.

Cederquist, J. N., J. R. Fienup, J. C. Marron, and R.G. Paxman, "Phase retrieval from experimental farfield speckle data", Optics Letters, 13 (8), pp. 619-621, 1988.

Crimmins, T.R., "Geometric filter for speckle reduction", Applied Optics, 24 (10), pp. 1438-1443, 1985.

Dainty, J. C., "Detection of images immersed in speckle noise", Optica Acta, 18 (5), pp. 327-339, 1971.

Dainty, J. C., "Diffraction-limited imaging of stellar objects using telescopes of low optical quality", Optical Communication, 7 (2), pp. 129 - 134, 1973.

Dainty, J. C., "The statistics of speckle patterns", in Progress in Optics, Vol. XIV, edited by E. Wolf, North Holland, Amsterdam, 1976, pp. 3 - 46.

Dainty, J. C., "An introduction to Gaussian speckle", SPIE Vol. 243, pp. 2 - 8, 1980.

Dainty, J. C., "Introduction", in Laser Speckle and Related Phenomenon, Vol 9, Topics in Applied Physics, edited by J.C. Dainty, Springer-Verlag, Heidelberg, 1984, pp. 1 - 7.

Dainty, J.C. and J.R. Fienup, "Phase retrieval and image reconstruction for astronomy", in Image Recovery: Theory and Application, edited by Henry Stark, Academic Press, Orlando, 1987, pp. 231-275.

Dianat, S.A. and M. R. Raghuveer, "Two-dimensional non-minimum phase signal reconstruction", paper presented at Workshop on Higher Order Spectral Analysis, Vail, CO, June 28-30, 1989.

Dianat, S.A. and M. R. Raghuveer, "Fast algorithms for phase and magnitude reconstruction from bispectra", Optical Engineering, 29 (5), pp. 504-512, 1990.

Enloe, L.H., "Noise-like structure in the image of diffusely reflecting objects in coherent illumination", Bell System Technical Journal, 46 (7), pp. 1479 - 1489, 1967.

Fienup, J.R., "Phase retrieval algorithms: a comparison", Applied Optics, 21 (15), pp. 2758-2769, 1982.

Forsythe, G.E., M.A. Malcolm and C.B. Moler, Computer Methods for Mathematical Computations. Prentice-Hall, Englewood Cliffs, NJ, 1977.

Freeman, J.D., J.C. Christou, F. Roddier, D. McCarthy, Jr., and M.L. Cobb, "Applications of bispectral analysis for phase recovery from one-dimensional infrared speckle data", JOSA-A, 5(3), pp. 406 ff, 1988.

Friedan, B.R., Probability, Statistical Optics and Data Testing. Springer-Verlag, Berlin, 1983.

Fujii, H., J. Uozumi and T. Asakura, "Computer simulation study of image speckle patterns with relation to object surface profile", JOSA,66(11), pp. 1222-1236, 1976.

Gaskill, J.D., Linear Systems, Fourier Transforms, and Optics, John Wiley & Sons, NY, 1985.

George, N., C.R. Christensen,J.S. Bennet and B.D. Guenther, "Speckle noise in displays", JOSA, 66 (11), pp. 1282 - 1290, 1976.

Goldfischer, Lester I., "Autocorrelation function and power spectral density of laser-produced speckle patterns", JOSA, 55 (3), pp. 247-253, 1965.

Gonzalez, R.C., and P. Wintz, Digital Image Processing, Addison-Wesley, Reading, 1987.

Goodman, J.W., Introduction to Fourier Optics, McGraw-Hill, NY, 1968.

Goodman, J.W., "Some fundamental properties of speckle", JOSA, 66 (11), pp. 1145-1149, 1976.

Goodman, J.W., "Statistical properties of laser speckle patterns", in Laser Speckle and Related Phenomenon, Vol 9, Topics in Applied Physics, edited by J.C. Dainty, Springer-Verlag, Heidelberg. 1984, pp. 9-75.

Goodman, J.W., Statistical Optics, John Wiley & Sons, NY, 1985.

Goodman, J.W., "A random walk through the field of speckle", Optical Engineering, 25 (5), pp. 6110-612, 1986.

Guenther, B.D., C.R. Christensen and A. Jain, "Digital processing of speckle images", IEEE Proc. Pattern Recognition and Image Processing. pp 85-89, 1978.

Haus, H.A., Waves and Fields in Optical Electronics, Prentice-Hall, Englewood Cliffs, NJ, 1984.

Hayes, M.H., "The unique reconstruction of multidimensional sequences from Fourier transform magnitude or phase", in Image Recovery: Theory and Application, edited by Henry Stark, Academic Press, Orlando, 1987, pp. 195-230.

Idell, P., J.R. Fienup and R.S. Goodman, "Image synthesis from nonimaged laser-speckle patterns", Optics Letters, 12 (11), pp. 858-860, 1987.

Jain, A.K. and C.R. Christensen, "Digital processing of images in speckle noise", Applications of Speckle Phenomena, SPIE Vol. 243, 1980.

Kaveh, M. and M. Soumekh, "Computer-assisted diffraction tomography", in Image Recovery: Theory and Application, edited by Henry Stark, Academic Press, Orlando, 1987, pp. 369-413.

Korwar, V.N. and J.R. Pierce, "Discrimination of form in images corrupted by speckle", Applied Optics, 20 (2), pp. 320-325, 1981.

Kozma, A. and C.R. Christensen, "Effects of speckle on resolution", JOSA, 66 (11), pp. 1257-1260, 1976.

Kuan, D.T., A.A. Sawchuk, T.C. Strand and P. Chavel, "Adaptive restoration of images with speckle" , IEEE Trans., Acoustics, Speech and Signal Processing, 35 (3), pp. 373 - 383, 1987.

Labeyrie, A., "Attainment of diffraction limited resolution in large telescopes by Fourier analyzing speckle patterns in star images", Astronomy and Astrophysics, 6, pp. 85-87, 1970.

Lim, J.S. and H. Nawab, "Techniques for speckle noise removal", Optical Engineering, 20 (3), pp. 472-480, 1981.

Lim, J.S. Two Dimensional Signal and Image Processing, Englewood Cliffs, NJ (1987).

Lohmann, A.W., G. Weigelt and B. Wirnitzer, "Speckle-masking in astronomy: triple correlation theory and applications", Applied Optics, 22 (24), pp. 4028-4037, 1983.

Lohmann, A.W. and B. Wirnitzer, "Triple correlations", Proc. of the IEEE, 72 (7), pp. 889-901, 1984.

Lowenthal, S. and H. Arsenault, "Image formation for coherent diffuse objects: statistical properties", JOSA, 60 (11), pp. 1478 -1483, 1970.

Marathay, A.S., "Phase function of spatial coherence from multiple intensity correlations", paper presented at Advanced Technology Optical Telescopes, III, Tucson, AZ, March, 1986.

Marathay, A.S., Y. Hu and P. S. Idell, "Object reconstruction using third and fourth order intensity correlations", paper presented at Workshop on Higher Order Spectral Analysis. Vail, CO, June 28-30, 1989.

Marron, J.C., P.P. Sanchez, and R.C. Sullivan,"Unwrapping algorithms for least-squares phase recovery from the modulo 2π bispectrum phase", JOSA-A, 7(1), pp. 14-20,1990,

Matsuoka, T. and T.J. Ulrych, "Phase estimation using the bispectrum", Proc. of the IEEE, 72 (10), pp. 1403-1411, 1984.

Mavroidis, T., J.C. Dainty and M.J. Northcott, "Imaging of coherently illuminated objects through turbulence: plane wave illumination", JOSA-A,7(3), pp. 348-355,1990.

McKechnie, T.S., "Speckle reduction", in Laser Speckle and Related Phenomenon, Vol 9, Topics in Applied Physics, edited by J.C. Dainty, Springer-Verlag, Heidelberg, 1984, pp. 123-171.

Miller, M.G., A.M. Scheiderman and P.F. Kellen, "Second-order statistics of laser-speckle patterns", JOSA, 65 (7), pp. 779-785, 1975.

Newman, D. and R. Van Vracken, "Photon correlation imaging for non-acoustic ASW", Eastman Kodak presentation (to be published in JOSA(1990), Jan. 1990.

Nikias, C.L. and M.R. Raghuveer, "Bispectrum estimation: a digital signal processing framework", Proc. of the IEEE, 75 (7), pp. 869-891, 1987.

Northcott, M.J.,G.R. Ayers, and J.C.Dainty, "Algorithms for image reconstruction from photon-limited data using the triple correlation", JOSA-A, 5(7), pp. 986-992, 1988.

Oppenheim, A.V. and R.N. Schafer, Digital Signal Processing, Prentice-Hall, Englewood Cliffs, NJ, 1975.

Oppenheim, A.V. and J.S. Lim, "The importance of phase in signals", Proc of the IEEE, 69(5), pp. 529-541, 1981.

Oppenheim, A.V., M.H. Hayes and J.S. Lim, "Iterative procedures for signal reconstruction from Fourier transform phase", Optical Engineering, 21 (1), pp. 122-127, 1982.

Papoulis, A., Fourier Integral and its Applications. McGraw-Hill Book Co., Inc, NY, 1962.

Raghuveer, M.R., S.A. Dianat, and G. Sundaramoorthy, "Reconstruction of non-minimum phase multidimensional signals using the bispectrum", paper presented at Third SPIE Conf. on Visual Communication and Image Processing, Cambridge, MA, November, 1988.

Sadjadi, Firooz A., "A perspective on techniques for enhancing speckled imagery", Optical Engineering. 29(1), pp. 25-30, 1990.

Safa, F. and G. Flouzat, "Example of morphological filtering of speckle in radar images", Photo-Interpretation, 5, 1988 .

Sato, T., S. Wadaka, J. Yamamoto and J. Ishii, "Imaging system using an intensity triple correlator", Applied Optics, 17 (13), pp. 2047-2052,1978.

Stark , H. and J.W. Woods, Probability, Random Processes, and Estimation Theory for Engineers. Prentice-Hall, Englewood Cliffs, NJ, 1986.

Stearns, S.D. and R.A. David, Signal Processing Algorithms, Prentice-Hall, Inc., Englewood Cliffs, NJ, 1988.

Sundaramoorthy, G., M.R. Raghuveer and S.A. Dianat, "Bispectral reconstruction of signal in noise: amplitude reconstruction issues", to be published in IEEE Trans. Acoustics, Speech and Signal Processing, July, 1990.

Swami, A. and G.B. Giannakis, "ARMA modeling and phase reconstruction of multidimensional non-gaussian processes using cumulants", International Conference on Acoustics, Speech, and Signal Processing, pp. 729-732, April,1988.

Takajo, H. and T. Takahashi, "Least squares phase estimation from the phase difference", JOSA-A, 5(3), pp. 416-425, 1988.

Tur, M., K.C. Chin and J.W Goodman, "When is speckle noise multiplicative?", Applied Optics, 21 (7), pp. 1157-1159, 1982.

Voelz, D.G., J.D. Gonglewski and P.S. Idell, "Imaging correlography: experimental results and performance evaluation based on SNR of the power spectrum estimate", in Statistical Optics, ed. by G.M. Morris, Proc. Soc. Photo-Opt. Instrum. Eng. 976, pp. 77-92, 1988.

Welford, W.T., "Speckle in images", JOSA, 66(11), pp. 1172-1174, November 1976.

Yariv, A., Optical Electronics, 3rd Ed., Holt, Rinehart, and Winston, NY, 1985.